QUANTUM PERSPECTIVES ON PHYSICAL AND INORGANIC CHEMISTRY

Thomas V. Grimes-Marchan, B.S.

Dissertation Prepared for the Degree of

DOCTOR OF PHILOSOPHY

UNIVERSITY OF NORTH TEXAS

December 2007

APPROVED:

Thomas R. Cundari, Major Professor
Weston T. Borden, Committee Member
Angela K. Wilson, Committee Member
Mohammad A. Omary, Committee Member
T. Brent Gunnoe, Committee Member
Michael G. Richmond, Chair of the Department of Chemistry
Sandra L. Terrell, Dean of the Robert B. Toulouse School of Graduate Studies

Grimes-Marchan, Thomas V., Quantum Perspectives on Physical and Inorganic Chemistry. Doctor of Philosophy (Physical Chemistry), December 2007, 120 pp., 18 tables, 13 illustrations, references, 236 titles.

Applications of computational quantum chemistry are presented, including an analysis of the photophysics of cyclic trinuclear coinage metal pyrazolates, an investigation into a potential catalytic cycle utilizing transition metal scorpionates to activate arene C-H bonds, and a presentation of the benchmarking of a new composite model chemistry (the correlation consistent composite approach, ccCA) for the prediction of classical barrier heights. Modeling the pyrazolate photophysics indicates a significant geometric distortion upon excitation and the impact of both metal identity and substituents on the pyrazolates, pointing to ways in which these systems may be used to produce rationally-tuned phosphors. Similarly, thermodynamic and structural investigations into the catalyst system points to promising candidates for clean catalytic activation of arenes. The ccCA was found to reproduce classical reaction barriers with chemical accuracy, outperforming all DFT, *ab initio*, and composite methods benchmarked.

TABLE OF CONTENTS

Page

LIST OF TABLES

Page

LIST OF FIGURES

Page

LIST OF CHARTS AND SCHEMES

Page

Charts

Schemes

CHAPTER I: INTRODUCTION

I.1 Overview

As quantum mechanics is one of the major underpinnings of modern chemistry, the advance of quantum mechanical computational methods to achieve convergence between theory and experiment is of paramount importance. In particular, the explosion of computational power has enabled chemists to probe chemical systems at the molecular level with unprecedented accuracy and insight. Concomitant with this newfound computational ability is the magnified scope of computational chemistry in general in terms of breadth of applications. This document focuses on two particular aspects of this burgeoning field, the quantum chemistry of transition metal complexes and the application of a new composite model chemistry to reaction barriers.

Transition metal complexes in general present challenges to both experimental and computational chemists. The density of states arising from the d-manifold as well as the generally non-negligible contribution of relativistic effects bestows a rich chemistry on these compounds. It is precisely this richness that establishes their importance for many applications in both the fine and bulk chemical industries. Beyond their obvious importance in catalysis of industrial processes, transition metals are found in some form in virtually every application from health and medicine (*e.g.*, the role of transition metal ions in biomolecular systems) to semiconductor and photonic devices.

From this broad spectrum, two particular projects have been chosen for discussion in this dissertation.

A computational investigation of cyclic trinuclear coinage metal (*i.e.*, Group 11) pyrazolate complexes is presented *vide infra*. These systems represent a fairly new class of compounds with fascinating photophysical properties. Specifically of interest in this study are the tunability of emission and absorption with modification of the coinage metal and the huge geometric change upon photoexcitation, which is evinced by the very large Stokes' shifts that have been observed experimentally and reproduced qualitatively in the current work. These compounds are therefore candidates for rational design of novel photonic devices avoiding the use of overly expensive (*e.g.*, Ru) or toxic (*e.g.*, Hg and Tl) metals.

Also included in this document is a study of aryl C-H bond activation by transition metal scorpionate complexes of the form TpM(X)(benzene), where M = Tc, Re, Ru, Co, Ir, Ni, or Pt and X = OH or NH_2. While a complete functionalization cycle has not yet been developed, experimental evidence for catalytic C-H activation in these systems is provided by the observation of H/D scrambling in solution at thermal energies. Currently, industrial methods for the functionalization of aromatic feedstocks require harsh conditions (*e.g.*, Friedel-Crafts chemistry), produce unacceptable waste products, and are intolerant of functional groups. The ability to catalytically activate aryl substrates without the need for such harsh conditions is therefore imperative for both increased atom and energy efficiency. The current work investigates the impact of

metal and activating ligand identity. This information is necessary for the extension of the observed H/D exchange to actual functionalization.

While the two topics above deal with transition metals from a more or less pragmatic perspective using DFT, the final topic is concerned with the development of a new composite model chemistry. The correlation consistent Composite Approach (ccCA) is formulated to use DFT to predict geometries and a sequence of *ab initio* calculations to predict the electronic energy. The energy is calculated as a series of additive corrections to a reference energy obtained by complete basis set extrapolation using Dunning's correlation consistent basis sets,[1] obtaining chemical accuracy at a cost less than that of a pure wavefunction-based method. The ccCA protocol has been employed with great success for the prediction of electronic properties of ground state systems containing main group (s- and p-block) elements[2] to within so-called "chemical accuracy," defined here as no more than ±1 kcal/mol error with respect to experiment. It is shown here that ccCA is useful for computing classical reaction barriers, being more accurate and reliable than the G3B composite methodology.

Incorporating both theory and application, transition metal and main-block chemistry, catalysis and photophysics, the current dissertation presents a spectrum of work all bound by the common theme of computational quantum chemistry. Specific applications addressed in this dissertation include the ground and excited state structure of coinage metal trimers, the identification of novel catalyst leads for direct functionalization of aromatic hydrocarbons, and the application of a novel composite chemical method to the calculation of activation barriers.

I.2 Coinage Metal Pyrazolates

Interesting chemical and photophysical properties result from the supramolecular assemblies with differing degrees of intertrimer and intratrimer metal-metal bonding displayed by coinage metal cyclic pyrazolate trimers (Chart 1). The interactions between the trimers are influenced by many factors, as shown particularly by Omary, Dias, and co-workers that the emission energies and unit cell dimensions of these materials have significant changes with temperature leading to *luminescence thermochromism*.[3,4] The manifold possibilities for modes of intertrimer interactions lead to a wide variety of supramolecular structures including extended linear and zigzag chains and dimer-of-trimers in which adjacent trimers are packed in various conformations that include chair, prismatic, star-shaped, step-ladder, *etc.*,[3,4,5,6] akin to those known for cyclic trinuclear coinage metal trimers of other bridging ligands besides pyrazolates.[7] Substituents on the bridging ligand and the coinage metal identity also determine the balance between acid/base behavior, electrostatic interactions, metallophilicity between d^{10}-metal pairs, and the luminescence behavior.[3,4,5,6] As a single example, the parent $[AuPz]_3$ is a basic complex, like most other Au^I cyclic trimers,[7,8] while addition of trifluoromethyl substituents to the pyrazolate rings yields a trimer that is acidic enough to form a binary adduct with toluene.[3] Pyykkö,[9,10] Hoffmann,[11] and others,[12,13] have explored the theoretical origin of metallophilicity, which describes d^{10} metal-metal interactions, and related these closed-shell interaction[7] to correlation effects

strengthened by relativistic effects[9,10] or to hybridization of *nd* orbitals with *(n+1)s* and *(n+1)p* orbitals.[11] Metallophilicity is expected to play an especially important role in the cyclotrimeric compounds treated in this dissertation because of the large number of close M···M pairs. Poblet and Bénard attempted to model similar systems in 1998 but they deemed that "a conclusive argument proving the existence of metallophilic interactions on such large systems is at present impossible to obtain from quantum chemical calculations."[13] This computation is now possible for $\{[MPz]_3\}_2$ coinage-metal dimer-of-trimers and even substituted systems such as $\{[M(3\text{-}CF_3)Pz]_3\}_2$, allowing direct comparison to experiment not only the ground-state metallophilic bonding but also for excited-state excimer M-M bonding. Direct experimental verification is now accessible by time-resolved single-crystal X-ray diffraction for these systems as demonstrated in a recent elegant study by Coppens and co-workers.[14]

Chart 1. Structure of $[M(3\text{-}(R),5\text{-}(R')Pz)]_3$ cyclic trimers.

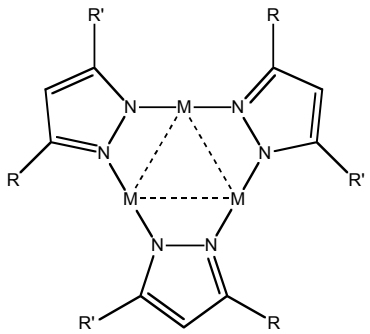

An important aspect of the present study is modeling the photophysics of coinage-metal pyrazolate trimers. In addition to bright, tunable phosphorescence, other fascinating luminescence properties of these systems found experimentally include

drastic sensitivities of the phosphorescence colors and lifetimes to solvent, temperature, concentration, rigidity of medium, substituents on the pyrazolate ring, and identity of the coinage metal.[3,4] Theoretical results giving values for the phosphorescence and excitation energies as well as the consequent Stokes' shifts representing the difference between the $T_1 \rightarrow S_0$ and $S_0 \rightarrow T_1$ vertical transition energies for various monomer-of-trimer and dimer-of-trimer models are presented. Known structures found in the Cambridge Structural Database[15] indicate a much larger variation in inter-trimer versus intra-trimer M···M distances for coinage metal pyrazolate trimers, consistent with the expectation of a soft interaction potential energy curve with respect to separation between the pyrazolate trimers. Understanding the nature of the bonding and photophysical properties for coinage metal trimers is vital to explain the luminescence properties of these compounds and how they can be tuned, leading to information for the rational design of new synthetic targets.

The current research presents computational evidence of a drastic change in the geometry of the emissive excited state of coinage-metal pyrazolate trimers. Intermolecular interactions of coinage metal pyrazolate trimers are modeled in dimeric models to yield a first approximation to the structure in the solid state and even solution, since these systems exhibit non-Beer's law behavior attributed to association in solution.[3] The manner in which M-M metallophilic and excimeric interactions differ between the ground and phosphorescent excited states of both $[MPz]_3$ monomer-of-trimer and $\{[MPz]_3\}_2$ dimer-of-trimer models is also addressed. Roles of the coinage metal identity and substituents on the pyrazolate bridges are also assessed in terms of

both the geometry of the S_0 and T_1 states and photophysical parameters. A discussion of intermolecular interactions between adjacent monomer-of-trimer units in the complexes is hardly complete without considering the relative role of metallophilic bonding versus electrostatic attraction, and is therefore included.

I.3 Aryl C-H Bond Activation

An important pursuit in modern chemistry is the development of catalysts for the functionalization of carbon-hydrogen bonds. There catalysts have the potential to positively impact both commodity and fine chemical markets. The stoichiometric metal-mediated activation of carbon-hydrogen bonds initiated by transition metal systems are known,[16] many of these systems functioning in ambient conditions. The most common mechanisms invoked for the C-H bond cleavage step itself include oxidative addition (OA), σ-bond metathesis (SBM), and electrophilic substitution (ES). Given the success of metal-mediated C-H activation, the paucity of incorporation of stoichiometric C-H activations into catalytic cycles is unfortunate.[17] This is especially true for functionalization of aliphatic hydrocarbons. A few well-known examples of such catalytic conversions include alkane dehydrogenation,[18,19,20] alkane metathesis,[21] alkane silation,[22] alkane borylation,[23] and hydrocarbon functionalization via Shilov-type metal electrophiles.[24] Vedernikov and Caulton have coupled alkane dehydrogenation with aziridination of the resultant olefins in an interesting tandem synthesis.[25]

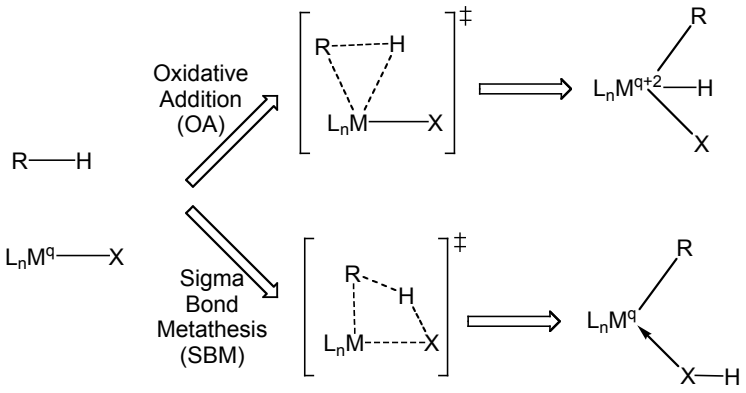

Scheme 1. Oxidative addition (OA) and σ-bond metathesis (SBM) mechanisms for C-H bond activation; q denotes the formal oxidation state of the metal.

The OA mechanism involves both the carbon and hydrogen of the C-H bond cleaved being transferred to a low-valent transition metal center via a three-centered transition state, Scheme 1.[26] In contrast to the OA three-center transition state, SBM is a concerted reaction involving four atomic centers including the metal center, the ligand that receives the transferred proton, and the C and H atoms of the bond being activated, Scheme 1. The SBM pathway does not change the formal oxidation state of the metal center. OA and SBM pathways of carbon-hydrogen bond activation were contrasted by Cundari upon examining the metal complex to substrate electron donation and backdonation.[27] Both OA and SBM are characterized by an "electrophilic" phase dominated by substrate to metal donation early in the reaction coordinate (*i.e.*, before the transition state). Metal complex to substrate backdonation comprises a "nucleophilic" phase and serves to delineate the mechanisms.[27] The metal center functions as both electrophile and nucleophile in the OA mechanism for typical (*i.e.*, monometallic) complexes and thus both ends of the C-H bond end up ligated to the

metal. When the mechanism is SBM, the donor orbital on the metal complex is a metal-ligand frontier orbital polarized towards the more electronegative ligand. Periana and Goddard *et al.* have proposed an oxidative-hydrogen migration (OHM)[28] mechanism for C-H activation by Ir(III) complexes in which the transition state is intermediate between OA and SBM[29] transition states and may be distinguished from the latter by more significant interaction between the metal and the hydrogen of the carbon-hydrogen bond being activated. Drawing distinctions between OA, OHM, and SBM is reminiscent of debates concerning the nature of chemical bonding: while technical distinctions exist and demarcation into categories can be useful, real mechanisms lie on a spectrum defined by these classifications.

The net 1,2-addition of C-H bonds across M-X (X = heteroatomic ligand such as amido, alkoxo, imido, oxo, *etc.*) bonds holds promise as a step in overall catalytic C-H functionalization.[30] perhaps via OA, SBM, or ES pathways. Relatively few examples of net 1,2-addition of C-H bonds across M-X bonds appear in the literature. For example, the Wolczanski[31] and Bergman[32] groups have studied the 1,2-addition of C-H bonds, including that of methane, across d^0 metal-imido (M=NR) bonds of early transition metals (*e.g.,* Ti and Zr). It has been established that the reaction is an overall $[2_\sigma+2_\pi]$ addition and that the transition state has a four-centered arrangement preceded by an alkane or arene adduct. Even though the resulting alkyl/aryl product is only a single C-N reductive elimination step away from substrate functionalization to produce amine, reductive elimination is difficult for electropositive early transition metal complexes. In contrast, there exists ample precedent for C-N and C-O reductive elimination from late

transition metals.[i] Thus, applying net 1,2-addition of C-H bonds to late transition metal systems may ultimately lead to incorporation into catalytic cycles for C-H functionalization.

Scheme 2 shows two possible pathways in which 1,2-addition of C-H bonds across M-X (X = O or NR) or M-XR bonds could be incorporated into a working catalytic cycle. Route A involves 1,2-addition of a C-H bond across a metal-heteroatom (M=X) bond, followed by reductive elimination of now-functionalized product (R-X-H). The active species is regenerated via an atom or group transfer reagent. This route is perhaps similar to metal-catalyzed insertion of carbenes into C-H bonds.[33] In contrast, Route B begins with functionalization of a metal-alkyl moiety via formal insertion of an oxygen atom or nitrene fragment into a metal-alkyl or metal-aryl bond. Following the insertion, hydrogen transfer from a hydrocarbon substrate produces the functionalized product and also regenerates the active metal-alkyl species. Mayer and Brown have reported high-valent Re-oxo complexes that undergo oxo insertion into Re-Ph bonds under photolytic and thermal conditions.[34] In addition, Periana *et al.* have recently reported remarkably facile conversions of the Re-Me bond of methylrheniumtrioxo to a methoxo ligand upon treatment with various oxidants,[35] with preliminary mechanistic studies suggesting that the inserted oxygen atom is not derived from a Re=O ligand.

---

i The proclivity of late transition metals for C-O and C-N elimination has been profitably exploited in, for example, the well-known Hartwig-Buchwald etheration and amination reactions. (a) Stuermer, R. *Organic Synthesis Highlights V* **2003**, 22. (b) Muci, A. R.; Buchwald, S. L. *Topics in Current Chemistry* **2002**, *219*, 131. (c) Hartwig, J. F. *Comprehensive Coordination Chemistry II* **2004**, *9*, 369.

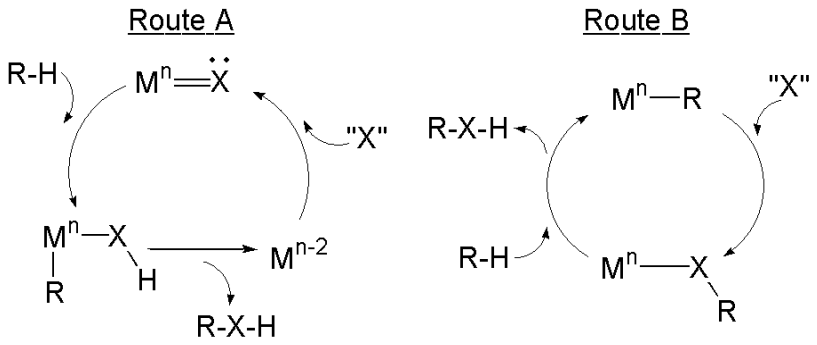

Scheme 2. Possible routes for catalytic C-H functionalization that involve net 1,2-addition of C-H bonds across M-X(R) bonds (X = O or NR).

Recently, there has been increasing interest in extending 1,2-addition of C-H bonds across M-X bonds to late transition metals in relatively low oxidation states. High valent late(r) transition metal-oxo and hydroxo/alkoxo complexes are prevalent in the functionalization of C-H bonds, but these systems typically activate C-H bonds through net radical hydrogen atom abstraction routes in which the metal center does not directly interact with the C-H bond. Instead, the metal serves as an oxidizing "electron reservoir."[36,37,38] The hypothesis used in this work is that lower oxidation states avoid the odd-electron radical chemistry and increase the propensity toward even-electron processes, such as intermolecular heterolytic C-H bond cleavage and intramolecular 1,2-addition reactions (Scheme 3).[39] For example, it has been demonstrated that coordinatively and electronically saturated octahedral Ru(II) and Fe(II) amido complexes may deprotonate (*i.e.*, an even-electron transformation) relatively acidic C-H bonds (*e.g.*, phenylacetylene, 1,4-cyclohexadiene, and triphenylmethane). Bergman *et al.* conducted a prominent study of the reactivity of *trans*-$(dmpe)_2Ru(H)(NH_2)$ toward

acidic C-H bonds.[40] Even very weakly acidic compounds (*e.g.*, toluene) react, though the reaction is endothermic.[40] Similar reactivity is observed in the corresponding Fe(II) analog,though it is less basic than the ruthenium complex,[41] $TpRuL_2X$ (X = NHR, OR; Tp = hydrido-*tris*(pyrazolyl)borate), and (PCP)Ru(L)(NHR) (PCP = *bis*-phosphine "pincer" ligand).[42,43,44] Note that these transformations involve *inter*molecular C-H bond cleavage (Scheme 3).

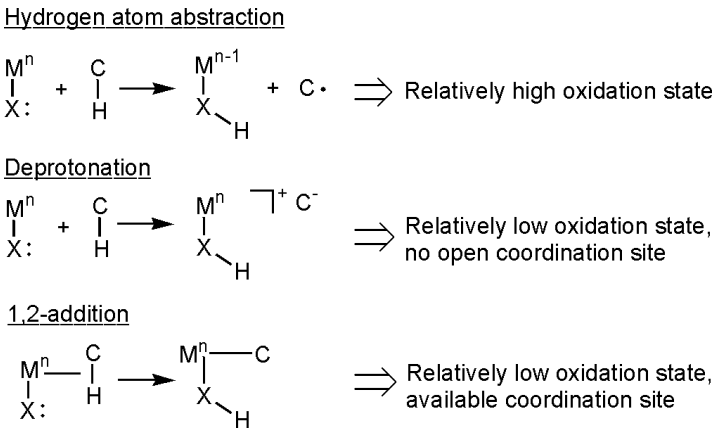

Scheme 3. Three pathways to cleave C-H bonds by transition metal systems with formally anionic heteroatomic ligands.

As has been previously suggested for reactions of $(PCP)Ru(CO)NH_2$,[43] the coordination of C-H bonds to similar systems[40,41] (*i.e.*, amido, hydroxo, or related complexes in low oxidation states) could possibly activate them toward net intramolecular deprotonation by the highly basic non-dative ligand "X" (Scheme 3). There is evidence for such reactions with $TpRu(PMe_3)X$ (X = OH, OPh, or NHPh) systems[30b,c], and Periana *et al.* have directly observed related reactions with an Ir(III)-

methoxo complex.[30a,45] To the author's knowledge, these reports are the only examples of 1,2-addition of C-H bonds across M-X (X = OR, NHR, O, or NR) bonds for late transition metals in low oxidation states. Macgregor *et al.* have reported the possible involvement of an Ir-acetate ligand in C-H bond activation[46] in related chemistry, and the 1,2-addition of a C-H bond across a Pt-Cl bond has been implicated in Shilov-type chemistry.[24] The paucity of literature relevant to the various factors that impact the energetics of the 1,2-additions compels the comprehensive computational study that is herein presented, addressing the influence of the identity of the non-dative ligand (OH versus NH_2) and metal [Tc(I), Re(I), Ru(II), Co(III), Ir(III), Ni(IV) and Pt(IV)] on the kinetics and thermodynamics of benzene C-H bond scission by 1,2-addition. Though the present studies are specifically focused on $[(Tab)M(PH_3)X]^n$ systems, guidance for the design of systems that are more active for C-H bond activation, particularly within a catalytic cycle for hydrocarbon functionalization, may be obtained by comparison with the current results.

I.4 ccCA Reaction Barrier Height Benchmarking

The use of composite model chemistries to accurately calculate energies at a reduced computational cost in the theoretical modeling of chemical species has made great stride in progress. Composite methods have progressed even to the point of predicting thermodynamic properties of ground state systems containing up to approximately a dozen heavy atoms to within ±1 kcal/mol from experimental values

(so-called "chemical accuracy"). Some composite methods even claim to be within 0.24 kcal/mol (1 kJ/mol) of experiment.[47,48] However, the prediction of kinetic rate constants, which implicitly require accurate energetics for both ground and transition states, has not, in general, enjoyed the same degree of success. The correlation consistent composite approach (ccCA) is a composite model chemistry that aims to achieve chemical accuracy without empirical parameters and at a reasonable computational cost in comparison to large basis set coupled cluster calculations.[49] The ccCA has been benchmarked against a large set of atomization energies, heats of formation, *etc.* for stable molecules, atoms, radicals and even s- and d-block metal systems.[2] Herein, the benchmarking of ccCA is extended to transition states and represents a first step toward accurate theoretical predictions of reaction kinetics using composite methods.

Two basic problems hinder any attempt at reproducing experimental kinetic data using theoretical methods. First, the chemical rate constant (k) has exponential dependence on the activation energy (E_a), as indicated by the Arrhenius equation ($k = A \exp[-E_a/RT]$). Even achieving chemical accuracy (±1 kcal/mol) for the activation barrier can still lead to very large errors in the predicted rate constant. Second, the nature of the E_a term itself is a problem. It is a purely phenomenological quantity in the Arrhenius equation: Arrhenius plots are never perfectly linear arbitrarily large temperature range. Furthermore, direct experimental measurement of classical barrier heights, *vis-à-vis* transition state energies, is not possible. The association of an observed activation barrier with the classical barrier height (the zero-point energy

corrected difference in energy between the transition and ground reaction states) is thus strictly incorrect, as can be easily rationalized by the fact that the adiabatic transition state geometry and energy do not change with temperature while the activation energy does. This particular association of activation energy and classical barrier height has led to substantial error in the comparison of predicted and observed rate constants (*e.g.*, see reference 50). Tunneling, barrier recrossing, diabatic effects (*i.e.*, coupling of different electronic states), the presence of multiple reaction channels, and potential van der Waals complexes in the reaction channels are all neglected within the simplest transition state theory. Thus, the observed rate constant depends on more than just the reactant and product asymptotes and a first-order adiabatic saddle point. Essentially the entire potential energy surface (PES) must be considered.

Choosing a transition state theory (TST) to model a particular reaction incurs a trade-off between accuracy and available resources, just as in thermochemistry modeling. Direct integration of the quantum mechanical scattering equations or the application of quantum statistical mechanics theoretically provides quantitatively accurate kinetic data. However, these procedures are so time consuming as to be impractical for all but the very smallest systems.[51] Application of a computationally expensive level of theory means fewer points on that PES can be feasibly computed within a reasonable amount of time, requiring a lower level of TST to keep the computational expense reasonable. A common application of this concept is the use of expensive levels of theory to calculate only the product/reactant asymptotes and a transition state (*i.e.*, conventional transition state theory).[52] Conversely, a cheaper level

of theory will allow more of the PES to be explored and a higher level of TST to be employed, but at the cost of uncertainty in those points. Whether the error comes from the electronic structure method or the flavor of TST, the error will propagate to the final result. In attempt to balance between the two possibilities just given, an alternative approach that is sometimes employed[53] is the use of a high level of electronic structure theory to calculate the product/reactant asymptotes and the transition stateand use a lower level of theory for a limited number of points on the PES (usually points along the minimum energy path, MEP). This may often offer a good compromise, yet this sort of "hybrid" methodologysuffers not only from reduced accuracy along the MEP, but also from a potential mismatch between PESs described at two different levels of theory. Therefore, a method that balances speed and accuracy uniformly across the PES is highly desirable. The natural next step is to try to extend composite model chemistries successful in predicting thermochemistry to such approaches to kinetic modeling.

Given the complexity of benchmarking against experimental observations directly and the convolution of error intrinsic to any TST, two databases of "best-estimate" transition state energies were used (HTBH38/04 and NHTBH38/04).[54] These databases contain barrier heights derived from either (a) TST adjusted against experimental rates combined with dynamical simulations[55] in order to extract a better estimate of the transition state energy (the classical barrier height), or (b) from very accurate *ab initio* calculations. A more balanced comparison of how ccCA performs for transition states in relation to the best available data is thus obtained by benchmarking against the database values. The benchmarking described in this paper does not directly yield an

estimate of how well ccCA predicts rate constants, but rather how well ccCA describes the adiabatic PES for the most important stationary points (reactant and product asymptotes and the transition state) relative to levels of theory currently employed in the literature for kinetic modeling.

Among composite model chemistries, G3 and G3B have a reported accuracy (mean unsigned error) of 0.99 and 1.01 kcal/mol, respectively, in the literature with respect to the G2/97 test set, for ground state energies.[56] The application of Gaussian-*n* methods to kinetics is frequently reported in the literature.[50,57,58] Results computed using G3B are given along with the ccCA results in this paper for the sake of comparison. Since both ccCA and G3B (a variant of G3 theory) model chemistries use B3LYP optimizations with comparable basis sets to provide the reference geometry, G3B was used in this research to provide the most even standard of comparison. Hybrid DFT methods are commonly thought to provide good transition state geometries.[59] Combining a fast, yet accurate geometry optimization provided by DFT with a carefully constructed series of additive basis set and correlation energy corrections allows computed from *ab initio* wavefunction-based methods, ccCA aims to provide more accurate thermochemical data than G3B at a computational expense much cheaper than W*n* model chemistries for ground state properties,[49] and forms the subject of this investigation.

CHAPTER II: COMPUTATIONAL METHODS

II.1 Coinage Metal Pyrazolates

II.1.a Methods

All of the geometry optimizations of coinage metal pyrazolate systems were performed at the B3LYP/CSDZ* level in Jaguar.[60] Since this method gave bond lengths and energies comparable to those obtained with B3LYP/LACV3P**++ on the $[CuPz]_3$ singlet and triplet structures, the computationally less expensive B3LYP/CSDZ* method was chosen for all subsequent calculations. The CSDZ* basis is the Stevens-Cundari effective core potential (ECP)[61] for elements heavier than argon; carbon, nitrogen and hydrogen are described by the 6-31G* basis set. For calculation of cuprophilicity, an approach suggested by Pyykkö was employed;[9] thus, LMP2 (localized 2nd-order Møller-Plesset perturbation theory[62])/CSDZ* and ROHF (restricted open-shell Hartree-Fock)/CSDZ* single-point calculations were run at the B3LYP/CSDZ*-optimized geometries of both singlet and triplet $\{[CuPz]_3\}_2$. In addition, the counterpoise method[63] was used to eliminate basis set superposition error (BSSE).

II.1.b Derivation of Intertrimer Metrics.

It was determined that the important interactions in the $\{[MPz]_3\}_2$ dimer-of-trimers systems are between the M_3 triangular metal cores. Therefore, a set of geometrical parameters defining the pertinent metrics of adjacent M_3 units was devised.

Each M_3 triangle was used to define a plane and a centroid. The direct distance between the centroids was one metric used to quantify the extent of intertrimer interaction, (Figure 1a). Also used were the perpendicular separation of the planes (Figure 1b), and the horizontal misalignment of the centroids (Figure 1c). Essentially, the latter two measures are the orthogonal projections of a vector from one centroid to the other, perpendicular to the planes and in the planes, respectively. Since in all cases the two trimers remained parallel, there was no ambiguity in selecting which plane to use as the reference. Further, the angle of rotation between two trimers (Figure 1d) was defined as the angle between the two centroid-vertex vectors as if they existed in the same plane and had the same origin. There is some ambiguity in the rotational angle, since the metal cores did not always form equilateral triangles, but the deviation of the measured angle with the choice of centroid-vertex pair was insignificant.

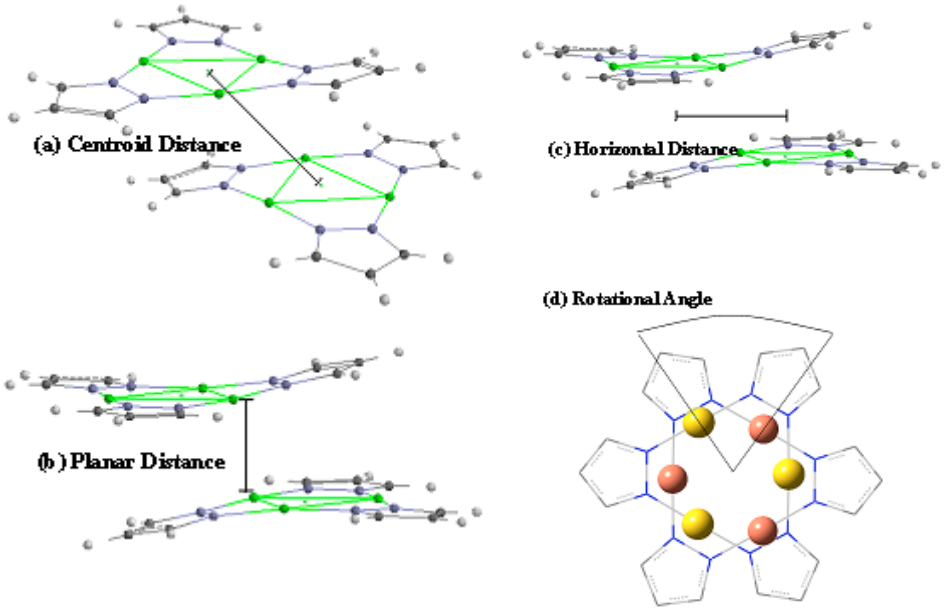

Figure 1: Metrics used to quantify interactions in $\{[MPz]_2\}_3$ dimer-of-trimers.

II.2 Aryl C-H Bond Activation

As in the pyrazolate systems above, all geometries pertinent to the aryl C-H bond activation systems were optimized within the Jaguar[60] program with density functional theory (DFT) using the B3LYP functional.[64] The Stevens effective core potential (ECP) and valence basis set was used,[65] with a *d*-polarization function on heavy main group elements (CSDZ* in Jaguar). Each structure (with exceptions as indicated) was confirmed as a minimum using an energy Hessian calculation. The *tris*-pyrazolyl borate (Tp) ligand was replaced with *tris*-azo borate (Tab), which was shown in previous work[66] to behave similarly in electronic, energetic, and steric impact to the full Tp ligand. Bader's Atoms In Molecules (AIM[67]) analysis was performed in Gaussian 03[68] using B3LYP/3-21G* (one of the largest all-electron basis sets for Ru available through EMSL[69]) with the B3LYP/CSDZ* geometries as optimized in Jaguar. An all-electron basis set is necessary to use the AIM analysis. Natural Population Analysis (NPA)[70] analyses were performed in Jaguar to calculate atomic charges.

II.3 ccCA Reaction Barriers

II.3.a Methods

Composite model chemistries attempt to produce very accurate predictions with reasonable computational costs by computing a series of additive basis set and electron

correlation corrections to a reference energy at a geometry provided by a lower level of theory. While G3 theory specifies the use of (all-electron) MP2/6-31G(d) geometries,[71] the G3B modification uses B3LYP/6-31G(d) geometries.[56] Since the most recent and successful formulation of ccCA uses B3LYP/6-311G(2df,p) geometries,[49b] the current study compares ccCA to G3B for prediction of barrier heights. Two major differences between G3B and ccCA are discussed below. Detailed analyses of G3B and ccCA for the prediction of ground state properties can be found in references 56 and 49, respectively.

While the Gaussian-*n* methods employ Pople-style basis sets for the computation of energies, ccCA attempts to systematically reduce basis set error using the correlation consistent basis sets originally developed by Dunning.[1] In the recommended formulation of ccCA, the reference energy is the result of extrapolating MP2 energies to the complete basis set (CBS) limit.[49] The two variants of ccCA, ccCA-S4 and ccCA-P, differ only in the fit function used in the reference energy extrapolation. The former fits MP2/aug-cc-pV*x*Z (*x* = T, Q) energies to the Schwartz fit function[72] given in equation 1, while the latter is a three-point fit for MP2/aug-cc-pV*x*Z (*x* = D, T, Q) energies to the Peterson equation[73] (equation 2),

$$E = E_0 + B\left(l_{\max} + \frac{1}{2}\right)^{-4} \qquad (1)$$

$$E = E_0 + B\exp\left[-(x-1)\right] + C\exp\left[-(x-1)^2\right] \qquad (2)$$

where l_{max} is the highest angular momentum function in the basis set, x is the cardinal number, E is the fit energy at the aug-cc-pVxZ level, E_0 is the extrapolated energy (*i.e.*, E for x, $l_{max} \rightarrow \infty$), and B and C are fit parameters.

The other significant difference between G3B and ccCA is the use of empirical corrections. G3 theory employs a higher-level correction (HLC) that originally corresponded to a physical quantity, the isogyric correction, in G1 theory.[74] Within subsequent Gn variants, the HLC was generalized to account for deficiencies of the model chemistry in an average way by being parameterized to minimize the magnitude of the mean signed deviation of the overall training set. The only "parameter" in ccCA is the harmonic vibrational scale factor, which is a non-optimized parameter used to account for well-known deficiencies in the harmonic approximation of vibrational frequencies, and not for deficiencies in the model chemistry as a whole. No zero-point energy corrections were used in the current work, so the vibrational scale factor is irrelevant for this specific application. All calculations were performed within the Gaussian 03 suite of programs.[68]

II.3.b Databases

To provide a standard of comparison, as indicated in the introduction, the HTBH38/04 and NHTBH38/04 reaction barrier databases (henceforth HTBH and NHTBH, respectively) compiled by Truhlar *et al.* were used.[75] The HTBH database contains 19 hydrogen transfer reactions with values for the forward and reverse classical barrier heights (*i.e.*, $\Delta E^{\neq}$ exclusive of zero-point corrections). All computed geometries and

energies are publicly available.[ii] The NHTBH database contains 19 reactions, including heavy-atom transfer, bimolecular nucleophilic substitution (S_N2), association, and unimolecular reactions.[75] Most of the barrier heights in NHTBH are derived from Weizmann-1 (W1) theory,[76] though some are derived from its successor (W2h[76]) or literature values from other levels of theory expected to be of at least chemical accuracy.

While it may seem undesirable to benchmark one composite method against another, W1 is designed to obtain the complete basis-set limit of CCSD(T) calculations and is expected to consistently give better than 1 kcal/mol accuracy for barrier heights.[75,iii] Although W1 contains a single fit parameter (the exponent for the valence correlation extrapolation), this parameter is derived from W2 theory rather than experiment. Confidence in the theoretically derived benchmark values is largely based on the known performance of W1 and W2 theories for stable molecules, producing errors on the order of only ±0.24 kcal/mol.[75,iii] A larger error is observed with W*n* theory for systems showing a high degree of nondynamical correlation effects, due to the inherent limits of CCSD(T).[77] The inclusion of higher-level excitations (connected quadruple, pentuple, *etc.*) in W3 and W4 theories was found to yield a better treatment of nondynamical correlation effects.[47b]

---

ii See EPAPS Document No. E-JCPSA6-127-302739 for all the relevant computed geometries and energies. This document can be reached via the EPAPS homepage (http://www.aip.org/pubservs/epaps.html).

iii W2h differs from W2 in that the former employs standard cc-pV*x*Z basis sets for elements in groups I, II, III, and IV rather than aug-cc-pV*x*Z basis sets for all elements. See J. M. L. Martin, and S. Parthiban; in *Quantum Mechanical Prediction of Thermochemical Data*; Ed. Cioslowski, J.; Kluwer: Dordrecht, 2001.

For the purposes of benchmarking, the "best estimate" values provided in the HTBH and NHTBH databases are assumed to be correct. All geometries used in this research were fully optimized and characterized by energy Hessian calculations at the level used for the geometry optimization [B3LYP/6-31G(d) for G3B and B3LYP/6-31G(2df,p) for ccCA] unless otherwise indicated.

CHAPTER III: RESULTS AND DISCUSSION

III.1 Coinage Metal Pyrazolates

III.1.a Cuprophilicity in the S_0 Ground State of $[(CuPz)_3]_2$

Metallophilicity is an attractive interaction between a pair of d^{10} atoms that is a result of long-range dispersion forces.[9-13] There has been some debate regarding the role of cuprophilicity versus electrostatic interaction and ligand assistance in binding Cu^I dimers in general,[12,13] though the specific case of intertrimer interactions in trinuclear Cu^I pyrazolates was suspected to be due to a genuine cuprophilic interaction.[4b,13] With multiple d^{10} atoms in close contact, metallophilicity may reasonably be expected to play an important role in understanding the dimer-of-trimers interactions in the singlet ground state of $\{[CuPz]_3\}_2$. Because metallophilicity is widely attributed to dynamic electron correlation,[9,10] it should be possible to separate cuprophilicity from electrostatic interactions by comparing the dimerization potential of the dimer-of-trimers calculated at the Hartree-Fock level with the potential using a correlated method (*e.g.*, local MP2, LMP2). This procedure was used by Pyykkö to investigate the attraction of Au^I ions in linear complexes.[9] The basis set superposition error (BSSE[63]) for the dimer-of-trimers is expected to be relatively large when calculating the dimerization energy, so the appropriate counterpoise calculations were performed to correct for this. Since LMP2 is designed to minimize BSSE and the counterpoise correction used with LMP2 has been found to overestimate BSSE,[78] only the HF calculations use the counterpoise correction.

The geometries for these single-point calculations came from optimization at the B3LYP/CSDZ* level.

Computational results are presented analyzing cuprophilicity in the $\{[CuPz]_3\}_2$ dimer-of-trimer, which models experimental systems that have led to short intertrimer Cu···Cu contacts according to the available crystallographic data. For example, $\{[3,5\text{-}(Me)_2Pz]Cu\}_3$,[4b,79] $\{[3,5\text{-}(i\text{-}Pr)_2Pz]Cu\}_3$,[4b,80] and $\{[2\text{-}(3\text{-}Pz)Py]Cu\}_3$[81] have shortest Cu···Cu intertrimer distances in the range 2.9-3.0 Å. The staggered conformation is the lowest-energy conformer at the level of theory used although the chair conformation is more common experimentally, likely due to steric and electronic effects associated with the substituents in the experimental $\{[M(3\text{-}(R),5\text{-}(R')Pz)]_3\}_2$ systems.[4,6,79-81] In the case of the unsubstituted staggered dimer-of-trimer $\{[CuPz]_3\}_2$ model, an HF single-point calculation predicts that the model is not intermolecularly bound in the singlet ground state (ΔE = +4.6 kcal/mol), giving rise to a net repulsion between the two adjacent trimers. However, the LMP2 calculations imply that cuprophilicity compensates for the repulsion and binds the dimer-of-trimers (ΔE = -13.5 kcal/mol). Since metallophilicity is an electron correlation effect, the difference between ROHF and LMP2 calculated energies, which results from dynamic electron correlation, is assumed to be due to cuprophilicity. Hence, the overall cuprophilic stabilization for this system is –18.1 kcal/mol. Pyykkö's MP2 optimization of the $[ClCu^{I}PH_3]_2$ dimer found an interaction potential of -3.07 kcal/mol.[82] While Pyykkö's value is the BSSE-corrected dimerization energy at the MP2 level, rather than the difference between the HF and MP2 energies, a useful comparison can still be made. There are a total of nine possible intertrimer Cu-

Cu pairs, six in the range 3.628 to 3.979 Å and three in the range 4.832 to 5.191 Å. Since cuprophilicity is expected to die off rapidly as a function of distance (approximate r^{-6} dependence), the most significant contributions to overall cuprophilicity will certainly be from the six closest contacts. Thus, counting six closest Cu-Cu intertrimer pairs, the cuprophilic stabilization is roughly equivalent to –3 kcal/mol per pair.

The comparison of the ROHF and LMP2 results shows that the dimer-of-trimers is bound by cuprophilicity rather than electrostatic attraction in its singlet ground state. The soft translational potential energy surface (PES) for these systems[3] is consistent with the weakness of metallophilic interactions and thus further strengthens the case for a substantial contribution to intertrimer bonding by cuprophilicity in the trimeric copper pyrazolate systems. It is amazing that the calculated average energy of each cuprophilic bond in $\{[CuPz]_3\}_2$ is similar to that in the simple dimeric model $[ClCu^{I}PH_3]_2$ despite the much longer Cu···Cu separations observed in the former (*vide supra*) than in the latter staggered dimer (3.137 Å). Furthermore, the total cuprophilic stabilization of –18.1 kcal/mol for $\{[CuPz]_3\}_2$ is drastically greater than the estimate given by Poblet and Bénard of -6 kcal/mol for the analogous $\{[CuL]_3\}_2$ model with L = 2-[3(5)-pyrazolyl]pyridine.[13,iv] We attribute these to a rather significant cooperativity of the cuprophilic bonding in $\{[CuPz]_3\}_2$. Precedents of cooperativity in metallophilic systems

iv The estimation in reference 13 was not based on quantum mechanical calculations for the dimer-of-trimer model. It was made simply by assigning a stabilization value for each intertrimer distance in the crystal structure of $\{[CuL]_3\}_2$ based on half the stabilization value inferred from Pyykkö's PES for $[ClCu^{I}PH_3]_2$.

have been reported for simple Hg_n linear clusters,[83] $[Au(CN)_2^-]_n$ and $[Au(CN)_2^-]_n$ oligomeric complexes,[84] and gold thiolate catenane systems.[9]

III.1.b Excimeric Bonding in the T_1 Excited State

The geometries of chair and staggered conformations of the $[(CuPz)_3]_2$ model were optimized using B3LYP/CSDZ* for both the lowest triplet excited state (T_1) responsible for phosphorescence and the singlet ground state (S_0). Figure 2 shows the frontier orbitals and optimized geometries for both S_0 and T_1 of the C_i staggered $[(CuPz)_3]_2$ model, which gave lower energy than the chair in the S_0 state. There are two doubly-degenerate highest occupied Kohn-Sham orbitals (HOKSOs) and a non-degenerate lowest unoccupied Kohn-Sham orbital (LUKSO) for the S_0 ground state (Figure 2).[v] In the phosphorescent T_1 state, on the other hand, the singly occupied Kohn-Sham orbitals (SOKSOs) are non-degenerate. Consistent with the singlet LUKSO, the upper SOKSO of T_1 shows increased intertrimer bonding. Upon absorption of a photon, an electron from the non-bonding HOKSO is promoted to the LUKSO; that the LUKSO of S_0 corresponds to the upper SOKSO of the non-optimized T_1 Franck-Condon excited state populated by the vertical electronic excitation transition has been confirmed by inspection of the relevant orbitals. Since the LUKSO of the S_0 state of $\{[CuPz]_3\}_2$ has an intertrimer Cu···Cu bonding character, a contraction of the separation between the trimer units is expected, and is indeed observed as shown in the calculated

v Kohn-Sham orbitals, *e.g.*, frontier orbitals HOKSO, LUKSO, and SOKSOs, are the DFT equivalent of molecular orbitals and may be similarly interpreted.

structure of the T_1 state upon which the contours of the SOKSOs are plotted in Figure 2. The planar distance (Figure 1b) exhibits a huge contraction, from 3.22 Å in S_0 to 2.50 Å in T_1 of $\{[CuPz]_3\}_2$! Even with the decreased planar distance, the Cu_3 cores of each monomer-of-trimer unit remain in parallel planes. In contrast, the pyrazolate ligands "ruffle" out of the plane described by the metal triangles for the triplet excited state.

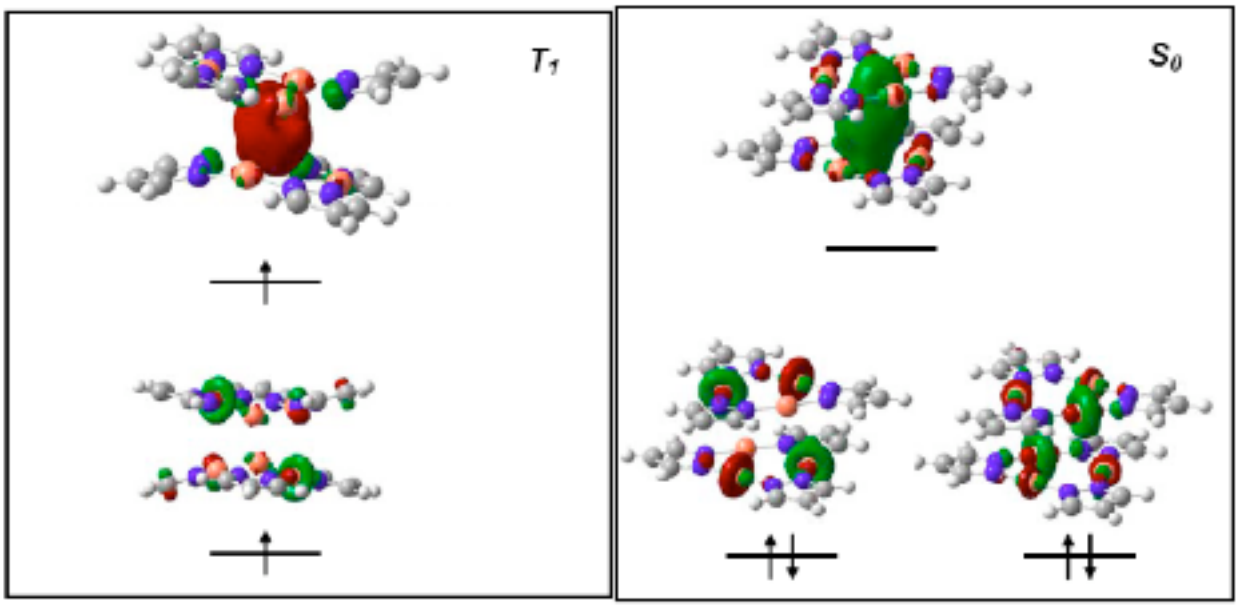

Figure 2: Contours of the frontier orbitals for the optimized S_0 and T_1 states of $\{[CuPz]_3\}_2$.

Since the HOKSO of the S_0 ground state of $\{[CuPz]_3\}_2$ is doubly-degenerate, Figure 2, the vertical excitation process is expected to attain Jahn-Teller instability within D_{3h}. To lower the degeneracy, the D_{3h} symmetry (an equilateral triangle) of the Cu_3 core can be reduced to C_{2v} (an isosceles triangle) or C_s (a scalene triangle).[85] In the S_0 form, both units within the dimer-of-trimer have D_{3h} symmetry individually, so all

intratrimer Cu-Cu bond lengths are equal. The Cu-Cu bond lengths in the optimized T_1 form of the $\{[CuPz]_3\}_2$ species studied are detailed below, Table 1, which also shows the bond lengths in the corresponding optimized S_0 form for comparison. The T_1 symmetry listed is the overall symmetry of the dimer-of-trimer. In order to better understand the effect of dimerization of $[CuPz]_3$ units, Table 1 and Figure 3 show the results for an isolated $[CuPz]_3$ monomer-of-trimer, which is also subject to photoinduced Jahn-Teller distortion.

Table 1: B3LYP/CSDZ* Optimized Intratrimer Cu-Cu Distances for $\{[CuPz]_3\}_2$ and $[CuPz]_3$ Models

	Bond Length (Å)				
Model	T_1		S_0		T_1 Symm.
$\{[CuPz]_3\}_2$, Chair	3.373	3.163	3.075	3.319	C_i
$\{[CuPz]_3\}_2$, Staggered	3.222	3.222	2.978	3.308	C_i
$\{[CuPz]_3\}_2$, Staggered[a]	3.283, 3.237	3.123, 3.143	3.019, 3.085	Not found	C_1
$[CuPz]_3$	3.165	2.489	2.489	3.329	C_{2v}

[a]Two sets of bond lengths are given, as symmetry did not constrain the $[CuPz]_3$ units to the same dimensions.

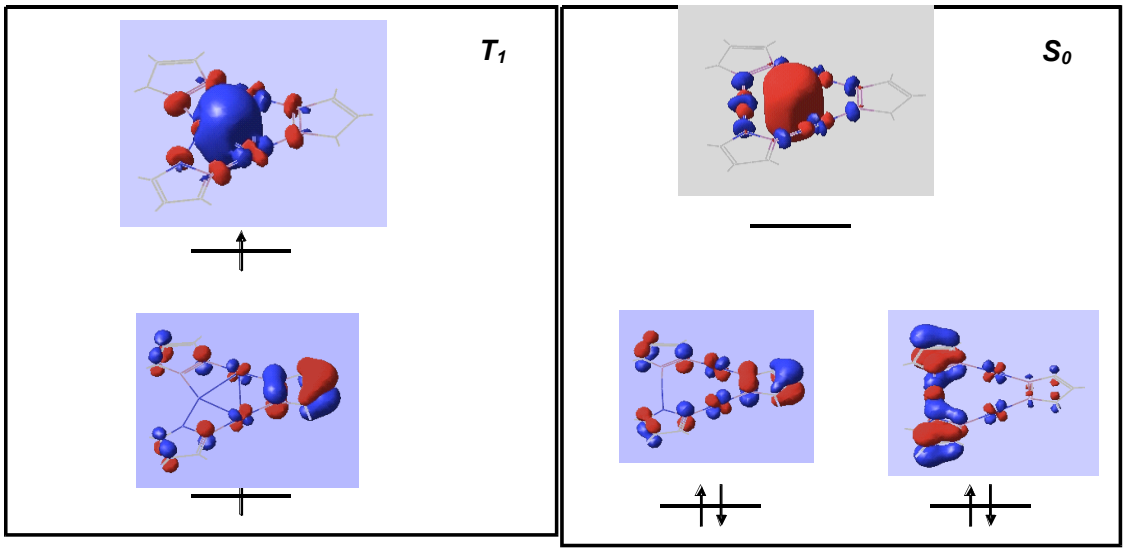

Figure 3: Contours of the frontier orbitals for the optimized S_0 and T_1 states of $[CuPz]_3$.

Not all the models show the same Jahn-Teller distortion. The isolated monomer-of-trimer triplet exciton (Figure 3) has two of the bonds shorten to 2.489 Å (Table 1), suggesting *bona fide* covalent Cu-Cu bonds. This is considerably more than the contraction of the third bond to 3.165 Å. Thus, the T_1 structure of isolated $[CuPz]_3$ represents an isosceles triangle with two short sides and a long side (Table 1). On the other hand, the staggered symmetric structure of $\{[CuPz]_3\}_2$ is calculated to undergo a photoinduced Jahn-Teller distortion to a C_{2v} symmetry by shortening one bond much more than the other two, forming a long-long-short isosceles. The chair and non-symmetric staggered structures show distortions to C_s geometries, forming scalene triangles.

Figure 4, Figure 5, and Figure 6 show the calculated optimized structures of the three $\{[CuPz]_3\}_2$ conformations represented in Table 1. Note that the T_1 state of each model has the shortest Cu-Cu distance as an intertrimer as opposed to an intratrimer

interaction. All S_0 models undergo molecular rearrangement upon photoexcitation, amounting to increased clustering of the Cu_6 unit in the T_1 state. In all cases, the spin density for the triplet states is located primarily on the copper atoms and is not limited to two Cu atoms, suggesting that cooperativity is also valid for excimeric Cu-Cu bonding. Although the Cu-Cu bonding is enhanced in the T_1 state, the situation herein is different from that in a simple $*[Cu^+]_2$ excimer such as that encountered by Zink and co-workers in doped β-alumina matrices.[86] While the latter excimer can be described by a conventional two-center/two-electron bond, the data herein for $\{[CuPz]_3\}_2$ and even $[CuPz]_3$ clearly indicate delocalized excimeric bonding across multiple Cu centers. Delocalized M-M excimeric bonding has been suggested upon one-photon absorption in other systems containing more than two adjacent transition metal atoms with a closed-shell ground state such as Hg_n atomic clusters[83] as well as clusters of other ligand-containing complexes.[87-89]

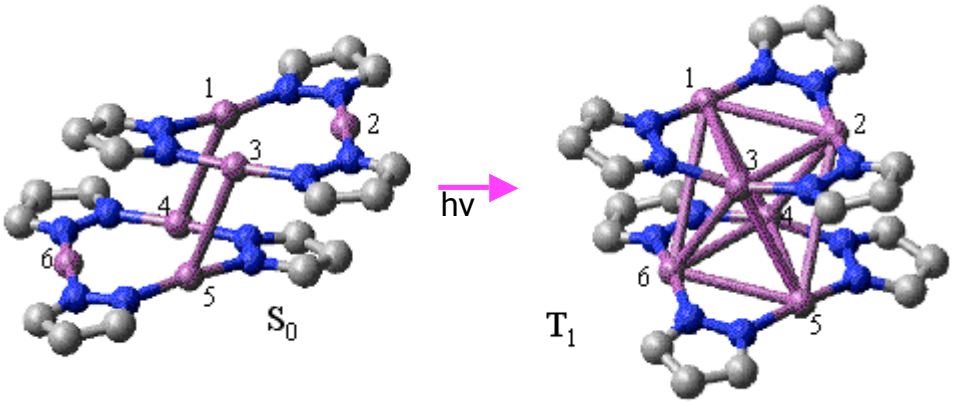

Figure 4: Optimized geometries of the S_0 and T_1 states of the chair conformation of $\{[CuPz]_3\}_2$. Cu-Cu distances (Å), S_0: 1-2=5-6= 3.315, 2-3=4-6= 3.325, 1-3=4-5= 3.316, 1-4=3-5=3.231; T_1: 1-2=5-6= 3.373, 2-3=4-6=3.075, 1-3=4-

5=3.163, 1-4=3-5=3.273, 2-4=3-6=2.885, 1-6=2-5=4.383, 3-4=2.813 (shortest intertrimer contact). Average (Cu-N, C-N, C-C) distances (Å), S_0: (1.904, 1.347, 1.395); T_1: (1.949, 1.348, 1.396).

It is interesting to note that the greatest intratrimer Cu-Cu contraction in the photoexcited dimer-of-trimers is only ~10% whereas the greatest contraction for an isolated monomer-of-trimer is roughly 25%. This underscores that the excimeric bonding is primarily an intertrimer Cu-Cu bonding effect in the T_1 excited state of $\{[CuPz]_3\}_2$ species (Figure 2, Figure 4, Figure 5, and Figure 6). In the absence of intertrimer effects (*e.g.*, in systems that can be described as monomer-of-trimer crystallographically or perhaps in higher excited states than T_1 in dimer-of-trimers in which the excimeric bonding is intratrimer), one would expect that the geometric perturbation should behave more similarly to isolated monomer-of-trimers (Figure 3). In the lowest energy staggered C_1 conformation of the T_1 structure of $\{[CuPz]_3\}_2$, Figure 6, the electronic energy is 3.35 eV higher than the electronic energy of the ground state singlet. The chair (C_i) conformation gives a similar T_e value (3.39 eV). For comparison, T_e for the $[CuPz]_3$ model is 3.48 eV. The transfer of an electron from the non-bonding HOKSO to the bonding LUKSO thus causes a large inter-ring contraction upon excitation to the lowest triplet state (Figure 6). A small intra-ring contraction of 0.17 Å (5%) in the Cu-Cu distances is observed. This is dwarfed, however, by the 0.73 Å (23%) decrease in inter-ring planar separation (Table 2). For comparison, a recent time-resolved X-ray diffraction experiment reported an inter-planar separation contraction of 0.65 Å (from

3.952(1) to 3.33(1) Å) for $\{[Cu(3,5\text{-}CF_3)_2Pz]_3\}_2$ while the intratrimer Cu-Cu separations had negligible contraction.[14] Given the additional steric bulk contributed by the CF_3 substituents on the pyrazolate ring, the experimental results are in excellent agreement with the theoretical analysis presented here.

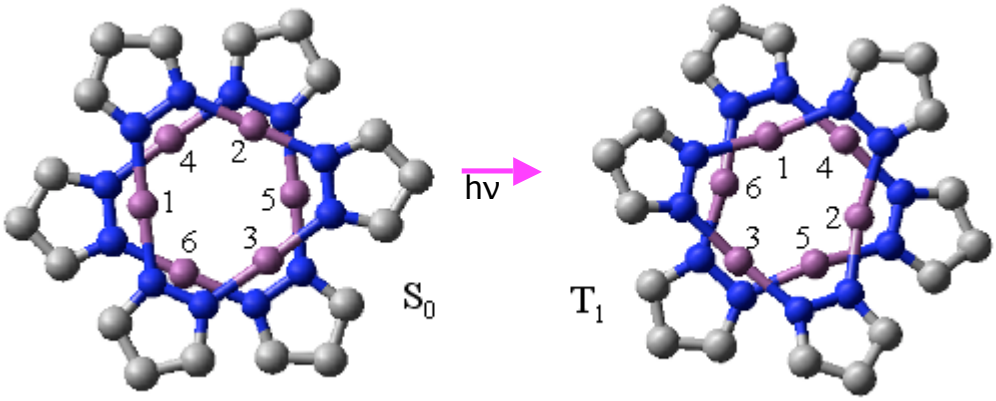

Figure 5: Optimized geometries of the S_0 and T_1 states of the staggered conformation of $\{[CuPz]_3\}_2$. Cu-Cu distances (Å), S_0: 1-2=5-6= 3.317, 2-3=4-6= 3.297, 1-3=4-5= 3.310, 1-4=3-5= 3.628, 2-4=3-6= 3.878, 1-6=2-5= 3.762; T_1: 1-2=5-6= 2.978, 2-3=4-6= 3.222, 1-3=4-5= 3.222, 1-4=3-5= 3.447, 2-4=3-6= 3.447, 1-6=2-5= 2.692 (shortest intertrimer contact). Average (Cu-N, C-N, C-C) distances (Å), S_0: (1.899, 1.346, 1.395); T_1: (1.947, 1.347, 1.396).

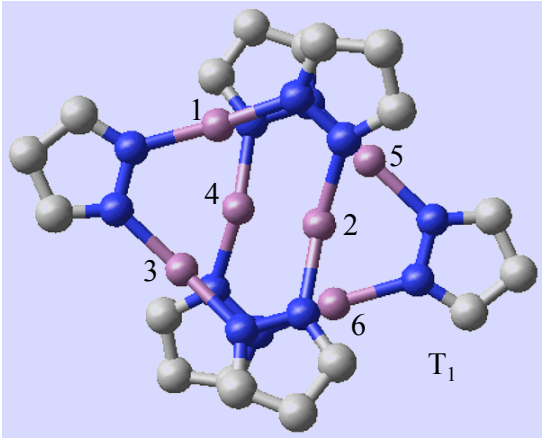

Figure 6: Optimized geometry of the T_1 state of the non-symmetric staggered conformation of $\{[CuPz]_3\}_2$. Cu-Cu distances (Å):1-2= 3.085, 4-5= 3.123, 1-3= 3.237, 4-6= 3.019, 2-3= 3.143, 5-6= 3.283, 1-4= 2.875, 3-4= 2.812, 2-5= 2.812, 2-6= 2.809 (shortest intertrimer contact), 2-4= 2.931. Average (Cu-N, C-N, C-C) distances (Å): (1.952, 1.348, 1.396).

Table 2: Metrics[a] for B3LYP/CSDZ*-optimized Geometries of $\{[MPz]_3\}_2$

Model	Planar Distance (Å)	Horizontal Distance (Å)	Centroid Distance (Å)	Avg. intra M-M dist (Å)
S_0, $[(CuPz)_3]_2$	3.224	0.280	3.236	3.308
T_1, $[(CuPz)_3]_2$	2.497	0.900	2.654	3.141
S_0, $[(AgPz)_3]_2$	3.223	0.708	3.300	3.572
T_1, $[(AgPz)_3]_2$	2.743	1.052	2.938	3.289
S_0, $[(AuPz)_3]_2$	3.595	0.480	3.627	3.560
T_1, $[(AuPz)_3]_2$	2.840	2.987	4.122	3.376

[a] See Figure 1 for a description of the various metrics.

III.1.c Role of the Coinage Metal in Excited State Distortions

Pyrazolate trimers of the entire coinage metal series display interesting chemical and photophysical properties,[3] and thus a computational study of possible excited state

distortions in $\{[AgPz]_3\}_2$ and $\{[AuPz]_3\}_2$ was initiated. Table 2 gives the salient features of the geometries of $\{[MPz]_3\}_2$ (M = Cu, Ag, Au) in both the S_0 and T_1 states. All of these structures are stationary points located using B3LYP/CSDZ* methods starting from a staggered conformation; this conformation was selected because it represents the lowest-energy dimer-of-trimer S_0 form of $[(CuPz)_3]_2$ and was thus assumed to be the same for the Ag and Au analogues. DFT calculations indicate the potential energy surface for the translation between the staggered conformation and the chair conformation is very soft (quantified by the horizontal misalignment, Figure 1c) and thus there are minimal relevant differences between the optimized structures produced from different starting geometries. The rotation angle (Figure 1d) between the monomer-of-trimers is always within 3º of the staggered conformation according to these DFT calculations.

The search reported herein of the CSD[15] shows that calculated intertrimer and intratrimer M···M distances are comparable with known coinage metal-pyrazolate complexes. Thirty coinage metal pyrazolate trimers, with differing pyrazolate substituents, were located to measure intratrimer distances (6 Cu, 2 Ag, 22 Au) and seventeen structures were located to measure intertrimer metal-metal distances (4 Cu, 13 Au). A summary of the experimental structural data is given in Table 3. Comparing the calculated geometries for the singlet structures of $\{[MPz]_3\}_2$ in Table 2 with the experimental data (Table 3) shows the calculated intertrimer and intratrimer M···M distances are well in line with what is expected for these systems.

Table 3: Experimental[15] Structural Data for Coinage Metal Pyrazolate Trimers

Metal	Intratrimer M···M distance (Å)			Intertrimer Plane separation (Å)		
	Avg.	Min	Max	Avg.	Min	Max
Cu	3.24	3.16	3.41	3.82	3.70	4.14
Ag	3.43	3.30	3.49	N/A	N/A	N/A
Au	3.36	3.26	3.43	4.12	3.49	4.85

The calculated horizontal distance (Figure 1c) in the singlet state (Table 2) follows the same order as the van der Waals radii:[90] Cu (1.40 Å) < Au (1.66 Å) < Ag (1.72 Å). This is also the same trend as that displayed by the intratrimer M···M bond lengths for the different metals according to the CSD search (Table 3). However, the trend is broken in the triplet state of $\{[MPz]_3\}_2$, for which the horizontal distances are Cu (0.9 Å) ≈ Ag (1.0 Å) << Au (3.0 Å). Examination of the upper SOKSO for $\{[CuPz]_3\}_2$ (Figure 2) and its Ag congener (Figure 7) indicates bonding in the triplet excited state that is distributed over all six metal ions. However, the upper SOKSO for $\{[AuPz]_3\}_2$ (Figure 7) shows significant bonding between two Au-Au pairs rather than the delocalized interaction found in the Cu and Ag derivatives.

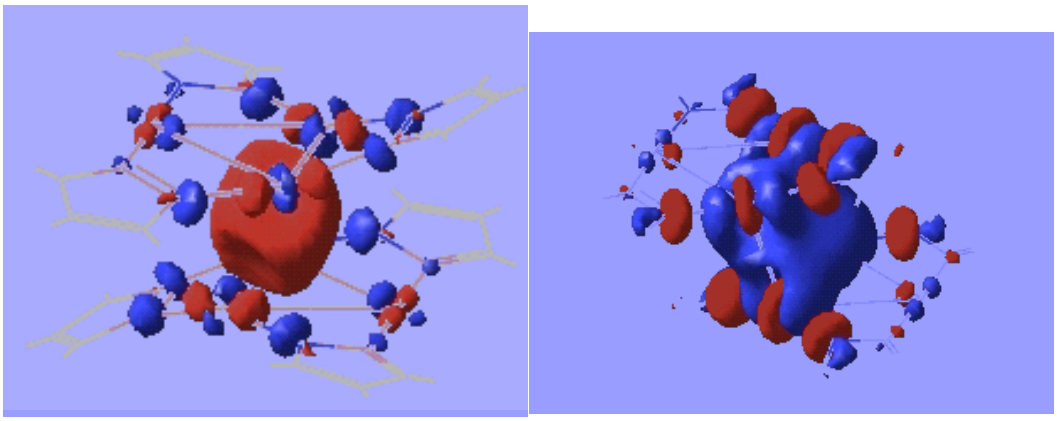

Figure 7: The higher SOKSO of the optimized T_1 state of $\{[AgPz]_3\}_2$ (left) and $\{[AuPz]_3\}_2$ (right).

The CSD data (Table 3) show a large variation in intertrimer distances and a smaller variation in the intratrimer distances. The intratrimer M-M bond distances vary by 0.25, 0.19, and 0.17 Å for Cu, Ag, and Au, respectively. The intratrimer metal-metal distances can be compared to the intertrimer variation of 0.44 Å in the copper-pyrazolate trimers compounds and a massive 1.36 Å in the gold compounds, Table 3. Given the structural diversity of the substituted pyrazolate ligands considered, this seems to be a good indication of the practicability of tuning the inter-trimer distance using different ligands, and hence the resultant emission wavelengths for the coinage metal pyrazolates (*vide infra*).

The most compelling finding derived from these computations on the triplet emissive state is the observation that contraction of the intertrimer M···M spacing in $\{[MPz]_3\}_2$ upon excitation is much greater than the contraction of the intratrimer M···M distances. The intertrimer contraction in the planar separation is 23%, 15%, and 21%

for Cu, Ag, and Au, respectively, giving an average contraction of 20% (Table 2). Within each monomer-of-trimer subunit, the contraction of the intratrimer M···M bond distance is 5% for Cu and Au, and 8% for Ag, giving an average of only 6%.

III.1.d Calculated Photophysical Properties

One of the interesting experimental features of these pyrazolate complexes is their large Stokes' shifts,[3] which implies significant excited state geometric distortion. DFT calculations above verified the geometric distortion, and so this section reports the calculated photophysical properties. Table 4 summarizes the $S_0 \rightarrow T_1$ excitation (λ_{exc}) and $T_1 \rightarrow S_0$ phosphorescent emission (λ_{em}) wavelengths calculated for the vertical transitions.

Table 4: DFT Calculated Photophysical Parameters for Coinage Metal Pyrazolate Systems

Complex	λ_{exc} (nm)	λ_{em} (nm)	Stokes' shift ($10^3 cm^{-1}$)
$[CuPz]_3$	256	401	14.1
$\{[CuPz]_3\}_2$	292	450	16.7
$[AgPz]_3$	262	452	16.0
$\{[AgPz]_3\}_2$	328	455	8.4
$[AuPz]_3$	237	321	11.0
$\{[AuPz]_3\}_2$	240	349	13.0
$[Cu(3\text{-}CF_3)Pz]_3$	277	403	11.3
$\{[Cu(3\text{-}CF_3)Pz]_3\}_2$	268	428	13.9
$[Cu(3,5\text{-}CF_3)_2Pz]_3$	[a]	498	[a]
$[Ag(3,5\text{-}CF_3)_2Pz]_3$	248	475	19.3
$[Au(3,5\text{-}CF_3)_2Pz]_3$	320	574	13.9

[a]The vertical excitation energy for this complex could not be computed due to SCF convergence failure.

Several observations are of interest with respect to the calculated photophysical properties. First, the calculated Stokes' shifts of the coinage metal pyrazolate monomer-of-trimers and dimer-of-trimers lie in the range of 8-20 × 10^3 cm^{-1}, similar to experimental values[3,4,6] and consistent with the drastic enhancement in the M-M bonding upon photon absorption for all monomer-of-trimer and dimer-of-trimer models as discussed above. Second, among the unsubstituted $[MPz]_3$ theoretical models, the Cu and Ag complexes are calculated to exhibit much more significant red shifts upon dimerization compared to the analogous gold complex in terms of both the excitation and phosphorescence energy; the latter energy shifts to the visible region for the Cu and Ag dimer-of-trimers but remains in the UV region for $\{[AuPz]_3\}_2$. It is somewhat surprising that dimerization of $[AgPz]_3$ does not significantly affect the emission energy while the excitation energy red-shifts by 7680 cm^{-1}. Both the excitation and emission energies are computed to be red-shifted significantly (by 4820 and 2720 cm^{-1}, respectively) upon dimerization of the unsubstituted copper complex. Third and more importantly, computed photophysical parameters are provided for the practical models with substituted pyrazolates, thus permitting direct comparison with experiment and/or facilitating the often-difficult assignment of the excitation and emission bands seen for the experimental systems.[3,4,6] The visible emissions in all CF_3-substituted models computed (Table 4) are consistent with experimental studies that gave rise to multiple visible phosphorescence bands attributed to different excited states of monomer-of-trimer and dimer-of-trimer excitons.[3,4] Basis set and method limitations, however,

preclude a quantitative comparison with the experimental systems. For example, the calculated $^1S \rightarrow {}^3D$ vertical excitation energies of the atomic systems Cu^+, Ag^+, and Au^+ using B3LYP/CSDZ* are higher than the state-weighted experimental[91] values by 6390, 4690, and 5520 cm^{-1}, respectively. Similar deviations are found in the literature for the $^1S \rightarrow {}^3P$ excitation energy of the mercury atom when similar methodologies are used.[83] Nevertheless, useful trends can be extracted from the computed photophysical energies herein. For example, among the monomer-of-trimers models in Table 4, the Cu and Au complexes are computed to undergo red shifts in the excitation energies with CF_3 substitution by 1600 and 10420 cm^{-1} for $[Cu(3\text{-}CF_3)Pz]_3$ and $[Au(3,5\text{-}CF_3)_2Pz]_3$, respectively, relative to the corresponding unsubstituted analogues. The red shift upon CF_3-substitution of the Au trimer is rather substantial even from a qualitative perspective. Contrary to the Cu and Au models, the vertical excitation wavelength is computed to undergo a substantial *blue shift* by 9930 cm^{-1} for $[Ag(3,5\text{-}CF_3)_2Pz]_3$ in comparison with $[AgPz]_3$. With these trends, it appears that, overall, the Cu and Au complexes behave similarly, whereas the trends are reversed for Ag complexes. However, the phosphorescence energy upon disubstitution in $[M(3,5\text{-}CF_3)_2Pz]_3$ models (M = Cu, Ag, Au) is computed to be red-shifted with respect to the corresponding unsubstituted analogues. Even then, the Cu and Au complexes are far more red-shifted (by 4860 and 13730 cm^{-1}, respectively) than the Ag complex (1070 cm^{-1}). These results are consistent with the available experimental data for $[M(3,5\text{-}CF_3)_2Pz]_3$ crystalline solids, in which the lowest-energy phosphorescence energy is significantly higher for the Ag trimer compared to the Cu and Au analogues,[3] especially given the

aforementioned result that the unsubstituted Ag trimer is computed to exhibit much lower sensitivity to dimerization than the Cu and Au analogues.

III.2 Aryl C-H Bond Activation

III.2.a Structure and Bonding Considerations

Previously reported evidence indicates that complexes of the type $TpRu(PMe_3)_2X$ (X = OH or NHPh; Tp = hydrido-*tris*(pyrazolyl)borate) initiate the 1,2-addition of aromatic C-H bonds across the Ru-X bond.[30b,c] Experimental and computational studies suggest that the transformations proceed via initial dissociation of PMe_3 and coordination of benzene to form $TpRu(PMe_3)$(benzene)X complexes, followed by C-H activation via 1,2-addition. Computational studies incorporated the smaller ligand models Tab (*tris*(azo)borate) and PH_3 in place of Tp and PMe_3, respectively. The proposed reaction pathway is depicted in Scheme 4.

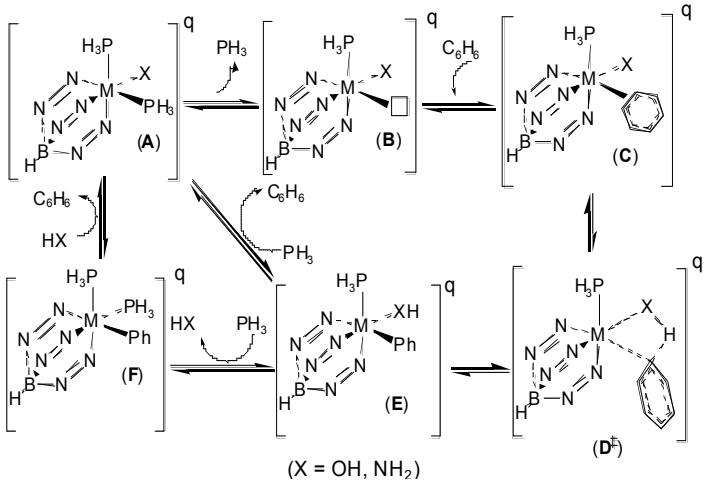

Scheme 4. Proposed reaction pathway for the 1,2-addition of benzene across M-X bonds studied by DFT calculations.

The following extends computational studies of the overall benzene C-H activation shown in Scheme 4 to a series of octahedral d^6 complexes in which the identity of the metal and ligand X are varied: $[(Tab)M(PH_3)_2X]^q$ (X = OH or NH_2; M = Tc or Re, q = -1; M = Ru, q = 0; M = Co or Ir, q = +1; M = Ni or Pt, q = +2). Since Tab is a tridentate, six-electron donor ligand, complexes **A**, **C**, **E**, and **F** are formally 18-electron, six-coordinate, and octahedral (Scheme 4). Species **B**, $[(Tab)M(PH_3)X]^q$, is formally a 16-electron, five-coordinate complex. However, the π-donation capability of X can render the active species (**B**) closer to 18-electron, as judged by the planar coordination mode at the nitrogen (when X = NH_2) of the amido ligand in these complexes (see below).[vi] All coordination geometries of optimized minima for complexes **A**, **E** and **F** are as expected, and the DFT calculations present no surprises in this regard. However, structures **C** and $\mathbf{D}^{\ddagger}$, the benzene adduct and the C-H activation transition state, respectively, vary among the complexes. More detailed analysis of these systems is given below.

III.2.b Benzene Adduct Geometries

For the overall C-H activation of benzene, the arene adducts (**C** in Scheme 4) can impact not only the rate of the overall reaction, but also enhance the Arrhenius prefactor. The benzene adducts in the proposed pathway for C-H activation serve to

---

vi For all metals, in **A** the amido ligand is pyramidal, suggesting σ-only donation. In the active species **B**, however, the amido ligand is planar, allowing two-electron π-donation to satisfy the 18-electron rule.

align the substrate arene with the activating ligand X, preparing the complex for carbon-hydrogen bond activation. The pertinent complexes shall be designated briefly as $[M\text{-}X]^q$ to indicate the specific metal (M), activating ligand (X) and overall charge of the complex (q).

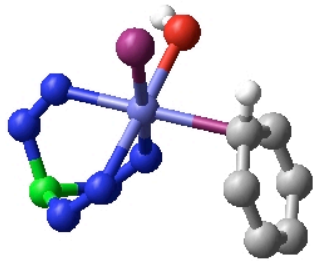

Figure 8. The calculated benzene adduct $[(Tab)Pt(PH_3)(benzene)OH]^{2+}$. All hydrogen atoms are omitted for clarity, except the hydroxo hydrogen and the hydrogen attached to the ligated carbon of benzene.

Benzene adducts were found for $[Ir\text{-}OH]^+$, $[Ni\text{-}OH]^{2+}$, $[Pt\text{-}OH]^{2+}$, $[Ni\text{-}NH_2]^{2+}$, and $[Pt\text{-}NH_2]^{2+}$ complexes with a representative structure shown in Figure 8 for $[(Tab)Pt(PH_3)(benzene)OH]^{2+}$. In contrast, related benzene adducts were not located for $[Tc\text{-}OH]^-$, $[Re\text{-}OH]^-$, [Ru-OH], $[Co\text{-}OH]^+$, $[Tc\text{-}NH_2]^-$, $[Re\text{-}NH_2]^-$, [Ru-NH_2], $[Co\text{-}NH_2]^+$ or $[Ir\text{-}NH_2]^+$. With the interaction of the benzene adducts occurring to a single carbon, the calculated adducts structurally resemble intermediates expected in electrophilic aromatic substitution (EAS). In the classical EAS mechanism, an electrophile attacks a carbon of the arene ring to form an arenium intermediate, and subsequent intermolecular deprotonation restores aromaticity to yield the substituted aromatic product. In the present EAS analogy, the base for metal-mediated C-H activation is the

ligand X, which serves as an intramolecular base.[vii] Since this mechanism is not expected to be restricted to aromatic substrates, the present mechanism may more properly be understood to be an example of internal electrophilic substitution (IES), in agreement with similar work by Oxgaard, Periana, Goddard *et al*.[45] This is similar in some respects to proposed C-H activation via electrophilic substitution by late transition metal complexes (with the exception that the proton transfer is generally considered an intermolecular reaction).[24]

Note that unlike previous computational studies[30b,c] of (Tab)Ru(PH_3)OH, an η^2-*C,C*- bound benzene adduct was not isolated in the present research, which may be a reflection of a slight downsizing of the Ru basis set (CSDZ* is valence double-zeta; previous simulations employed the full triple-zeta contraction for the Stevens' valence basis sets[65c]) or, more likely, the inherent weakness of the metal-benzene interaction in neutral complexes of this type. In a previous study of benzene C-H activation by full TpRu(L)R complexes (L = CO, PR_3 or CNH; R = alkyl or aryl),[92] it was observed that while benzene binding was weakly exothermic, an unfavorable entropic contribution rendered this event endergonic. Thus, consistent with the current calculation, the previous calculations of TpRu-methyl complexes suggest relatively weak benzene coordination. In addition, the previous studies revealed that the details of the metal-benzene interaction are subtle. For example, while benzene bonding modes in

---

vii Even for cationic complexes, benzene adducts **C** are not as strongly bound as, for example, a quintessential EAS intermediate such as protonated benzene (B3LYP/6-311++G(d,p) geometry optimization), which has a very long "Bz CC" (1.47 Å) and large "Bz C-H oop" (30°). See Table 1 for a discussion of these metrics, and comparable $[M\text{-}X]^{q+}$ values.

TpRu(Ph)(CO)(benzene) and TpRu(Ph)(CNH)(benzene) were calculated to be η^2-*C,C*, the related complex TpRu(Ph)(PMe_3)(benzene) showed η^2-*C,H* bonding of the benzene, which is quite similar to the adducts calculated herein, due to steric reasons.[92] Thus, given the previous subtlety of benzene coordination mode for TpRu(L)R systems, it is not surprising that coordination of benzene by [(Tab)M(PH_3)X]^q is highly dependent on M and X.

Table 5 presents pertinent geometric data for calculated benzene adducts. Several structural trends as a function of metal and activating ligand are observed. Strongly bound benzene adducts only occur for cationic complexes, *e.g.,* [Ni-OH]$^{2+}$, [Pt-OH]$^{2+}$ and [Ir-OH]$^{+}$ among the hydroxo complexes, and [Pt-NH_2]$^{2+}$ among the amido complexes. As expected for electrophilic addition to benzene, dicationic Group 10 metal complexes show structural evidence of stronger benzene binding as compared to cationic Group 9 species (*e.g.*, compare benzene adducts of [Ir-OH]$^{+}$ and [Pt-OH]$^{2+}$, Table 5). The structural assessments are made primarily on the basis of the long metal-carbon(benzene) bond distances found in the congeners containing earlier (neutral or anionic) transition metal complexes, which substantially shortens for the later (cationic) complexes. Other structural indicators of greater benzene/complex interaction and activation for cationic complexes include longer C-C bond lengths for the benzene bond closest to the metal, and pyramidalization of the carbon in the proximal C-H bond (Figure 8). Such changes as a function of overall charge are expected, and partly reflect the lack of solvent effects in the modeling. What is perhaps more unexpected and interesting is the role of metal (M) for a given molecular charge. Benzene binding is

stronger for heavier congener within a triad (*e.g.*, compare benzene adducts of [Co-OH]$^+$ versus [Ir-OH]$^+$ or [Ni-NH_2]$^{2+}$ versus [Pt- NH_2]$^{2+}$, Table 5).

Table 5. Representative Geometric Data for Calculated Benzene Adducts [(Tab)M(PH_3)(benzene)X]^{q} [a]

(Tab)M(PH_3)(benzene)OH

Metal	MC_1 (Å)	MC_2 (Å)	Bz CC (Å)	Bz C-H oop (°)
Tc	4.41	4.37	1.40	0.3
Re	4.41	4.44	1.40	0.5
Ru	3.95	4.23	1.40	1.5
Co	3.07	3.30	1.40	4.5
Ir	2.59	3.02	1.42	14.8
Ni	2.42	3.03	1.43	17.7
Pt	2.40	3.09	1.44	27.6

(Tab)M(PH_3)(benzene)NH_2

Metal	MC_1 (Å)	MC_2 (Å)	Bz CC (Å)	Bz C-H oop (°)
Tc	4.26	4.39	1.40	0.1
Re	4.56	4.95	1.40	0.0
Ru	5.14	5.18	1.40	0.5
Co	4.59	4.76	1.40	3.0
Ir	4.69	4.97	1.40	2.3
Ni[b]	2.61	3.13	1.42	14.1
Pt	2.49	3.13	1.43	23.6

[a] C_1 and C_2 are the two benzene carbon atoms closest to the metal center. 'Bz C-H oop' is the out-of-plane bending angle of the activated H from the plane of the benzene ring.

[b] A benzene adduct was located for Ni-NH_2 using a different SCF convergence algorithm (iacscf=1 in Jaguar). At the optimized geometry, the usual SCF algorithm reports a small imaginary mode of 13*i* cm^{-1}.

The degree of metal-NH_2 π-interaction in the amido complexes, as well as its response to modification of the complex, is interesting and can be assessed by the "flap" angle of the amido plane (*i.e.*, the H···H-N-M improper dihedral). When the metal-benzene interaction is very weak, the amido flap angle is close to 180°, as it is for Tc, Re, Ru, Co, and Ir amido complexes (179° for each). Figure 9 shows the calculated geometry of species **C** for $[Co\text{-}NH_2]^+$, for which the benzene and Co essentially do not interact. The structural results for some amido complexes thus imply that there is significant π-donation from the amido ligand to the metal center that competes with the coordination of benzene. Alternatively, the enhanced amido-to-metal π-bonding compensates for the lack of metal-benzene bonding. The amido flap angle in those cases in which the amido is not planar is reduced toward the 109.5° value expected for σ-only bonding for $[Ni\text{-}NH_2]^{2+}$, Figure 9, and $[Pt\text{-}NH_2]^{2+}$ (123° and 116°, respectively), implying that coordination of the benzene effectively saturates the metal, thus ameliorating the degree of metal-amido $d\pi$–$p\pi$ interaction. The foregoing comments must be tempered to some degree as planarity of a metal amido ligand may also arise in the limit of a significantly ionic ($L_nM^+NH_2^-$) bonding description.[93]

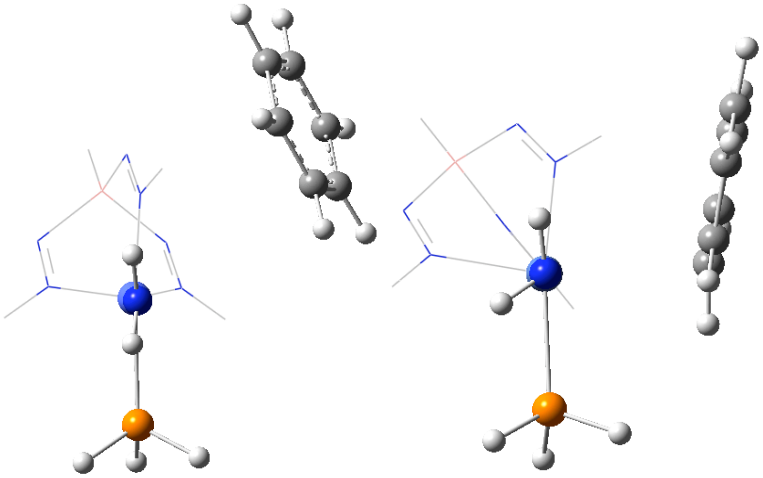

Figure 9. The benzene adducts of $[(Tab)Co(PH_3)(benzene)NH_2]^+$ (left) and $[(Tab)Ni(PH_3)(benzene)NH_2]^{2+}$ (right). The Tab ligand is shown in wireframe for clarity. Pertinent metric data given in Table 5.

Investigation of the electronic structure of benzene adducts (**C** in Scheme 4) reveals an increasing interaction between the metal and benzene as the acidity of the metal increases. The acidity of 16-electron complex **B** was assessed using the LUKSO (lowest unoccupied Kohn-Sham orbital[v]) energy and NPA (Natural Population Analysis) charge on the metal. A lower LUKSO energy and a more positive NPA charge imply a more acidic metal center. Since NH_2^- is a stronger base than OH^- (based on gas-phase proton affinities[94]), the metal center is expected to be less acidic for the amido complexes as compared to the hydroxo complexes, and indeed this is the case. For each hydroxo species **B**, the corresponding amido species is calculated to be less acidic as indicated by the LUKSO energies and NPA charge on the metal, Table 6.

For both the hydroxo and amido systems containing Tc, Re, and Ru, no benzene adducts were found via DFT geometry optimization. The HOKSO (highest occupied

Kohn-Sham orbital[v]) energy of benzene at the level of theory used is -0.246 a.u. Analysis of LUKSO energies in Table 6 indicates that benzene binds only in the limit that $\varepsilon_{LUKSO}([M\text{-}X]^q) < \varepsilon_{HOKSO}$(benzene), supporting the conclusion made above as to the correlation between the acidity of **B** and its ability to form a stable adduct **C**. Caution is needed, however, in interpretation of the present results, as experiments are conducted in condensed media. The overall charge of the complex is an obvious factor in regulating the interaction between the active species **B** and benzene. In the absence of solvation, charge effects will dominate. However, the comparison of NPA and LUKSO data in Table 6 for systems with equivalent charge make it apparent that both M and X can modify the acidity/basicity of **B**, and thus provide evidence for the important electronic role that the metal M and the ligand X play in modifying the overall activity toward C-H bond cleavage.

Table 6. Electronic Properties of 16-electron [(Tab)M(PH_3)(X)][a]

	LUKSO[b] Energy (a.u.)		NPA Charge on metal (e^-)	
Metal	OH	NH_2	OH	NH_2
Tc	0.090	0.098	0.153	0.062
Re	0.086	0.095	0.277	0.195
Ru	-0.082	-0.072	0.330	0.233
Co	-0.283	-0.268	0.705	0.628
Ir	-0.269	-0.253	0.690	0.597
Ni	-0.502	-0.485	0.863	0.831
Pt	-0.477	-0.457	0.907	0.851

[a] Lowest unoccupied Kohn-Sham orbital (LUKSO) energies in atomic units are determined at the calculated minima of [TabM(PH_3)(X)] using the B3LYP/CSDZ* level of theory. NPA = Natural Population Analysis.

[b] For comparison purposes, the highest occupied Kohn-Sham orbital (HOKSO) energy of benzene at the same level of theory is -0.246 au.

III.2.c Transition States for Benzene C-H Activation

As expected from previous studies,[28,30,66] the transition states (TSs) for C-H bond activation of benzene by the M-X bond of $[(Tab)M(PH_3)(benzene)X]^q$ have a four-centered arrangement with a kite-shaped geometry resulting from the obtuse angle about the hydrogen being transferred. The imaginary frequencies in these transition states correspond almost exclusively to C···H and X···H bond forming/breaking via motion of the active hydrogen. The TS structure results in a relatively short metal-hydrogen distance since the M···C and M···X distances in such transition states are typically only marginally longer (~10–20%) than normal covalent bond lengths. A representative example of the calculated transition state for benzene C-H activation by $[(Tab)Pt(PH_3)OH]^{2+}$ is shown in Figure 10. In these transition states the benzene ring is more or less perpendicular to the plane defined by the X···M···C···H ring.

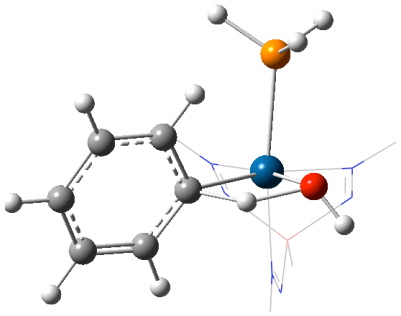

Figure 10. Calculated transition state for C-H activation of benzene by $[(Tab)Pt(PH_3)OH]^{2+}$. Tab ligand is shown in wireframe.

Short M···H distances in SBM transition states have been used in the past as a gauge of metal-hydrogen interaction.[95] For the systems studied herein, the "reduced" M-H distances (calculated by subtracting the sum of the covalent radii[96] of the metal and hydrogen from the M···H distance in transition state $\mathbf{D}^{\ddagger}$) were calculated. A plot of this metric is given in Figure 11, showing the metric as a function of metal and ligand X. In relative terms, the M···H "bond" in the transition states are on average 8% longer than covalent estimates in the hydroxo systems and 12% longer in the amido complexes, which could be taken as an indicator of significant bonding between the metal and the hydrogen of the C-H bond being activated. However, a metric analysis may be too simplistic as there must also be electron density along the internuclear axis.

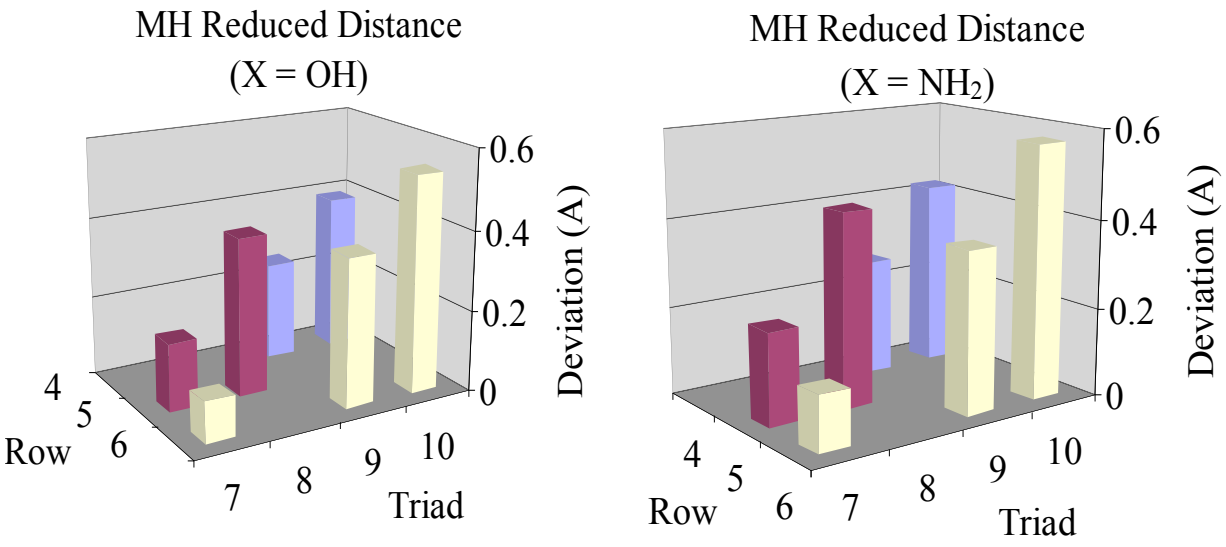

Figure 11. Reduced M-H bond distance (*i.e.*, M...H distance in transition state minus sum of covalent radii of metal and hydrogen) by row and group and by X group.

To analyze the nature of the bonding in the transition state, AIM (Atoms in Molecules[67]) analyses were performed for representative [Ru-OH] and [Ru-NH_2] benzene C-H activation transition states. The AIM technique is a topological analysis of the calculated electronic structure of a molecule, which, among other procedures, searches for critical points (stationary points) in the total electron density. Such critical points are taken to indicate that bonding exists among two or more atoms. The AIM analysis indicates four bond critical points (M···X, X···H, C···H and M···C), thus implying a M···X···H···C four-membered ring, which is confirmed by the identification of a ring critical point in the electron density within the proposed cycle. No bond critical point could be located between the X···C pairs. What is more intriguing is that the AIM analysis does not indicate a bond critical point between the metal and hydrogen in the active site of the transition state. Hence, the bond connectivity in Scheme 5 (right) is

suggested for these transition states. In the limit of a M···H bond, one would also expect two ring critical points for the individual three-membered cycles (Scheme 5, left).

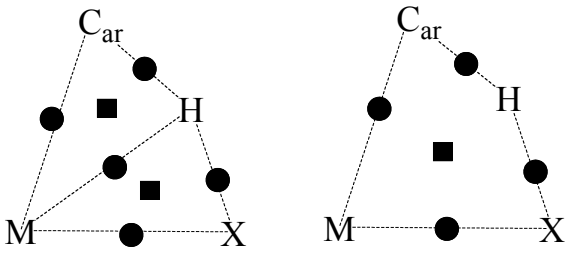

Scheme 5. Two possible depictions from atoms in molecules (AIM) analyses for benzene CH activation transition states. A square indicates a ring critical point; a circle indicates a bond critical point. The AIM analysis is more consistent with the depiction on the right for [Ru-OH] and [Ru-NH_2] transition states.

The OHM description is thus contraindicated for these transition states on the basis of the lack of significant M-H interaction as determined by the AIM analysis. In considering the nature of the transition state for C-H activation, a useful comparison can be made between the SBM transition state indicated by the AIM analysis and IES (see above) mechanism. The major difference between SBM and IES is the participation of the lone pair on the ligand "X" in the C-H activation step. It has been previously suggested that the lone pair plays an important part in activation of dihydrogen and intramolecular C-H activation by (PCP)Ru(CO)NH_2.[43] Scheme 6 provides a comparison of the calculated distances for the four atoms that comprise the active site for benzene C-H activation by (Tab)Ru(PH_3)(C_6H_6)X for X = CH_3,[30c,97] NH_2 and OH.

It is readily apparent from the metric data that the X groups with a lone pair (NH_2 and OH) are quite similar to each other, while the methyl activating ligand is more disparate. Thus, the metric data for the calculated transition states indicate a substantial difference between X = Me and X = OH/NH_2. The origin of this difference is likely the presence of a lone pair on the amido and hydroxo ligands. What is particularly noticeable is the much shorter Ru···H distance in the transition state for X = CH_3. It is herein proposes that the directed sp^3 hybrid of the methyl activating ligand less effectively "bridges" both the transfer hydrogen and the metal, and thus must compromise in binding with each of these moieties. As a result, the Ru-X-H angle is small and the resulting Ru···H distance short. Bercaw *et al.* presented a similar analysis for the preference of H over alkyl for the transfer group in their classic study of SBM by scandium-alkyl complexes.[29] For complexes with amido and hydroxo activating ligands, the presence of available lone pairs makes these ligands more effective at "bridging" M and H, and thus the Ru-X-H angle can expand and Ru···H be longer, as depicted in Scheme 6.

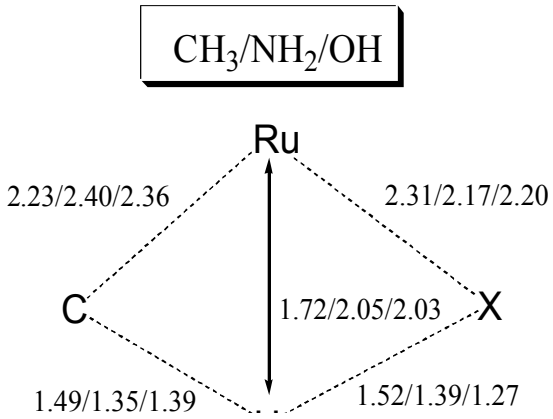

Scheme 6. Calculated metric data for C-H activation of benzene by TabRu(PH_3)(X), where X = CH_3,[97] NH_2 or OH.

Table 7. Early versus Late CH Activation Transition States[a]

	X = OH			X = NH_2		
Metal	Δ(C···H) (%)	Δ(O···H) (%)	TS type	Δ(C···H) (%)	Δ(N···H) (%)	TS type
Tc	27	10	Late	23	19	Late
Re	24	13	Late	21	21	Middle
Ru	22	15	Late	19	23	Middle
Co	19	18	Middle	14	28	Early
Ir	22	18	Middle	13	32	Early
Ni	15	22	Early	12	31	Early
Pt	15	25	Early	11	36	Early

[a] Δ(C···H) and Δ(X···H) is the calculated percent lengthening of the particular bond in the transition state versus typical covalent single bond lengths.

As a measure of the relative position of the transition state on the reaction coordinate (*i.e.*, early versus late transition states), the percent deviations from a typical single C-H and X-H bond length (as determined by the sum of covalent radii) for

both hydroxo and amido ligands are presented in Table 7. Inspection of the data in Table 7 indicates that the transition states are late for structures with electron-rich (anionic) metal centers (*e.g.*, $[Tc\text{-}OH]^-$, $[Re\text{-}OH]^-$ and $[Tc\text{-}NH_2]^-$) and becomes progressively earlier for more acidic (cationic) metal centers. The calculations are consistent with more electron-rich metal centers being more efficient at promoting the donation of electron density into the C-H σ^* orbital, causing a longer (later) C-H bond length in the transition state.[27] The amido transition states are relatively early as compared to their hydroxo congeners, Table 7, which is expected of the more basic amido ligand under the EAS analogy.

Table 8. Comparison of M-X Bond Lengths (Å) between the Active Species, Transition State, and Product[a]

Metal	X	Active Species (**B**)	Transition State ($\mathbf{D}^{\ddagger}$)	Product (**E**)	Percent Completion
Tc	OH	2.03	2.30	2.44	66%
Re	OH	2.00	2.28	2.40	68%
Ru	OH	1.97	2.20	2.30	69%
Co	OH	1.77	1.94	2.06	60%
Ir	OH	1.92	2.15	2.23	75%
Ni	OH	1.76	1.92	2.07	53%
Pt	OH	1.92	2.11	2.25	58%
Tc	NH_2	2.01	2.23	2.31	75%
Re	NH_2	1.99	2.21	2.29	75%
Ru	NH_2	1.95	2.17	2.25	74%
Co	NH_2	1.77	1.95	2.05	66%
Ir	NH_2	1.95	2.12	2.19	70%
Ni	NH_2	1.77	1.95	2.05	63%
Pt	NH_2	1.91	2.11	2.20	69%

[a] Percent completion is the ratio of the transition state bond length to the product bond length, relative to the active species' bond length, *e.g.,* 50% completion

means the transition state bond length is exactly halfway between the active species and product bond lengths.

One might ask why oxidative hydrogen migration was observed as the mechanism in similar systems[29b,30,97,98] but not here. The ligand receiving the transferred hydrogen is an alkyl group in systems showing OHM as a mechanism (*e.g.*, (Tab)Ru(L)(C_6H_6)R), but the current research employs heteroatomic hydroxo and amido as the activating ligands. The most obvious difference between these X groups is the existence of lone pairs on the hydroxo and amido ligands that are missing in the alkyl systems. Indeed, an AIM analysis of the X = CH_3 transition state lacks a four-membered ring critical point and instead indicates true Ru-H(*ipso*) interaction as prescribed by the OHM mechanism. It is reasonable that rather than a metal dπ orbital,[27] perhaps an available lone pair on X is responsible for the donation of electron density to the activated hydrogen.[27] That is, when the ligand X possesses a lone pair, it functions as an intramolecular base, which is consistent with the IES mechanism and highlights a fundamental difference between heteroatom and hydrocarbyl activating ligands. In fact, based on this premise, it is suggested that SBM/IES type C-H activation might be inherently more facile when the "receiving ligand" is anionic and heteroatomic than for hydrocarbyl ligands. Future efforts will address this issue in more detail. To assess the role of the X group using metric data, the M-X bond lengths from the active species (**B**), the transition states ($\mathbf{D}^{\ddagger}$) and products (**E**) are compared. If the donation to σ^*_{CH} is primarily from the ligand, the M-X bond length in the transition state

is expected to more closely resemble the product. Conversely, if the donation to σ^*_{CH} is primarily from the metal center (*i.e.*, substantial M-H interaction), the transition state M-X bond length should be no greater than halfway between the corresponding values calculated for **B** and **E**. In all cases, the M-X bond lengths in the transition states are closest to the product values (Table 8) on average 64% for hydroxo and 70% for amido, a structural indicator of a more significant contribution to C-H bond scission from the ligand than the metal.

These results suggest that the mechanism for C-H activation by $[(Tab)M(PH_3)X]^n$, where X = formally anionic heteroatomic ligand such as hydroxo or amido, fragments is perhaps best viewed as an intramolecular proton transfer or IES as defined by Goddard, Periana *et al.* (Scheme 7).[45] An important mechanistic distinction between IES and an aromatic substitution is based on the interaction of the metal with the C-H bond rather than the arene π-system. Upon coordination to the metal center, acidic character is imparted to the C-H bond resulting in relatively facile proton transfer to the basic ligand "X." Calculated results for the transition state of benzene C-H activation that are consistent with the intramolecular proton transfer view include: 1) shorter Ru-H bond distance for X = Me than for X = OH or NH_2, 2) shorter M-H bond distances for less basic OH ligands than for NH_2 ligands, and 3) longer M-H bond distances for later and more electrophilic metals (Figure 11). Such a reaction is similar to net heterolytic cleavage of dihydrogen by transition metal amido complexes and has been previously discussed for intramolecular C-H activation by a Ru(II) parent amido system.[39,43,99] In addition, related mechanistic issues and conclusions have been discussed recently in an

excellent detailed computational analysis including an interesting explicit investigation of orbital transformations involved in C-H activation by an Ir(III) methoxo complex.[45]

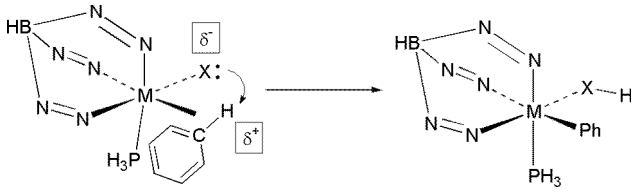

Scheme 7. Proposed mechanism for C-H activation by $[(Tab)M(PH_3)(C_6H_6)X]^n$ (X = OH or NH_2) is best described as an intramolecular proton transfer.

III.2.d Kinetic and Thermodynamic Considerations

Analysis of the structural and electronic properties of the various stationary points along the reaction pathway for 1,2-addition of the C-H bond of benzene has revealed a considerable degree of sensitivity to modification of the metal, including overall complex charge, and activating ligand X. It is also likely that exchange of the phosphine ligand (PH_3 for the calculations) also influences the energetics of C-H activation.[92] From the perspective of rational design of activating complexes, this flexibility is highly desirable as it suggests considerable ability to tune d^6 TpM(L)X complexes toward optimal activity and selectivity. Attention is now turned to issues of kinetics and thermodynamics to probe whether the calculated molecular and electronic structural changes discussed above are manifested in the energetics of C-H bond activation of benzene by the model scorpionate complexes.

An overview of the proposed reaction pathway for benzene C-H activation is given in Scheme 4. The overall transformation involves the loss of phosphine from the

18-electron precursor $[(Tab)M(PH_3)_2X]^q$ (**A**) to generate the formally 16-electron species $[(Tab)M(PH_3)X]^q$ (**B**). Benzene then coordinates to **B** to form the adduct $[(Tab)M(PH_3)(benzene)X]^q$ (**C**), which is followed by the transition state for benzene C-H activation ($\mathbf{D}^{\ddagger}$) leading to 18-electron product $(Tab)M(HX)(PH_3)(Ph)$ (**E**). The dative ligand XH may then be replaced by the original PH_3 to yield *bis*-phosphine complex $(Tab)M(PH_3)_2(Ph)$ (**F**).[30b,c] Calculated free energies for these steps are depicted in Figure 12 for $[M\text{-}OH]^q$ (top) and $[M\text{-}NH_2]^q$ (bottom) complexes.

Three thermodynamic criteria were used to assess the suitability of different metal/ligand combinations for C-H bond activation of benzene. The first criterion evaluated is the energetic barrier to the formation of the unsaturated species **B** from the precursor **A**, as C-H activation of benzene requires coordination to the metal center. Second, the magnitude of the benzene C-H activation transition state $\mathbf{D}^{\ddagger}$ relative to starting materials **A** is considered. The third criterion assessed here is the thermoneutrality of the H-transfer step (**B** + PhH → **E**), which is related to incorporation of the C-H activation sequence into potential catalytic cycles. For efficient catalysis, this reaction should be close to thermoneutral in order to avoid thermodynamic "sinks."

III.2.d.i Generation of 16-electron Active Species

The generation of the active species **B** plays an obviously important role in determining the overall rate of benzene C-H activation. If the unsaturated complex is too high in energy, activation of the C-H bond will be hampered by a low concentration

of active species **B** or, alternatively, require a larger concentration of the precursor complex **A**. The free energies to create the 16-electron active species are given in Table 9. In general, the extrusion of phosphine becomes more endergonic as the charge on the complex becomes more positive, which is consistent with tighter binding of the Lewis basic phosphine to a more acidic metal center. However, given the favorable entropy for a bond dissociation process, the overall $\Delta G_{bind}(PH_3)$ for this step is not inordinate for any complex, being less than 28 kcal/mol for even the most tightly bound system, $[Pt\text{-}OH]^{2+}$, and much less than this for all other complexes studied.

Phosphine loss is more favorable for the amido complexes than their hydroxo counterparts, suggesting an advantage for the former in the way of a greater concentration of active species for $[M\text{-}NH_2]$ than for the corresponding [M-OH] complexes. The working hypothesis is that this difference is a consequence of greater π-donation for the amido ligands versus hydroxo ligands, as discussed above, which nominally puts the active species closer to a more stable 18-electron count. Hence, from the perspective of generation of 16-electron active species **B**, amido complexes are expected to have an advantage over their hydroxo counterparts.[viii]

---

viii In some cases, the loss of phosphine is calculated to have a slightly favorable change in Gibbs free energy due to entropic factors. Since these are gas-phase calculations, the effects of entropy in the dissociation step are magnified beyond what is expected in solvent. However, the contribution of TΔS is roughly constant (within 1.8 kcal/mol) across all metals for this step. Further, the entropic contribution to the **A**→**B** and **B**→**C** steps roughly cancel each other (within 4.5 kcal/mol) and the remaining steps are unimolecular, effectively eliminating solvation concerns for the purposes of this study.

Table 9. Free Energies (kcal/mol) for Generation of 16-electron Active Species $[(Tab)M(PH_3)X]^q$ (B) from $[(Tab)M(PH_3)_2X]^q$ (A)[a]

M	X = OH	X = NH_2
Tc	-4.2	-5.7
Re	-2.2	-5.0
Ru	-0.9	-4.6
Co	7.8	-1.8
Ir	13.6	2.8
Ni	18.7	10.6
Pt	27.6	14.9

[a] This is the B3LYP/CSDZ* calculated free energy for the reaction, $TabM(X)(PH_3)_2 \rightarrow TabM(X)(PH_3) + PH_3$

III.2.d.ii Kinetic Barrier to C-H Bond Activation of Benzene

In terms of targeting new systems capable of facile C-H activation via 1,2-addition across M-X bonds, the most pertinent energetic parameter is the activation barrier for the C-H bond-breaking event. For convenience and ease of comparison, this barrier is defined as the calculated free energy difference between the precursor complex $(Tab)M(PH_3)_2X$ (**A**) and the transition states ($\mathbf{D}^{\ddagger}$, Table 10).

Table 10. Free Energies (kcal/mol) of Activation of Benzene C-H Bond starting from $(Tab)M(PH_3)_2X$ (A)[a]

M	X = OH	X = NH_2
Tc	26.5	27.0
Re	33.0	32.4
Ru	29.6	29.1
Co	28.7	25.5
Ir	35.2	32.0
Ni	19.4	18.9
Pt	24.1	22.4

[a] This is the B3LYP/CSDZ* calculated free energy difference between transition state $\mathbf{D}^{\ddagger}$ and reactants **A**.

The transition states for benzene C-H activation, $\mathbf{D}^{\ddagger}$, fall within the free energy range of ~19 kcal/mol ($[Ni\text{-}X]^{2+}$ for X = OH, NH_2) to ~35 kcal/mol ($[Ir\text{-}OH]^{+}$) above precursors **A**. For systems with the same total charge, progressing from a 1st or 2nd row transition metal to the 3rd row is calculated to increase the barrier to benzene C-H activation. For example, the free energies of activation for the heavier rhenium complexes are ~6 kcal/mol higher than the lighter technetium congeners. Likewise, there is an increase in free energy of activation for Ir as compared to Co by 6.5 kcal/mol (for both X = OH and NH_2) and also platinum versus nickel (difference of 4.7 kcal/mol for X = OH and 3.5 kcal/mol for X = NH_2).

With one exception (Tc), the calculated barriers for the amido complexes are lower than their hydroxo counterparts by an average of 1.6 kcal/mol for the remaining six systems. The largest calculated difference is 3.2 kcal/mol for the Co and Ir systems, while the smallest magnitude difference is 0.5 kcal/mol for Tc and Ni. The magnitude of the free energy change for **A** → $\mathbf{D}^{\ddagger}$ is smaller for variation of X than the change due to variation of metal (same ligand X) within a triad. Computational studies of 1,2-addition of a C-H bond of methane across the Ir-X (X = OH, OMe, OCF_3, or NH_2) bond of the model complexes $Ir(Me)_2(NH_3)_2(X)(CH_4)$ reveal a difference in $\Delta H^{\ddagger}$ that is less than 2 kcal/mol for variation of X, which is similar in magnitude to the calculated differences upon variation of X for (Tab)M complexes.[45] However, this comparison of activation

barriers for hydroxo versus amido are for *overall reactions* that involve phosphine dissociation, benzene coordination and the C-H activation step. For a more direct comparison to the results for $Ir(Me)_2(NH_3)_2(X)(CH_4)$ systems, the $\Delta\Delta G^{\ddagger}$ for 1,2-addition of the C-H bond of benzene starting from $[(Tab)Ir(PH_3)(C_6H_6)X]^+$ complexes is calculated. The $\Delta G^{\ddagger}$ for the 1,2-addition is 17.6 kcal/mol for X = OH and 28.9 kcal/mol for $X = NH_2$.

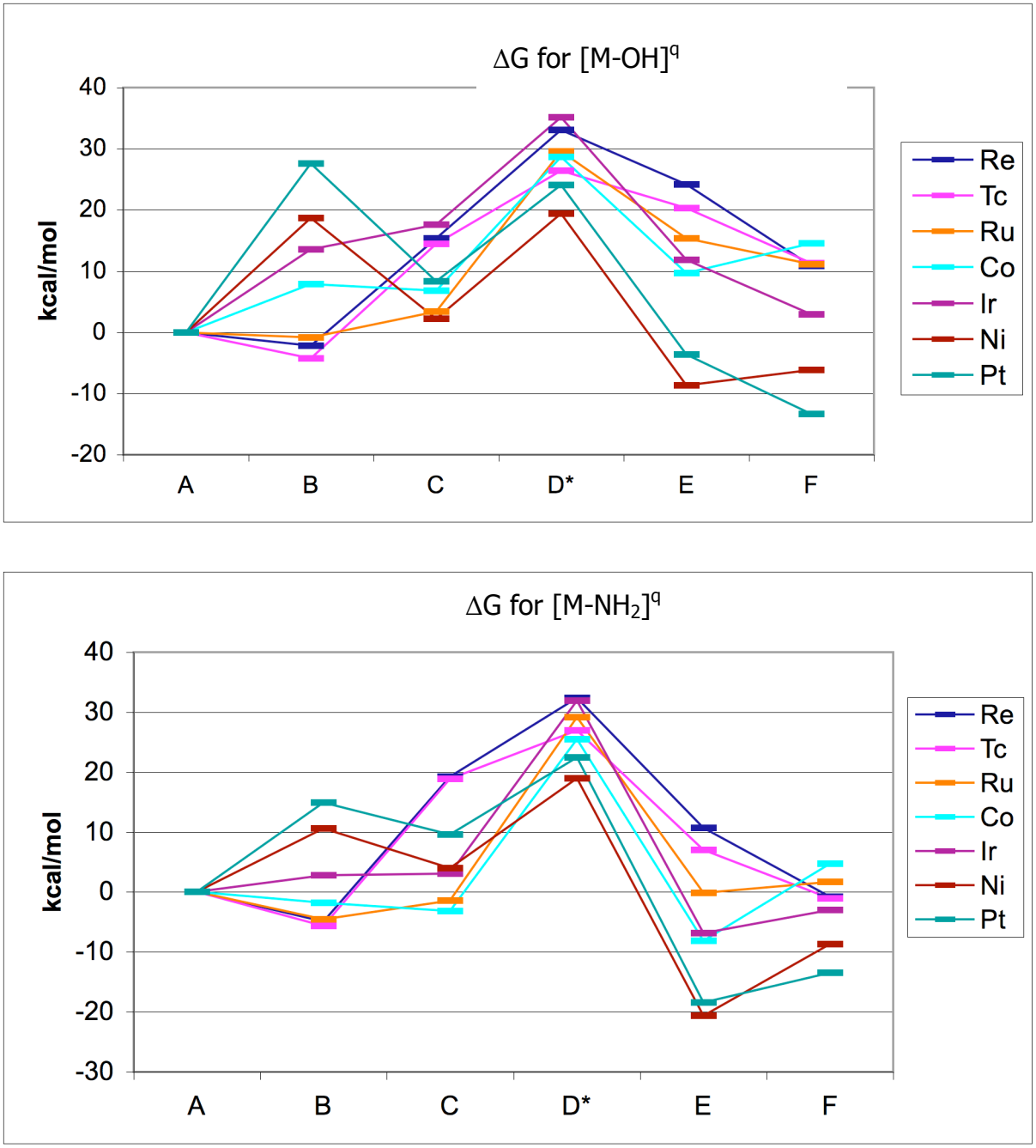

Figure 12. Calculated ΔG for benzene C-H activation by the complexes (Tab)M(PH_3)$_2$X for X = OH (top) and X = NH_2 (bottom). D* represents the transition state for C-H activation.

Thus, a much more substantial change in activation barrier upon substitution of OH with NH_2 for (Tab)Ir(PH_3)(C_6H_6)X systems is found, with $\Delta\Delta G^{\ddagger}$ = 11.3 kcal/mol [compared to ≤ 2 kcal/mol difference for Ir(Me)$_2$(NH_3)$_2$(X)(CH_4)]. In part, these differences may reflect the impact of gas phase calculations that incorporate entropy (this study) versus changes in enthalpy (previous study of Ir system[45]). Combined with the structural evidence discussed above, the calculations yield an emerging picture that catalysis will be significantly influenced by both the metal M and the activating ligand X.

III.2.d.iii Thermoneutrality of Hydrogen Transfer

For the possible incorporation of the C-H activation sequences into catalytic cycles, the overall thermodynamics of the H-transfer step (*i.e.*, ΔG_{trans}, the free energy of the reaction (Tab)M(PH_3)X [**B**] +PhH → (Tab)M(PH_3)(HX)Ph [**E]**) are important. Effective catalysis implies that these transformations be neither too favorable nor too unfavorable, as indicated in previous theory-experiment investigations of the observed efficient H/D exchange.[30c] The Ni, Pt, and Ir complexes for both activating ligands X and the Co-amido complex are exergonic for the conversion of **B** plus benzene to **E** (Table 11), implying these metals may be prime candidates for direct observation of benzene C-H activation and functionalization. Consistent with the present calculations, Periana *et al.* have observed the conversion of an Ir(III)-methoxo complex and benzene to methanol and the corresponding Ir(III)-phenyl system.[30a] However, for the Ni and Pt model systems, the benzene C-H activations are calculated to be highly exergonic,

implying that these systems may be less suitable for incorporation into catalytic sequences. The systems for which the **B** → **E** transformation are calculated to be closest to thermoneutral are the $[Co\text{-}OH]^+$ and $[Ir\text{-}OH]^+$ complexes.

Table 11. Free Energies (kcal/mol) of Hydrogen Transfer[a]

M	X = OH	X = NH_2
Tc	24.5	12.7
Re	26.4	15.6
Ru	16.2	4.4
Co	1.9	-6.4
Ir	-1.7	-9.6
Ni	-27.4	-31.2
Pt	-31.2	-33.3

[a] This is the B3LYP/CSDZ* calculated free energy difference between active species **B** plus benzene and 18-electron product **E**, TabM(HX)(PH_3)(Ph).

For a given metal, the amido ligand lowers ΔG for conversion of $[(Tab)M(PH_3)X]^q$ (**B**) plus benzene to $[(Tab)M(PH_3)(XH)Ph]^q$ (**E**), the free energy change for the hydrogen transfer step, in comparison to the hydroxo ligand. The differences in Gibbs free energy range from 12.8 kcal/mol for Tc to 2.1 kcal/mol for Pt. In general, the difference between hydroxo and amido decreases from left to right in the transition series.[ix]

ix For example, the average difference is 11.8 kcal/mol for group 7, 11.8 kcal/mol for group 8, 8.1 kcal/mol for group 9 and 2.9 kcal/mol for group 10.

III.3 ccCA Reaction Barrier Height Benchmarking

III.3.a Problematic Structures

While DFT often provides good geometries,[100,101] even for transition states,[59] like any theory it is not infallible. In particular, there are three systems for which the default B3LYP-based geometry optimization failed.

a) The $H+F_2 \rightarrow HF+F$ transition state

This reaction is apparently barrierless at the B3LYP/6-31G(2df,p) level of theory, as suggested by a scan of the PES. As a consequence, the QCISD/MG3[102] optimized transition state geometry provided by Truhlar[103] was used without modification for both the ccCA and G3B calculations. At the given geometry, both B3LYP/6-31G(2df,p) and B3LYP/6-31G(d) methods have one imaginary frequency corresponding to the correct transition mode.

b) The $CH_3+FCl \rightarrow CH_3F+Cl$ transition state

No transition state could be located using B3LYP/6-31G(2df,p) or B3LYP/6-31G(d) methods. The reaction is assumed to be barrierless at these levels of theory, so the transition state geometry provided by Truhlar[103] was used. At the given geometry, B3LYP/6-31G(2df,p) calculations predict one imaginary frequency corresponding to the correct transition mode. Using the B3LYP/6-31G(d) level of theory, a reasonable transition mode is found ($459i$ cm^{-1}), plus two small imaginary modes corresponding to C-F-Cl linear bending modes ($37i$ and $36i$ cm^{-1}).

c) The $F^{-}\cdots CH_3Cl$ ion pair

The stationary point corresponding to this separated ion pair (a stable minimum, not a transition state) could not be located using B3LYP/6-31G(2df,p), B3LYP/6-31G(d), or even B3LYP/cc-pVTZ. Upon attempted geometry optimization using these basis sets, the product ion pair $CH_3F\cdots Cl^{-}$ resulting from moving through the transition state is always obtained. S_N2 reactions typically have a double-well structure[58] corresponding to a bound ion pair in the entrance and exit channels of the reaction. Martin and Parthiban found it impossible to obtain this bound ion pair using B3LYP/6-311G(2d,d,p),[104] but were able to find it once diffuse functions were added to the basis set. [58] To investigate basis set and correlation effects, optimizations were attempted at the CCSD/cc-pVTZ, B3LYP/cc-pVQZ, and B3LYP/MG3 levels of theory to locate this elusive ion pair. The bound ion pair geometry could not be located at the CCSD/cc-pVTZ, B3LYP/MG3, and B3LYP/aug-cc-pVTZ levels, but not using the B3LYP/cc-pVQZ method. To retain consistency with the above-mentioned troublesome stationary points, the QCISD/MG3 geometry was used.[103] Both B3LYP/6-31G(2df,p) and B3LYP/6-31G(d) predict two small imaginary modes (nearly degenerate 157*i* and 145*i* cm^{-1}, respectively) at the QCISD/MG3 geometry, roughly corresponding to linear F-C-Cl bending.

Besides being in the NHTBH database, all three problematic structures have one feature in common. The transition state geometry for each "problem" reaction is predicted to be close to the reactants, via the Hammond Postulate.[105] That is, the

forward barrier is small, leading to a transition state that strongly resembles the reactants both in energy and in structure. The linear interpolation proposed independently by Agmon[106] and Miller[107] for quantitative application of the Hammond postulate can be used to estimate the degree of completion of a reaction at the transition state using the known forward and reverse reaction barrier heights. While quantitative formulations of the Hammond Postulate have been compared to results using Marcus theory,[108] the use of these parameters as an estimation of how well DFT will perform appears to be unique to the current study. The completion estimates for the three troublesome reactions above are given in

Table 12. All of the NHTBH reactions have completion estimates ranging from 2% to 59%, and it is noticeable that the troublesome reactions mentioned above have completion estimates less than 12%, *i.e.*, have very "early" transition states. There is one other reaction ($H + C_2H_4 \rightarrow CH_3CH_2$) in the NHTBH set and one reaction in the HTBH set ($F + H_2 \rightarrow HF + H$) with completion estimates under 12% (4% and 5%, respectively) but B3LYP geometries were found for the corresponding transition states for these reactions. It is notable that all the transition states for proton-transfer reactions were found, despite the small completion estimates for two of them. This leads one to believe that the completion estimates of Agmon[106] and Miller[107] may be a good indicator of when a transition state for non-proton-transfer reactions will be difficult (if not impossible) to locate using DFT and perhaps whether modification of the geometry optimizations will be necessary.

Table 12: Hammond Postulate Analysis of Problematic Species[a]

Reaction	V_f	V_r	Completion at TS
$H + F_2 \rightarrow HF + F$	2.27	106.18	2%
$CH_3 + FCl \rightarrow CH_3F + Cl$	7.43	60.17	11%
$F^{-}\cdots CH_3Cl \rightarrow FCH_3\cdots Cl^{-}$	2.89	29.62	9%

[a] V_f and V_r are the benchmark values of the forward and reverse barrier heights, respectively, in kcal/mol. The completion estimate is defined as $V_f/(V_f+V_r)$

III.3.b "Black Box" Method Performance

Analysis of the reaction set is slightly complicated by the fact that the forward and reverse reactions are not absolutely independent because both the forward and reverse barriers depend on the transition state structure and energy. The reverse and forward barriers are inextricably linked through the equilibrium constant, which is a thermodynamic quantity dependent on ground state energies that is thus expected to be accurately predicted by composite methods. For non-symmetric reactions, the dependency is irrelevant from a statistical standpoint because two degrees of freedom are produced (forward and reverse barriers) from two independent variables (transition state energy with respect to reactants and products). However, the products and reactants are identical in symmetric reactions and the corresponding energies are constrained to be equal. Therefore, the forward barrier is not independent of the reverse barrier (they are, of course, equal). Truhlar's reported statistics double-count symmetric reactions (2 in the HTBH set and 5 in the NHTBH set),[54,75] so both unique and "double-counted" statistical approaches were investigated (Table 13 and Table 14, respectively). There are only minor differences in the reported error arising from

double-counting symmetric reactions, as is expected of randomly distributed error. Detailed comparisons of the calculated values versus best estimates is given elsewhere[ii] and summarized in Table 13. Overall results are reported for ccCA and G3B.

Table 13: Error Metrics (in kcal/mol) for ccCA and G3B

	ccCA-S4	ccCA-P	G3B
HTBH – Forward reaction barriers			
MSE	-0.15	-0.15	1.03
MUE	0.79	0.79	1.59
Max Error	2.12	2.14	5.04
HTBH – Reverse reaction barriers			
MSE	-0.11	-0.11	1.44
MUE	0.99	1.01	1.75
Max Error	2.88	2.95	4.92
NHTBH – Forward reaction barriers			
MSE	-0.29	-0.27	0.62
MUE	1.01	1.00	1.82
Max Error	3.19	3.26	6.70
NHTBH – Reverse reaction barriers			
MSE	0.06	0.06	2.31
MUE	0.76	0.77	2.57
Max Error	3.67	3.75	6.68
HTBH Aggregate (36 independent data points)			
MSE	-0.10	-0.10	1.25
MUE	0.91	0.92	1.71
Max Error	2.88	2.95	5.04
NHTBH Aggregate (32 independent data points)			
MSE	-0.19	-0.18	1.41
MUE	0.98	0.99	2.28
Max Error	3.67	3.75	6.70
HTBH+NHTBH Aggregate			
MSE	-0.14	-0.14	1.32
MUE	0.94	0.95	1.98
Max Error	3.67	3.75	6.70

Table 14: "Double-counted" Statistics for Direct Comparison with Other Benchmarks[a]

	ccCA-S4	ccCA-P	G3B
HTBH			
MSE	-0.13	-0.13	1.23
MUE	0.89	0.90	1.67
NHTBH			
MSE	-0.11	-0.11	1.47
MUE	0.89	0.89	2.20
HTBH+NHTBH			
MSE	-0.12	-0.12	1.35
MUE	0.89	0.89	1.94

[a] All errors are defined as expected minus calculated, *e.g.*, a positive error indicates that the calculated value is lower than the true value. MSE = mean signed error; MUE = mean unsigned error.

III.3.b.i ccCA versus G3B

In a global sense, the mean unsigned error for the entire data set (aggregate HTBH + NHTBH, Table 13 and Figure 13) indicates that ccCA (MSE of -0.14 kcal/mol and MUE of 0.95 kcal/mol) achieves chemical accuracy for the prediction of reaction barrier heights. On the other hand, G3B performs less well with a mean unsigned error of 1.98 kcal/mol for the entire set. Furthermore, the maximum error of the ccCA method is 3.67 and 3.75 kcal/mol for ccCA-S4 and ccCA-P, respectively, whereas the maximum error for G3B is much higher (6.70 kcal/mol). The consistently negative mean signed error for ccCA (except for the NHTBH reverse barrier subset: see Table 13) means the transition state energy is consistently overestimated, whereas the positive mean signed error for G3B indicates that the barrier is consistently underestimated.

Figure 13: Graph of computed versus best estimate reaction barriers for ccCA and G3B.

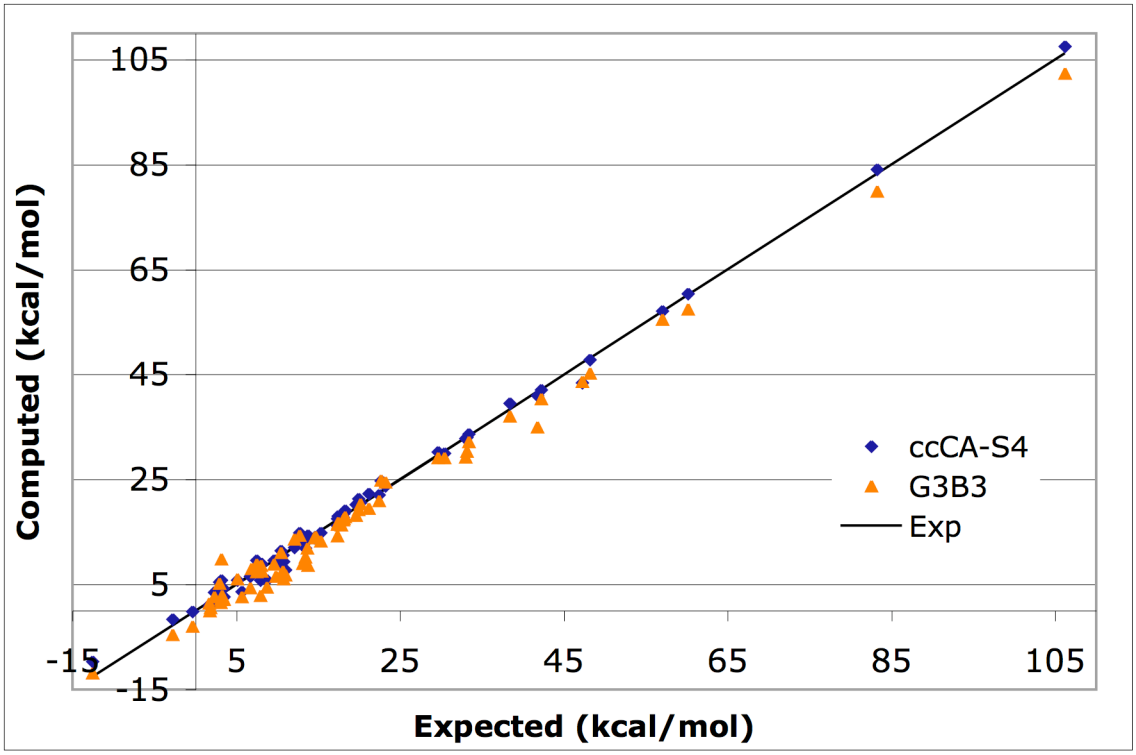

III.3.b.ii ccCA versus Density and Wavefunction Based Methods

Since the NHTBH and HTBH databases were used, a comparison can be made between the accuracy of ccCA and G3B versus the 29 DFT functionals and 6 *ab initio* wavefunction-based methods benchmarked in reference 75. The original benchmark calculations are equivalent to *X*/MG3S[x]//QCISD/MG3 (where *X* is a DFT functional) or *Y*/MG3//QCISD/MG3 (where *Y* is an *ab initio* wavefunction method). Analysis of the

---

x According to Zhao *et al.*, "The MG3S basis is the same as MG3 except it omits the diffuse functions on hydrogens." (*cf.* reference 75)

mean unsigned errors indicates that four DFT functionals (MPW1K, BB1K, MPWB1K, and MPWKCIS1K) and 1 *ab initio* method, QCISD(T), outperform G3B for the calculation of activation barriers. It is perhaps unsurprising that the DFT functionals specifically parameterized for kinetics (hence the capital K at the end of their acronyms) outperform G3B for this data set. However, both the ccCA-P and ccCA-S4 variants outperform *all* methods benchmarked in this study, including the highest *ab initio* level reported by Truhlar *et al.*:[54] QCISD(T). The overall MSE and MUE for QCISD(T) are 0.64 and 1.10 kcal/mol, respectively, whereas ccCA (both variants) gives -0.12 and 0.89 kcal/mol, respectively. Although the MG3(S) basis sets are fairly large (equivalent to the 6-311+G(3d2f,2df,2p) Pople basis set), there remains the possibility that the difference can be attributed to a better treatment of basis set completeness in ccCA. Furthermore, extrapolation to the basis set limit as is done in ccCA should also ameliorate basis set superposition error (BSSE);[109] the BSSE was not explicitly corrected for in the benchmarked calculations.[75]

III.3.c Reliability: ccCA versus G3B

As a measure of reliability, the reactions with the largest error for ccCA and for G3B in both HTBH and NHTBH sets are given in Table 15. (that is, only the reaction with the greatest error for each method and subset is selected). Reactions 1 and 2 (H_2+Cl → H+HCl in HTBH and $F^{-}\cdots CH_3OH$ → $HO^{-}\cdots CH_3F$ in NHTBH, respectively) are the reactions for which ccCA has the greatest error. Both ccCA variants perform similarly: the average difference between the unsigned errors for ccCA-S4 and ccCA-P for all

reactions is only 0.03 kcal/mol, with a maximum deviation of 0.09 kcal/mol, therefore the worst reactions for either ccCA variant are the same and are listed only once in Table 15. Similarly, reactions 3 and 4 ($O+CH_4 \rightarrow HO+CH_3$ in HTBH and $H+CO \rightarrow HCO$ in NHTBH, respectively) are the reactions for which G3B shows the greatest error. For reactions 1 and 2, ccCA and G3B yield similar reaction barriers (*ca.* 3-4 kcal/mol lower than the benchmark value), but the ccCA predicted barriers are significantly closer to the best estimate values than G3B for reactions 3 and 4 (*ca.* 1 and 3 kcal/mol error for ccCA; *ca.* 5 and 7 kcal/mol for G3B). The fact that both methods err in the same direction and with roughly the same magnitude for reactions 1 and 2 reactions whereas ccCA provides superior barrier heights for the other two reactions potentially indicates a limitation of G3B that is not in common with ccCA, Table 15.

Table 15: Problematic Reactions (1 and 2 for ccCA; 3 and 4 for G3B)[a]

Reaction	Lit $V^{\neq}$	ccCA-S4	ccCA-P	G3B
1) $H_2+Cl \rightarrow H+HCl$	8.70	5.82	5.75	4.59
2) $F^{-}\cdots CH_3OH \rightarrow HO^{-}\cdots CH_3F$	47.20	43.53	43.45	43.67
3) $O+CH_4 \rightarrow HO+CH_3$	13.70	14.37	14.36	8.66
4) $H+CO \rightarrow HCO$	3.17	5.82	5.92	9.87

[a] All energies are in kcal/mol.

The accuracy of the calculated barrier height is affected not only by the performance of the method for the transition state, but also by the accuracy with which the reactant and product energies can be predicted. It is therefore useful to investigate the reliability of ccCA and G3B by comparing the unsigned errors (*i.e.*, calculated versus

best estimate from databases) of ccCA[xi] to the unsigned errors of G3B for each reaction rather than just the mean unsigned error across an entire set. If both methods have similar absolute errors for a particular reaction, then both are similarly reliable for that reaction (and presumably for analogous reactions). Across the HTBH and NHTBH databases, the ccCA unsigned error is more than 1 kcal/mol greater than the unsigned error of G3B for only one reaction ($F^- + CH_3Cl \rightarrow FCH_3 + Cl^-$, in the NHTBH set). Conversely, the G3B unsigned error is greater than the ccCA unsigned error by more than 1 kcal/mol for no fewer than 28 reactions in the aggregate set.

III.3.d Effect of Modifying the Methods

III.3.d.i Effect of HLC on Calculated Barrier Heights

Another test of reliability is to modify the methods to determine what impact a particular component has on the performance of the composite method as a whole. Rather than perform an exhaustive study of each individual correction, which is outside the scope of this research, two specific perturbations were selected as the most interesting: the impact of removing the higher-level correction (HLC) from G3B, and placing the geometries used by each method on equal footing. When the empirical HLC is removed from G3B, the mean signed and unsigned errors improve noticeably while the maximum error gets worse (Table 16). In the HTBH set, none of the reactions to

---

xi Given how close the ccCA-P and ccCA-S4 values are to each other (*vide supra*), the average of the unsigned error for the ccCA variants for each reaction was taken as the ccCA unsigned error for the reaction.

which the HLC contributes[xii] are improved by inclusion of the HLC. In fact, the HLC degrades all of the reactions to which it contributes by an average of 1.13 kcal/mol for the HTBH set.

Table 16: HLC-exclusive Error Metrics for G3B[a]

Database	MSE	MUE	Max
HTBH	0.74	1.24	4.57
NHTBH	1.08	2.21	7.93
HTBH+NHTBH	0.90	1.70	7.93

[a] MUE = mean unsigned error; MSE = mean signed error; Max = maximum error; values quoted in kcal/mol. Unique forward and reverse reactions were combined for each database, as in Table 13.

Of the 15 reactions in the NHTBH set for which the HLC contributes, 7 are improved by addition of the HLC (the unsigned error is reduced an average of 0.44 kcal/mol), and 8 are degraded by the addition of the HLC (0.64 kcal/mol on average) resulting in an average degradation of 0.13 kcal/mol across the NHTBH set. It is apparent, therefore, that the HLC in G3B contributes to both the systematic and nonsystematic error. Across the entire reaction set (HTBH and NHTBH combined), the HLC improves the accuracy (as determined by the unsigned error against best estimate) only 10% (7/67) of the time, while it actually degrades the accuracy 34% (23/67) of

xii Note that since the HLC is calculated solely using the number of paired and unpaired electrons, many reaction barriers have no contribution from the HLC.

the time. Perhaps more troubling than the net loss of accuracy due to the HLC[xiii] is the unpredictability with which it will improve or degrade the computed values.

Since the HLC distinguishes between atoms and molecules, a transition state-consistent variant of Gn methods may reasonably be expected to have a separate set of HLC parameter values for transition states.[xiv] Indeed, Truhlar et al. encountered this very problem while formulating a variant of G3 (multi-coefficient G3, MCG3[110]) that could be used to examine any arbitrary point on the potential energy surface (PES) rather than being confined to minima. Since MCG3 parameterizes the contribution of each explicit correction, the HLC was completely removed for consistent treatment at every point on the PES. From a physical interpretation, the fact that the atomic and molecular HLC parameters differ in the G3 method indicates that the parameters are linked in same way to the electronic environment of the system. Since transition states almost invariably have at least one bond that is stretched beyond a normal covalent equilibrium length, the electronic environment of the stretched bond is expected to be

---

xiii Assuming the databases used provide a good sampling of reactions, on average the HLC is expected to degrade accuracy by (0.96 kcal/mol)*(23/67)-(0.44 kcal/mol)*(7/67) = 0.28 kcal/mol. Or, looking just at cases in which the HLC contributes, an average degradation of (0.96 kcal/mol)*(23/30)-(0.44 kcal/mol)*(7/30) = 0.63 kcal/mol results.

xiv Since the HLC is calibrated for stable species, there is no *a priori* reason to believe it is appropriate for transition states. Further, the HLC cancels unless (a) at least one of the reactants is an atomic species, or (b) the spin multiplicity of the transition state is different from the infinitely-separated reactants, leading to an inconsistency in the way the HLC is handled for general points on the PES. Specifically, a large class of reactions will not have any contribution from the HLC, which, as the empirical fit parameter set for the method, is intended to account for higher-order physical effects not explicitly accounted for elsewhere.

somewhere between an equilibrium bond (molecular HLC parameters) and a broken bond (atomic HLC parameters).

III.3.d.ii Effect of Geometry on Calculated Barrier Heights

To decouple G3 and ccCA from dependence on the ability of the B3LYP functional to predict geometries, all structures were re-optimized at the CCSD/6-31G(d) level of theory. The error metrics, analogous to Table 13, are reported in

Table 17 for the values computed at these new geometries. As with B3LYP, the structure for the $F^{-}\cdots CH_3Cl$ bound ion pair could not be located, and hence the QCISD/MG3 geometry from Truhlar[103] was used as discussed above. Strictly speaking, the use of geometries obtained by levels of theory other than B3LYP/6-31G(d) requires a reoptimization of the HLC component of G3B. However, the standard HLC parameters in G3B were used without modification for the sake of simplicity and because the reoptimized parameters are not expected to differ greatly from the standard values.[xv]

xv In fact, when G3 was modified to use DFT geometries and ZPE (the G3B method), the HLC parameters changed from [A, B, C, D] = [6.386, 2.977, 6.219, 1,185 mHartree] to [6.760, 3.233, 6.786, 1.269 mHartree] (*cf.* reference 56). That is a maximum change of 0.567 mHartree for the C parameter, corresponding to the correction for electron pairs in atomic species.

Table 17: Error Metrics for ccCA and G3B, Modified to Use the CCSD/6-31G(d) Geometry

	ccCA-S4	ccCA-P	G3B
HTBH – Forward reaction barriers			
MSE	-0.35	-0.34	0.60
MUE	0.69	0.70	1.38
Max Error	2.07	2.08	4.27
HTBH – Reverse reaction barriers			
MSE	-0.30	-0.30	0.99
MUE	0.68	0.68	1.53
Max Error	2.15	2.18	3.86
NHTBH – Forward reaction barriers			
MSE	-0.30	-0.29	0.47
MUE	0.88	0.89	1.58
Max Error	2.71	2.80	6.66
NHTBH – Reverse reaction barriers			
MSE	0.06	0.06	2.15
MUE	1.01	1.02	2.38
Max Error	3.58	3.54	4.59
HTBH Aggregate (36 "independent" reactions)			
MSE	-0.30	-0.30	0.88
MUE	0.69	0.69	1.49
Max Error	2.15	2.18	4.27
NHTBH Aggregate (32 "independent" reactions)			
MSE	-0.11	-0.11	1.35
MUE	1.05	1.06	2.15
Max Error	3.58	3.54	6.66
HTBH+NHTBH Aggregate			
MSE	-0.21	-0.21	1.10
MUE	0.86	0.86	1.80
Max Error	3.58	3.54	6.66

[a] The mean signed error (MSE), mean unsigned error (MUE) and maximum error (Max Error) are quoted in kcal/mol.

The use of CCSD/6-31G(d) geometries systematically improves the G3B values, though the mean errors still indicate chemical accuracy is not achieved (MUE decreases

from 1.98 to 1.80 kcal/mol across the entire database, see Table 13 and

Table 17). On the other hand, ccCA performs only slightly better with CCSD-based geometries than with the standard DFT-based geometries (MUE is decreased from 0.95 to 0.86 kcal/mol). The maximum error across all subsets and the mean unsigned error of the HTBH subset is decreased,

Table 17, but the mean signed error becomes more negative and the mean unsigned error of the NHTBH subset is very slightly increased. The more negative mean signed error indicates that the reaction barrier is predicted consistently too high (as compared to the best estimate values), but the spread of the error and its magnitude is decreased overall. The reactions causing the maximum error for ccCA and G3B with the CCSD geometries are given in Table 18. It is interesting to note that the two reactions with the most error from ccCA (reactions 1 and 2, Table 7) are not the same as with the standard B3LYP geometries (cf. Table 15), whereas G3B errs most significantly for the same reactions as before (reactions 3 and 4, Table 18), potentially indicating a systematic error in G3B that may not be present in ccCA.[xvi] Again, for reactions 1 and 2, ccCA and G3B produce similar values, but ccCA gives much better values than G3B for reactions 3 and 4, once again suggesting that ccCA is more reliable than G3B for predicting barrier heights.

Table 18: Problematic Reactions (1 and 2 for ccCA; 3 and 4 for G3B) Using CCSD/6-31G(d) Geometries[a]

---

xvi To further disambiguate errors arising from geometry selection versus a fundamental limitation in the G3B protocol, the G3B barrier heights were recomputed using QCISD/MG3 geometries from Truhlar *et al.*[103] MG3 is a much larger basis than 6-31G(d), *vide supra*, and should clearly illustrate any issues arising from basis set deficiencies in the computed geometries. The improvement in calculated geometries effected no clear improvement, increasing the overall MSE from 1.35 kcal/mol to 1.36 kcal/mol and decreasing the overall MUE from 1.94 kcal/mol to 1.65 kcal/mol (all "double-counted" values), reinforcing the idea of a fundamental limitation in the G3B protocol that cannot be resolved by using a more accurate geometry.

Reaction	Lit $V^{\neq}$	ccCA-S4	ccCA-P	G3B
1) $H_2O+NH_2 \rightarrow HO+CH_4$	12.70	14.85	14.88	15.14
2) $FCH_3+Cl^- \rightarrow F^-+CH_3Cl$	20.11	16.53	16.57	16.68
3) $O+CH_4 \rightarrow HO+CH_3$	13.70	14.51	14.50	9.43
4) $H+CO \rightarrow HCO$	3.17	5.88	5.97	9.83

[a] All energies are in kcal/mol.

CHAPTER IV: CONCLUSIONS

IV.1 Coinage Metal Pyrazolates

A comprehensive computational study of the structural and spectral properties of the ground and phosphorescent excited states of trimeric coinage metal pyrazolates is presented. Several important conclusions have been reached as a result of this research. First, cuprophilic stabilization in the singlet ground state of $\{[CuPz]_3\}_2$ is 18.1 kcal/mol, overcoming electrostatic repulsion between the like-charged d^{10} metal centers. This cuprophilic interaction is, however, still relatively weak, leading to a soft PES. The large variation in inter-trimer separations found in ground state coinage metal pyrazolates supports a relatively weak, hence tunable, inter-trimer interaction. Second, the emissive triplet excited state of $\{[MPz]_3\}_2$ is predicted by density functional calculations to show major geometric perturbations due to a Jahn-Teller distortion and excimeric M-M bonding. Specifically, population of the lowest unoccupied Kohn-Sham orbitals enhances M···M bonding, contracting both the intratrimer and intertrimer distances. The intertrimer M···M distances contract much more than intratrimer contraction (20% versus 6%), while the percent contraction does not change significantly with the coinage metal used. Third, intertrimer M···M contractions in the T_1 state are roughly equal for the copper and gold complexes (20%) and slightly less for the silver congener (15%). Furthermore, the geometry of the phosphorescent triplet excited state of $\{[AuPz]_3\}_2$ indicates that the M···M bonding is more localized

than in the copper and silver analogues. Fourth, the calculated photophysical properties indicate less sensitivity in the excitation wavelength (λ_{exc}(avg.) ~ 270 ± 30 nm), but more variability in the phosphorescence wavelength (λ_{em} (avg.) ~ 440 ± 70 nm) with coinage metal and pyrazolate substituent modification, consistent with experimental spectroscopic data. Furthermore, significant Stokes' shifts are calculated (*ca.* 15,000 cm^{-1}), similar to those reported for the relevant experimental models.

Taken together, the observations deduced from these calculations point to the great potential of tuning the emission properties of coinage metal pyrazolate trimers through judicious choice of the metal and pyrazolate substituents and allow the prediction of the excited-state structures. Although the latter can now be determined experimentally by time-resolved diffraction,[14] the limited range and accessibility of such experimental investigations render it essential that computational methods be utilized for such purposes, especially given the excellent agreement of the calculated ground- and excited-state structures herein with the experimental ones even for such large dimer-of-trimer systems. Currently, experiments and computations are underway to further explore these implications for the design of improved light-emitting devices.

IV.2 Aryl C-H Bond Activation

The feasibility and kinetic accessibility of the C-H activation step in a catalytic cycle like that shown on the right side of Scheme 2 have been demonstrated (at least for benzene activation) using Ru and Ir complexes.[28,30] Although much remains to be

learned about these transformations, it can now be said that such reactions are accessible with late transition metal systems and that the activation barriers for C-H activation are reasonably low for implementation into catalytic cycles. The second key step, net oxygen atom insertion into an M-R or M-Ar bond is at least equally challenging. Despite the utility and interest in these reactions, insertion of oxygen into metal-alkyl or –aryl functionalities has rarely been directly observed.[34,35] Mayer and Brown have reported the conversion of Re(VII) oxo complexes with phenyl ligands to the corresponding phenoxo complexes, and in at least one case the transformation occurs under thermal conditions.[34] More recently, Periana *et al.* have reported the reaction of methylrheniumtrioxo (MTO) with external oxidants (*e.g.*, hydrogen peroxide, pyridine-*N*-oxide, periodate, and iodosyl benzene) to form $Re(OMe)O_3$.[35] Importantly, these transformations occur relatively rapidly at room temperature, and preliminary mechanistic studies indicate that the oxygen atom in the final methoxo ligand does not originate from a Re-oxo moiety. A mechanism similar to the classic Baeyer-Villiger organic reaction[111] has been proposed.

Thus, the two key steps in the catalytic cycle depicted on the right side of Scheme 2 have been observed; however, the C-H activations have been observed for systems with high d-electron counts [*i.e.*, d^6 for Ru(II) and Ir(III)],[28,30] while the transformation of M-R into M-OR have only been observed for systems in high oxidation states (and thus low d-electron counts).[34,35] For the present models the d-electron count has been fixed at six, which has necessitated variation of the overall charge. While the precise relationship between the kinetics and thermodynamics of these

transformations *vis-à-vis* d-electron counts and metal formal oxidation states is not entirely understood, it is reasonable to expect that a marriage of these two transformations may require a catalyst that satisfies both requirements (such as Co^{III}, Pt^{IV}, *etc.*).

Tables 9 - 11 provide a comparison of the three criteria considered to quantify the efficacy of (Tab)M complexes toward C-H activation and their possible use as catalysts (*i.e.*, generation of the active species, overall H-transfer barrier, and thermoneutrality of the H-transfer step) for hydrocarbon functionalization. As expected, generation of the coordinatively unsaturated species $[(Tab)M(PH_3)X]^q$ (**B**) via loss of phosphine from the 18-electron precursors **A** becomes less favorable as the effective charge on the metal complex becomes more positive. As the charge on the metal complex becomes more positive, $\Delta G^{\ddagger}$ (**A** +PhH → **D**‡) and ΔG (**B** + PhH → **E**) for C-H activation step are both reduced (*i.e.*, become more favorable). However, the present calculations suggest that the metal plays a primary role in the kinetic and thermodynamic feasibility of arene C-H bond activation and functionalization.

In addition to the identity of the metal, the ligand X impacts the calculated reaction energetics.[xvii] Pt is the metal most "tunable" by the ligand X, with a mean absolute change of 11.5 kcal/mol in ΔG due to change of ligand "X." On average, the generation of the 16-electron active species **B** from **A** by phosphine loss is ~7 kcal/mol

---

xvii For each step, the average range of free energy values is *ca.* 20 kcal/mol (holding the ligand constant, for both ligands), whereas the range of the *difference* between the two ligands for each step (*i.e.*, holding the metal constant) is *ca.* 13 kcal/mol, only 65% of the variation due to the metal.

more facile for the amido than their hydroxo congeners, Table 9. Likewise, the **A** + PhH → $\mathbf{D}^{\ddagger}$ activation barriers are ~1 – 3 kcal/mol lower for X = NH_2 than X = OH. Both of these observations suggest an advantage for amido over hydroxo complexes. It is interesting to note that the energetic discrepancy between hydroxo and amido complexes becomes greater for these two criteria as one moves from left to right in the transition series. For the thermoneutrality (of hydrogen transfer) criterion, hydroxo and amido complexes are comparable in a global sense, with the early metals being closer to thermoneutral for the amido than the hydroxo complexes and vice versa for the later metal models.

Here it should be noted that while the C-H activation step is important and is the rate-determining step for most calculated systems, the energetics of PH_3/benzene exchange is also a potentially significant contributor to the success of C-H activation. This underscores the point that hydrocarbon coordination is often as challenging as the actual C-H bond cleavage step. Thus, when considering the impact of variation of the ligand "X," the influence on hydrocarbon coordination should also be considered, especially when varying "X" from alkyl or aryl to π-donor heteroatomic ligands such as OR or NHR, which can impact ligand coordination dramatically. For example, the complexes $TpRu(PMe_3)_2X$ (X = OPh, OH or NHPh) exhibit more rapid rates of dissociative phosphine exchange compared to $TpRu(PMe_3)_2R$ (R = Ph or Me).[15c]

A simple linear catalyst scoring function can be constructed using the calculated ΔG values for the three criteria enumerated above (see Tables 9 – 11) to suggest a

good balance between competing catalytic trends.[xviii] Assigning a lower priority to the free energy to formation of the active species (**A** → **B**)[xix] indicates $[Co\text{-}OH]^+$, $[Ir\text{-}OH]^+$, $[Ru\text{-}NH_2]$, $[Co\text{-}NH_2]^+$, and $[Ir\text{-}NH_2]^+$ are the best candidates for further experimental study, *i.e.*, they have the lowest catalyst scores. It is worth noting that the catalyst scoring function is robust in that the top candidates did not change upon variation of the weights over a reasonable range of values. Moreover, it is interesting to note that the catalyst scoring function independently arrives at models of two heavily studied and successful hydroarylation catalysts, i.e., Ru(II) and Ir(III) complexes.[28,30] These candidates have free energies to formation of the active species less than 10 kcal/mol (except $[Ir\text{-}OH]^+$, which has a barrier of 14 kcal/mol), overall barriers to C-H activation (**A** → $\mathbf{D}^{\ddagger}$) of less than 30 kcal/mol (except $[Ru\text{-}NH_2]$, with a value of 34 cal/mol due to the stability of **B**), and are thermoneutral in the H-transfer step to within 10 kcal/mol. The Co and Ir species have the additional advantage of forming reasonable benzene adducts, leading to potential enhancement in the Arrhenius prefactor for the H-transfer step. It is also interesting to note that none of these candidates exhibit a late transition state structure (see Table 7). Among all the candidates, $[Co\text{-}OH]^+$ has the most favorable "score"[xviii,xix] and appears to be the most promising for further research and tuning to optimize the potential catalytic activity on the basis of an accessible barrier to

---

xviii The weighted sum of the ΔG values of the corresponding criteria may be combined to produce a score, $S=w_{act}\Delta G_{act}+w_{barrier}\Delta G_{barrier}+w_{xfer}|\Delta G_{xfer}|$, with lower scores being more desirable (see Tables 9 - 11 for ΔG values).

xix Specifically, $w_{act}=1$ and $w_{barrier}=w_{xfer}=2$.

H-transfer (21 kcal/mol), near thermoneutrality for H-transfer (+2 kcal/mol), and small barrier to formation of the active species (8 kcal/mol).

The AIM analysis as well as calculated structural metrics and energy barriers implicate a fundamental shift in the nature of the bonding in the transition state upon going from an X with no available lone pairs (*i.e.*, X = methyl) to heteroatom X groups with available lone pairs such as OH and NH_2. While the mechanism of C-H activation for X = hydrocarbyl is more akin to an OHM/SBM description, the transition states for X = OH, NH_2 more closely resemble those envisaged for Shilov-type systems in which the proton transfer is an intramolecular process. In terms of development, X = heteroatom systems may provide more profitable systems for design and fine-tuning of hydrocarbon functional catalysts, generally, and hydroarylation catalysts, specifically. Indeed, such integrated theory-experiment studies are currently underway.

IV.3 ccCA Reaction Barrier Height Benchmarking

A standard benchmark suite of reactions from the literature[54] was employed to compare the accuracy of ccCA to G3B for the prediction of reaction barrier heights. The mean signed and unsigned errors as well as the maximum error metrics were computed to support the assertion that both variants of ccCA (ccCA-S4 and ccCA-P) achieve chemical accuracy whereas G3B does not. Since a standard database was used,[54] ccCA was also compared to several DFT and wavefunction-based methods and found to yield

greater accuracy for reaction barriers, including the highest wavefunction-based theory tested, QCISD(T).

Unmodified, G3B was found to have a mean signed error of +1.32 kcal/mol (*i.e.*, barriers predicted too low on average) and a mean unsigned error of 1.98 kcal/mol with respect to the test set. The largest error for G3B was 6.70 kcal/mol. A mean signed error of –0.14 kcal/mol (*i.e.*, barriers predicted slightly too high on average) and a mean unsigned error of 0.94 kcal/mol as well as a maximum error of 3.67 kcal/mol were computed for ccCA.[xx] An analysis of the problematic reactions for ccCA and for G3B indicates that in addition to being more accurate, ccCA is more reliable than G3B for the reaction set used.

The impact of modified reference geometries and removal of the HLC for G3B was also investigated. Even with the modifications, ccCA is still more accurate and more reliable (mean signed error of –0.22 kcal/mol, mean unsigned error of 0.86 kcal/mol) than G3B (mean signed error of 1.11 kcal/mol, mean unsigned error of 1.86 kcal/mol) for the prediction of transition state properties. Hence, the ccCA methodology represents a chemically robust composite approach for the modeling of both the thermodynamics and kinetics of chemical reactions with chemical accuracy.

---

xx For simplicity, the ccCA-S4 variant results are quoted. The ccCA-P results are similar.

ENDNOTES

1 (a) Dunning, Jr., T. H.; J. Chem. Phys. **90**, 1007 (1989). (b) Dunning, Jr., T. H.; Peterson, K. A.; Wilson, A. K.; J. Chem. Phys. **114**, 9244 (2001). (c) Wilson, A. K.; Woon, D. E.; Peterson, K. A.; Dunning, Jr., T. H.; J. Chem. Phys. **110**, 7667 (1999). (d) Wilson, A. K.; Woon, D. E.; Peterson, K. A.; Dunning, Jr., T. H.; Abstr. Pap. – Am. Chem. Soc. **213**, 60 (1997). (e) Kendall, R. A.; Dunning, Jr., T. H.; Harrison, R. J.; J. Chem. Phys. **96**, 6796 (1992). (f) Woon, D. E.; Dunning, Jr., T. H.; J. Chem. Phys. **100**, 2975 (1994). (g) Woon, D. E.; Dunning, Jr., T. H.; J. Chem. Phys. **103**, 4572 (1995). (h) Woon, D. E.; Dunning, Jr., T. H.; J. Chem. Phys. **117**, 10548 (2002).

2 (a) N. J. DeYonker, K. A. Peterson, G. Steyl, A. K. Wilson, and T. R. Cundari; J. Phys. Chem. A *in press* (2007). (b) D. S. Ho, N. J. DeYonker, A. K. Wilson, and T. R. Cundari; J. Phys. Chem. A **110**, 31, (2006). (c) N. J. DeYonker, D. S. Ho, A. K. Wilson, and T. R. Cundari; *J. Phys. Chem. A,* **2007**, *26*, 910.

3 Omary, M. A.; Rawashdeh-Omary, M. A.; Gonser, M. W. A.; Elbjeirami, O.; Grimes, T.; Cundari, T. R.; Diyabalanage, H, V. K.; Palehepitiya Gamage, C. S.; Dias, H. V. R. *Inorg. Chem.* **2005***, 44*, 8200.

4 (a) Dias, H. V. R.; Diyabalanage, H. V. K.; Rawashdeh-Omary, M. A.; Franzman, M. A.; Omary, M. A. *J. Am. Chem. Soc.* **2003**, *125*, 12072. (b) Dias, H. V. R.; Diyabalanage, H. V. K.; Eldabaja, M. G.; Elbjeirami, O.; Rawashdeh-Omary, M. A.; Omary, M. A. *J. Am. Chem. Soc.* **2005***, 127,* 7489.

5 Burini, A.; Bravi, R.; Fackler, J. P., Jr.; Galassi, R; Grant, T. A.; Omary, M. A; Pietroni, B. R. ; Staples, R. J. *Inorg. Chem.* **2000**, *39*, 3158.

6 Yang, G.; Raptis, R. G. *Inorg. Chem.* **2003**, *42*, 261.

7 For reviews, see: (a) Burini, A.; Mohamed, A. A.; Fackler, J. P., Jr. *Comments Inorg. Chem.* **2003**, *24*, 253. (b) Omary, M. A.; Mohamed, A. A.; Rawashdeh-Omary, M. A.; Fackler, J. P., Jr. *Coord. Chem. Rev.* **2005**, *249*, 1372.

8 (a) Rawashdeh-Omary, M. A.; Omary, M. A.; Fackler, J. P., Jr.; Galassi, R.; Pietroni, B. R.; Burini, A. *J. Am. Chem. Soc.* **2001**, *123*, 9689. (b) Burini, A.; Fackler, J. P., Jr.; Galassi, R., Grant, T. A.; Omary, M. A.; Rawashdeh-Omary, M. A.; Pietroni, B. R.; Staples, R. J. *J. Am. Chem. Soc.* **2000**, *122,* 11264.

9 For reviews, see: (a) Pyykkö, P.; *Chem. Rev.*, **1997**, *97*, 597. (b) Pyykkö, P. *Angew. Chem. Int. Ed.* **2004**, *43*, 4412.

10 Mendizabal, F.; Pyykkö, P.; Runeberg, N. *Chem. Phys. Lett.*, **2003**, *370*, 733.

11 (a) Merz, K. M., Jr.; Hoffmann, R. *Inorg. Chem.* **1988**, *27*, 2120. (b) Jiang, Y.; Alvarez, S.; Hoffmann, R. *Inorg. Chem.* **1985**, *24*, 749. (c) Mehrotra, P. K.; Hoffmann, R. *Inorg. Chem.* **1978**, *17*, 2187. (d) Dedieu, A.; Hoffmann, R. *J. Am. Chem. Soc.* **1978**, *100*, 2074.

12 Carvajal, M. A.; Alvarez, S.; Novoa, J. J. *Chem. Eur. J.* **2004**, *10*, 2117.

13 Poblet, J. M.; Bénard, M. *Chem. Commun.*, **1998**, 1179.

14 Vorontsov, I. I.; Kovalevsky, A. Y.; Chen, Y.-S.; Graber, T.; Gembicky, M.; Novozhilova, I. V.; Omary, M. A.; Coppens, P. *Phys. Rev. Lett.* **2005**, *94*, 193003

15 Allen, F. H. *Acta Crystallogr.*, *Sect. B* **2002**, *58*, 380.

16 *Jaguar*, version 5.5; Schrodinger, Inc.: Portland, OR (www.schrodinger.com).

17 Cundari, T. R.; Stevens, W. J.; Sommerer, S. O. *J. Chem. Phys.*, **1993**, *98*, 5555.

18 Sæbø, S.; Pulay, P. *Theor. Chim. Acta* **1986**, *69*, 357.

19 Boys, S.; Bernardi, F. *Mol. Phys.*, **1970**, *90*, 553.

20 Sæbø, S.; Tong, W. *J. Chem. Phys.*, **1993**, *98*, 2170.

21 Ehlert, M. K.; Rettig, S. J.; Storr, A.; Thompson, R. C.; Trotter, J. *Can. J. Chem.* **1990**, *68*, 1444.

22 Fujisawa, K.; Ishikawa, Y.; Miyashita, Y.; Okamoto, K.-I. *Chem. Lett.* **2004**, *33*, 66.

23 (a) Singh, K.; Long, J. R.; Stavropoulos, P. *J. Am. Chem. Soc.* **1997**, *119*, 2942. (b) Singh, K.; Long, J. R.; Stavropoulos, P. *Inorg. Chem.* **1998**, *37*, 1073.

24 Pyykkö, P.; Runeberg, N.; Mendizabal, F. *Chem. Eur J.*, **1997**, *3*, 1451.

25 Omary, M. A.; Sinha, P.; Bagus, P. S.; Wilson, A. K. *J. Phys. Chem. A* **2005***, 109,* 690.

26 See, for example, Table 5 in: Omary, M. A.; Webb, T. R.; Assefa, Z.; Shankle, G. E.; Patterson. H. H. *Inorg. Chem*. **1998**, *37*, 1380, and Tables 3 - 4 and Figure 9 in: Rawashdeh-Omary, M. A.; Omary, M. A.; Patterson, H. H. *J. Am. Chem. Soc.* **2000**, *122,* 10371.

27 Burdett, J. *Molecular Shapes*; John Wiley & Sons: New York, NY, 1980; p 173.

28 (a) Hollingsworth, G.; Barrie, J. D.; Dunn, B.; Zink, J. I. *J. Am. Chem. Soc.* **1988**, *110*, 6569. (b) Barrie, J. D.; Dunn, B.; Holilingsworth, G.; Zink, J. I. *J. Phys. Chem*. **1989**, 93, 3958.

29 (a) Clodfelter, S. A.; Doede, T. M.; Brennan, B. A.; Nagle, J. K.; Bender, D. P.; Turner, W. A.; LaPunzia, P. M. *J. Am. Chem. Soc.* **1994**, *116*, 11379. (b) Nagle, J. K.; Brennan, B. A. *J. Am. Chem. Soc.* **1988**, *110*, 5931.

30 (a) White-Morris, R. L.; Olmstead, M. M.; Jiang, F.; Tinti, D. S.; Balch, A. L. *J. Am. Chem. Soc.* **2002**, *124*, 2327. (b) White-Morris, R. L.; Olmstead, M. M.; Jiang, F.; Balch, A. L. *Inorg. Chem.* **2002**, *41*, 2313.

31 (a) Omary, M. A.; Patterson, H. H. *J. Am. Chem. Soc.* **1998**, *120*, 7696. (b) Rawashdeh, M. A.; Omary, M. A.; Patterson, H. H.; Fackler, J. P., Jr. *J. Am. Chem. Soc.* **2001**, *123,* 11237.

32 Winter, M. *WebElements (Professional Edition).* http://www.webelements.com/

33 Moore, C.E. *Atomic Energy Levels*; Nat. Bur. Stand.: Washington, 1958; Vol. III.

34 (a) Labinger, J. A.; Bercaw, J. E. *Nature* **2002**, *417*, 507. (b) Arndtsen, B. A.; Bergman, R. G.; Mobley, T. A.; Peterson, T. H. *Acc. Chem. Res.* **1995**, *28*, 154. (c) Jones, W. D.; Feher, F. J. *Acc. Chem. Res.* **1989**, *22*, 91. (d) Crabtree, R. H. *Chem. Rev.* **1985**, *85*, 245. (e) Crabtree, R. H. *Chem. Rev.* **1995**, *95*, 987. (f) *Activation and Functionalization of C-H Bonds*; Goldberg, K.I., Goldman, A.S., Eds.; ACS Symposium Series 885; American Chemical Society: Washington, D.C., **2004** (g) Guari, Y.; Sabo-Etienne, S.; Chaudret, B. *Eur. J. Inorg. Chem.* **1999**, 1047. (h) Jones, W. D.; *Acc. Chem. Res.* **2003**, *36*, 140.

35 (a) Sen, A. *Acc. Chem. Res.* **1998**, *31*, 550. (b) Crabtree, R. H. *J. Chem. Soc., Dalton Trans.* **2001**, 2437. (c) Periana, R. A.; Bhalla, G.; Tenn, W. J., III; Young,

K. J. H.; Liu, X. Y.; Mironov, O.; Jones, C. J.; Ziatdinov, V. R. *J. Mol. Catal. A* **2004**, *220*, 7. (d) Goj, L. A.; Gunnoe, T. B. *Curr. Org. Chem.* **2005**, *9*, 671. (e) Ritleng, V.; Sirlin, C.; Pfeffer, M. *Chem. Rev.* **2002**, *102*, 1731. (f) Dyker, G. *Angew. Chem. Int. Ed.* **1999**, *38*, 1698.

36 (a) Belli, J.; Jensen, C. M. *Organometallics* **1996**, *15*, 1532. (b) Zhu, K.; Achord, P. D.; Zhang, X.; Krogh-Jespersen, K.; Goldman, A. S. *J. Am. Chem. Soc.* **2004**, *126*, 13044. (c) Renkema, K. B.; Kissin, Y. V.; Goldman, A. S. Journal *J. Am. Chem. Soc.* **2003**, *125*, 7770. (d) Krogh-Jespersen, K.; Czerw, M.; Summa, N.; Renkema, K. B.; Achord, P. D.; Goldman, A. S. *J. Am. Chem. Soc.* **2002**, *124*, 11404. (e) Kanzelberger, M.; Singh, B.; Czerw, M.; Krogh-Jespersen, K.; Goldman, A. S. *J. Am. Chem. Soc.* **2000**, *122*, 11017. (f) Liu, F.; Pak, E. B.; Singh, B.; Jensen, C. M.; Goldman, A. S. *J. Am. Chem. Soc.* **1999**, *121*, 4086.

37 Liu, F.; Pak, E. B.; Singh, B.; Jensen, C. M.; Goldman, A. S. *J. Am. Chem. Soc.* **1999**, *121*, 4086.

38 Renkema, K. B.; Kissin, Y. V.; Goldman, A. S. *J. Am. Chem. Soc.* **2003**, *125*, 7770.

39 Goldman, A. S.; Roy, A. H.; Huang, Z.; Ahuja, R.; Schinski, W.; Brookhart, M. *Science* **2006**, *312*, 257.

40 (a) Sadow, A. D.; Tilley, T. D. 224th ACS National Meeting, Boston, MA, August 18-22, 2002, INOR-563. (b) Sadow, A. D.; Tilley, T. D. *J. Am. Chem. Soc.* **2005**, *127*, 643.

41 (a) Chen, H.; Schlecht, S.; Semple, T. C.; Hartwig, J. F. *Science* **2000**, *287*, 1995. (b) Webster, C. E.; Fan, Y.; Hall, M. B.; Kunz, D.; Hartwig, J. F. *J. Am. Chem. Soc.* **2003**, *125*, 858.

42 (a) Periana, R. A.; Taube, D. J.; Gamble, S.; Taube, H.; Satoh, T.; Fujii, H. *Science* **1998**, *280*, 560. (b) Periana, R. A.; Taube, D. J.; Evitt, E. R.; Loffler, D. G.; Wentrcek, P. R.; Voss, G.; Masuda, T. *Science* **1993**, *253*, 340. (c) Shilov, A. E.; Shul'pin, G. B. *Chem. Rev.* **1997**, *97*, 2879. (d) Lin, M.; Chen, S.; Garcia-Zayas, E. A.; Sen, A. *J. Am. Chem. Soc.* **2001**, *123*, 1000. (e) Jones, C. J.; Taube, D. J.; Ziatdinov, V. R.; Periana, R. A.; Nielsen, R. J.; Oxgaard, J.; Goddard, W.A., III *Angew. Chem., Int. Ed.* **2004**, *43*, 4626. (f) Xu, X.; Fu, G.; Goddard, W. A., III; Periana, R. A. *Studies Surf. Sci. Catal.* **2004**, *147*, 499. (g) Stahl, S.; Labinger, J. A.; Bercaw, J. E. *Angew. Chem., Int. Ed.* **1998**, *37*, 2181. (h) Shilov, A. E.; Shteinman, A. A. *Acc. Chem. Res.* **1999**, *32*, 763. (i) Periana, R. A.; Ortmann, D. A.; Dagmara, A.; Mironov, O. A. 224th ACS National Meeting,

Boston, MA, August 18-22, **2002**, INOR-465. (j) Kua, J.; Xu, X.; Periana, R. A.; Goddard, W. A., III *Organometallics* **2002**, *21*, 511. (k) Periana, R. A.; Ortmann, D. A. 223rd ACS National Meeting, Orlando, FL, April 7-11, **2002**, INOR-157.

43 Vedernikov, A. N.; Caulton, K. G. *Chem. Comm.* **2004**, *2*, 162.

44 (a) Jones, W. D. *Acc. Chem. Res.* **2003**, *36*, 140. (b) Jones, W. D.; Feher, F. J. *Acc. Chem. Res.* **1989**, *22*, 91.

45 Cundari, T.R. *J. Am. Chem. Soc.* **1994**, *116*, 340.

46 Oxgaard, J.; Muller, R. P.; Goddard, W. A., III,; Periana, R. A. *J. Am. Chem. Soc.* **2004**, *126*, 352.

47 (a) Thompson, M. E.; Baxter, S. M.; Bulls, A. R.; Burger, B. J.; Nolan, M. C.; Santarsiero, B. D.; Schaefer, W. P.; Bercaw, J. E. *J. Am. Chem. Soc.* **1987**, *109*, 203. (b) Lam, W. H.; Jia, G.; Lin, Z.; Lau, C. P., Eisenstein, O.; *Chem. Eur. J.* **2003**, *9*, 2775.

48 (a) Tenn, W. J., III; Young, K. J. H.; Bhalla, G.; Oxgaard, J.; Goddard, W. A., III; Periana, R. A. *J. Am. Chem. Soc.* **2005**, *127*, 14172. (b) Feng, Y.; Lail, M.; Barakat, K. A.; Cundari, T. R.; Gunnoe, T. B.; Petersen, J. L. *J. Am. Chem. Soc.* **2005**, 127, 14174. (c) Feng, Y.; Lail, M.; Foley, N. A.; Gunnoe, T. B.; Barakat, K. A.; Cundari, T. R.; Petersen, J. L. *J. Am. Chem. Soc.* **2006**, *128*, 7982.

49 (a) Cummins, C. C.; Baxter, S. M.; Wolczanski, P. T. *J. Am. Chem. Soc.* **1988**, *110*, 8731. (b) Cummins, C. C.; Schaller, C. P.; Van Duyne, G. D.; Wolczanski, P. T.; Chan, A. W. E.; Hoffmann, R. *J. Am. Chem. Soc.* **1991**, *113*, 2985. (c) Schaller, C. P.; Wolczanski, P. T. *Inorg. Chem.* ***1993***, *32*, 131. (d) Bennett, J. L.; Wolczanski, P. T. *J. Am. Chem. Soc.* **1994**, *116*, 2179. (e) Schaller, C. P.; Bonanno, J. B.; Wolczanski, P. T. *J. Am. Chem. Soc.* **1994**, *116*, 4133. (f) Schaller, C. P.; Cummins, C. C.; Wolczanski, P. T. *J. Am. Chem. Soc.* **1996**, *118*, 591. (g) Bennett, J. L.; Wolczanski, P. T. *J. Am. Chem. Soc.* **1997**, *119*, 10696. (h) Schafer, D. F., II; Wolczanski, P. T. *J. Am. Chem. Soc.* **1998**, *120*, 4881. (i) Slaughter, L. M.; Wolczanski, P. T.; Klinckman, T. R.; Cundari, T. R. *J. Am. Chem. Soc.* **2000**, *122*, 7953. (j) Cundari, T. R.; Klinckman, T. R.; Wolczanski, P. T. *J. Am. Chem. Soc.* **2002**, *124*, 1481. (k) Cundari, T. R. *J. Am. Chem. Soc.* **1992**, *114*, 10557.

50 (a) Hoyt, H. M.; Michael, F. E.; Bergman, R. G. *J. Am. Chem. Soc.* **2004**, *126*, 1018. (b) Walsh, P. J.; Hollander, F. J.; Bergman, R. G. *J. Am. Chem. Soc.* **1988**, *110*, 8729.

51 (a) Braga, A. A. C.; Maseras, F.; Urbano, J.; Caballero, A.; Mar Diaz-Requejo, M.; Perez, P. J. *Organometallics* **2006**, *25*, 5292. (b) de Fremont, P.; Stevens, E. D.; Fructos, M. R.; Mar Diaz-Requejo, M.; Perez, P. J.; Nolan, S. P. *Chem. Comm.* **2006**, *19*, 2045. (c) Doyle, M. P. *J. Org. Chem.* **2006**, *71*, 9253. (d) Doyle, M. P. *Topics in Organometallic Chemistry* **2004**, 203.

52 Brown, S. N.; Mayer, J. M. *J. Am. Chem. Soc.* **1996**, *118*, 12119; Brown, S. N.; Mayer, J. M. *Organometallics* **1995**, *14*, 2951; Brown, S. N.; Mayer, J. M. *J. Am. Chem. Soc.* **1994**, *116*, 2219.

53 Conley, B. L.; Ganesh, S. K.; Gonzales, J. M.; Tenn, W. J., III; Young, K. J. H.; Oxgaard, J.; Goddard, W. A., III; Periana, R. A. *J. Am. Chem. Soc.* **2006**, *128*, 9018.

54 (a) Mayer, J. M. *Acc. Chem. Res.*, **1998**, *31*, 441. (b) Bryant, J. R.; Taves, J. E.; Mayer, J. M. *Inorg. Chem.* **2002**, *41*, 2769. (c) Larsen, A. S.; Wang, K.; Lockwood, M. A.; Rice, G. L.; Won, T. J.; Lovell, S.; SadЛek, M.; Tureček, F.; Mayer, J. M. *J. Am. Chem. Soc.* **2002**, *124*, 10113. (d) Jonas, R. T.; Stack, T. D. P. *J. Am. Chem. Soc.* **1997**, *119*, 8566. (e) Schilstra, M. J.; Veldink, G. A.; Vliegenthart, J. F. G. *Biochemistry* **1994**, *33*, 3974. (f) Goldsmith, C. R.; Jonas, R. T.; Stack, T. D. P. *J. Am. Chem. Soc.* **2002**, *124*, 83. (g) Mayer, J. M.; Made, E. A.; Roth, J. P.; Bryant, J. R.; Matsuo, T.; Dehestani, A.; Bales, B. C.; Watson, E. J.; Osako, T.; Vallient-Saunders, K.; Lam, W. H.; Hrovat, D. A.; Borden, W. T., Davidson, E. R. *J. Mol. Catal. A* **2006**, *251*, 24. (h) Roth, J. P.; Yoder, J. C.; Won, T. J.; Mayer, J. M. *Science* **2001**, *294*, 2524. (i) Mayer, J. M. *Annu. Rev. Phys. Chem.* **2004**, *55*, 363. (j) Bales, B.; Brown, P.; Dehestani, A.; Mayer, J. M. *J. Am. Chem. Soc.* **2005**, *127*, 2832. (k) *Biomimetic Oxidations Catalyzed by Transition Metal Complexes*; Meunier, B. Ed.; Imperial College Press: River Edge, NJ, **1999**.

55 (a) Eckert, N. A.; Vaddadi, S.; Stoian, S.; Flaschenriem, C. J.; Cundari, T. R.; Munck, E.; Holland, P. L. *Angew. Chem., Int. Ed.* **2006**, *45*, 6868. (b) Bach, T.; Korker, C. *Eur. J. Org. Chem.* **1998**, *5*, 1033. (c) Verma, A. K.; Nazif, T. N.; Achim, C.; Lee, S. C. *J. Am. Chem. Soc.* **2000**, *122*, 11013. (d) Brown, S. D.; Betley, T. A.; Peters, J. C. *J. Am. Chem. Soc.* **2003**, *125*, 322. (e) Betley, T. A.; Peters, J. C. *J. Am. Chem. Soc.* **2003**, *125*, 10782. (f) Jensen, M. P.; Mehn, N. P.; Que, L. *Angew. Chem. Int. Ed.* **2003**, *42*, 4357. (g) Brown, S. D.; Peters, J. C. *J. Am. Chem. Soc.* **2004**, *126*, 4538. (h) Bart, S. C.; Lobkovsky, E.; Bill, E.; Chirik, P. J. *J. Am. Chem. Soc.* **2006**, *128*, 5302. (i) Thyagarajan, S.; Shay, D. T.; Incarvito, C. D.; Rheingold, A. L.; Theopold, K. H. *J. Am. Chem. Soc,* **2003,** *125,* 4440. (j) Hu, X.; Meyer, K. *J. Am. Chem. Soc.* **2004**, *126*, 16322. (k) Jenkins, D. M.; Betley, T. A.; Peters, J. C. *J. Am. Chem. Soc.* **2002**, *124*, 11238.

(l) Kogut, E.; Wiencko, H. L.; Zhang, L.; Cordeau, D.; Warren, T. H. *J. Am. Chem. Soc.* **2005,** *127*, 11248. (m) Mindiola, D. J.; Hillhouse, G. L. *J. Am. Chem. Soc*. **2001**, *123*, 4623. (n) Mindiola, D. J.; Hillhouse, G. L. *Chem. Comm.* **2002**, *17*, 1840. (o) Waterman, R.; Hillhouse, G. L. *J. Am. Chem. Soc*. **2003**, *125*, 13350.

56 Au, S. M.; Huang, J. S.; Yu, W. Y.; Fung, W. H.; Che, C. M.; *J. Am. Chem. Soc.* **1999**, *121*, 9120.

57 Gunnoe, T. B.; *Eur. J. Inorg. Chem.* **2007**, 1185.

58 (a) Fulton, J. R.; Bouwkamp, M. W.; Bergman, R. G *J. Am. Chem. Soc.* **2000**, *122*, 8799. (b) Fulton. J. R.; Sklenak, S.; Bouwkamp, M. W.; Bergman, R. G. *J. Am. Chem. Soc.* **2002**, *124*, 4722. (c) Holland, A. W.; Bergman, R. G. *J. Am. Chem. Soc.* **2002**, *124*, 14684.

59 Fox, D. J.; Bergman, R. G. *Organometallics* **2004**, *23*, 1656.

60 (a) Jayaprakash, K. N.; Conner, D.; Gunnoe, T. B. *Organometallics* **2001**, *20*, 5254. (b) Conner, D.; Jayaprakash, K. N.; Gunnoe, T. B.; Boyle, P. D. *Inorg. Chem.* **2002**, *41*, 3042. (c) Conner, D.; Jayaprakash, K. N.; Wells, M. B.; Manzer, S.; Gunnoe, T. B.; Boyle, P. D. *Inorg. Chem.* **2003**, *42*, 4759. (d) Feng. Y.; Gunnoe, T. B.; Grimes, T. V.; Cundari, T. R. *Organometallics* **2006**, *25*, 5456.

61 Conner, D.; Jayaprakash, K. N.; Cundari, T. R.; Gunnoe, T. B.; *Organometallics* **2004**, *23*, 2724.

62 Zhang, J.; Gunnoe, T. B.; Petersen, J. L.; *Inorg. Chem.* **2005**, *44*, 2895.

63 Oxgaard, J.; Tenn, III, W. J.; Nielsen, R. J.; Periana, R. A.; Goddard, W. A., III; *Organometallics* **2007**, *26*, 1565.

64 Davies, D. L.; Donald, S. M. A.; Macgregor, S. A. *J. Am. Chem. Soc.* **2005**, *127*, 13754; Davies, D. L.; Donald, S. M. A.; Al-Duaij, O.; Macgregor, S. A.; Pölleth, M. *J. Am. Chem. Soc.* **2006**, *128*, 4210.

65 Becke, A. D. *J. Chem. Phys.* **1993**, *98*, 5648.

66 (a) Binkley, J. S.; Pople, J. A.; Hehre, W. J. *J. Am. Chem. Soc.* **1980**, *102*, 939. (b) Stevens, W. J.; Basch, H.; Krauss, M. *J. Chem. Phys.* **1984**, *81*, 6026. (c) Stevens, W. J.; Krauss, M.; Basch, H.; Jasien, P. G. *Can. J. Chem.* **1992**, *70*, 612.

67 Bergman, R. G.; Cundari, T. R.; Gillespie, A. M.; Gunnoe, T. B.; Harman, W. D.; Klinkman, T. R.; Temple, M. D.; White, D. P. *Organometallics* **2003**, *22*, 2331.

68 Bader, R.F.W.; *Atoms in Molecules – A Quantum Theory*, Oxford University Press, Oxford, **1990**.

69 Gaussian 03, Revision C.02, Frisch, M. J. *et al.* Gaussian, Inc., Wallingford CT, **2004**.

70 Schuchardt, K.L.; Didier, B.T.; Elsethagen, T.; Sun, L.; Gurumoorthi, V.; Chase, J.; Li, J.; Windus, T.L.; *J. Chem. Inf. Model* **2007**, 10.1021/ci600510j

71 Weinhold, F.; Landis, C. R. *Chem. Ed.: Research and Practice in Europe* **2001**, *2*, 91.

72 Foley, N. A.; Lail, M.; Lee, J. P.; Gunnoe, T. B.; Cundari, T. R.; Petersen, J. L. *J. Am. Chem. Soc.* **2007**, 129, 6765.

73 Grotjahn, D. B.; Sheridan, P. M.; Jihad, I. A.; Ziurys, L. M. *J. Am. Chem. Soc.* **2001**, *123*, 5489.

74 Linstrom, P. J., Mallard, W.G., Eds., *NIST Chemistry WebBook, NIST Standard Reference Database Number 69*, **2005**, National Institute of Standards and Technology, Gaithersburg MD, 20899 (http://webbook.nist.gov).

75 See, for example, Cundari, T. R.; Gordon, M. S. *J. Am. Chem. Soc.* **1993**, 115, 4210.

76 WebElements Scholar, http://www.webelements.com/, Accessed January **2007**.

77 Lail, M.; Bell, C. M.; Cundari, T. R.; Conner, D.; Gunnoe, T. B.; Petersen, J. L. *Organometallics* **2004**, *23*, 5007.

78 (a) Oxgaard, J.; Periana, R. A.; Goddard, W. A., III; *J. Am. Chem. Soc.* **2004**, *126*, 11658. (b) Oxgaard, J.; Goddard, W. A., III; *J. Am. Chem. Soc.* **2004**, *126*, 442.

79 (a) Sandoval, C. A.; Ohkuma, T.; Muniz, K.; Noyori, R.; J. Am. Chem. Soc. **2003**, *125*, 13490. (b) Murata, K.; Konishi, H.; Ito, M.; Ikariya, T.; Organometallics **2002**, *21*, 253. (c) Guo, R.; Morris, R. H.; Song, D.; J. Am. Chem. Soc. **2005**, *127*, 516. (d) Clapham, S. E.; Hadzovic, A.; Morris, R. H.; Coord. Chem. Rev. **2004**, *248*, 2201. (e) Abdur-Rashid, K.; Clapham, S. E.; Hadzovic, A.; Harvey, J. N.; Lough, A. J.; Morris, R. H.; J. Am. Chem. Soc. **2002**, *124*, 15104. (f) Abdur-

Rashid, K.; Faatz, M.; Lough, A. J.; Morris, R. H.; J. Am. Chem. Soc. **2001**, *123*, 7473. (g) Heiden, Z. M.; Rauchfuss, T. B.; J. Am. Chem. Soc. **2006**, *128*, 13048. (h) Fryzuk, M. D.; Montgomery, C. D.; Rettig, S. J.; Organometallics **1991**, *10*, 467.

80 Brink, G. J.; Arends, I. W. C. E.; Sheldon, R. A. *Chem. Rev.* **2004**, *104*, 4105.

81 (a) Martin, J. M. L.; de Oliveira, G.; J. Chem. Phys. **111**, 5 (1999). (b) Boese, A. D.; Oren, M.; Atasoylu, O.; Martin, J. M. L.; Kállay, M.; Gauss, J.; J. Chem. Phys. **120**, 9 (2004). (c) Karton, A.; Rabinovich, E.; Martin, J. M. L.; Ruscic, B.; J. Chem. Phys. **125**, 144108 (2006).

82 Tajti, A.; Szalay, P. G.; Császár, A. G.; Kállay, M.; Gauss, J.; Valeev, E. F.; Flowers, B. A.; Vázquez, J.; Stanton, J. F.; J. Chem. Phys. **121**, 23 (2004).

83 (a) DeYonker, N. J.; Cundari, T. R.; Wilson, A. K.; J. Chem. Phys. **124**, 114104 (2006). (b) DeYonker, N. J.; Grimes, T. V.; Yockel, S.; Dinescu, A.; Mintz, B.; Cundari, T. R.; Wilson, A. K.; J. Chem. Phys. **125**, 104111 (2006).

84 Blowers, P.; Zheng, X.; Homan, K.; Chem. Eng. Comm. **190**, 1233 (2003).

85 Althorpe, S. C.; Clary, D. C.; Annu. Rev. Phys. Chem. **54**, 493 (2003).

86 Fernández-Ramos, A.; Miller, J. A.; Klippenstein, S. J.; Truhlar, D. G.; Chem. Rev. **106**, 4518 (2006).

87 (a) Truong, T. N.; Evans, T. J.; J. Phys. Chem. **98**, 9558. (1994) (b) Corchado, J. C.; Espinosa-García, J.; Hu, W.-P.; Rossi, I.; Truhlar, D. G.; J. Phys. Chem. **99**, 687 (1995). (c) Corchado, J. C.; Espinosa-García, J.; Roberto-Neto, O.; Chuang, Y.-Y.; Truhlar, D. G.; J. Phys. Chem. A **102**, 4899 (1998). (d) Xu, Z.-F.; Li, S.-M.; Yu, Y.-X.; Li, Z.-S.; Sun, C.-C.; J. Phys. Chem. A **103**, 4910 (1999).

88 Zhao, Y.; González-García, N.; Truhlar, D. G.; J. Phys. Chem. A **109**, 2012 (2005).

89 Lynch, B. J.; Fast, P. L.; Harris, M.; Truhlar, D. G.; J. Phys. Chem. A **104**, 4811 (2000).

90 Baboul, A. G.; Curtiss, L. A.; Redfern, P. C.; Raghavachari, K.; J. Chem. Phys. **110**, 7650 (1999).

91 (a) Jodkowski, J. T.; Rayez, M.-T.; Rayez, J.-C.; Bércez, T.; Dóbé, S.; J. Phys. Chem. A **103**, 3750 (1999). (b) Hand, M. R.; Rodriquez, C. F.; Williams, I. H.;

Balint-Kurti, G. C.; J. Phys. Chem. A **102**, 5958 (1998). (c) Fridgen, T. D.; McMahon, T. B.; J. Phys. Chem. A **107**, 668 (2003). (d) Fast, P. L.; Sánchez, M. L.; Truhlar, D. G.; Chem. Phys. Lett. **306**, 407 (1999). (e) Bryukov, M. G.; Slagle, I. R.; Knyazev, V. D.; J. Phys. Chem. A **105**, 6900 (2001). (f) Basch, H.; Hoz, S.; J. Phys. Chem. A **101**, 4416 (1997). (g) So, S. P.; Chem. Phys. Lett. **313**, 307 (1999). (h) Schwartz, M.; Marshall, P.; Berry, R. J.; Ehlers, C. J.; Petersson, G. A.; J. Phys. Chem. A **102**, 10074 (1998). (i) Korchowiec, J.; Kawahara, S.; Matsumura, K.; Uchimaru, T.; Sugie, M.; J. Phys. Chem. A **103**, 3548 (1999). (j) Jursic, B. S.; Theochem **499**, 223 (2000). (k) Yu, X.; Li, S.-M.; Liu, J.-Y.; Xu, Z.-F.; Li, Z.-S.; Sun, C.-C.; J. Phys. Chem. A **103**, 6402 (1999). (l) Wang, B.; Hou, H.; Gu, Y.; J. Phys. Chem. A **105**, 156 (2001). (m) Yu, Y.-X.; Li, S.-M.; Xu, Z.-F.; Li, Z. S.; Sun, C.-C.; Chem. Phys. Lett. **302**, 281 (1999). (n) Xu, Z.-F.; Li, S.-M.; Yu, Y.-X.; Li, Z.-S.; Sun, C. C.; J. Phys. Chem. A **103**, 4910 (1999). (o) Pu, J.; Truhlar, D. G.; J. Phys. Chem. A **109**, 773 (2005). (p) Aliagas, I.; Gronert, S.; J. Phys. Chem. A **102**, 2609 (1998). (q) Goumri, A.; Rocha, J.-D. R.; Laakso, D.; Smith, C. E.; Marshall, P.; J. Phys. Chem. A **103**, 11328 (1999). (r) Goumri, A.; Rocha, J.-D. R.; Laakso, D.; Smith, C. E.; Marshall, P.; J. Chem. Phys. **101**, 9405 (1994). (s) Goumri, A.; Laakso, D.; Rocha, J.-D. R.; Smith, C. E.; Marshall, P.; J. Chem. Phys. **102**, 161 (1995).

92 Parthiban, S.; Oliveira, G.; Martin, J. M. L.; J. Phys. Chem. A **105**, 895 (2001).

93 Lynch, B. L.; Truhlar, D. G.; J. Phys. Chem. A **105**, 2936 (2001).

94 Curtiss, L. A.; Raghavachari, K.; Redfern, P. C.; Rassolov, V.; Pople, J. A.; J. Chem. Phys. **109**, 7764 (1998).

95 Martin, J. M. L.; Chem. Phys. Lett. **259**, 669 (1996).

96 Peterson, K. A.; Woon, D. E.; Dunning, Jr., T. H.; J. Chem. Phys. **100**, 7410 (1994).

97 Pople, J. A.; Head-Gordon, M.; Fox, D. J.; Raghavachari, K.; Curtiss, L. A.; J. Chem. Phys. **90**, 5622 (1989).

98 Zhao, Y.; González-García, N.; Truhlar, D. G.; J. Phys. Chem. A **109**, 2012 (2005).

99 Martin, J. M. L.; Oliveira, G.; J. Chem. Phys. **111**, 1843 (1999).

100 Parthiban, S.; Martin, J. M. L.; J. Chem. Phys. **114**, 6014 (2001).

101 Bauschlicher, C. W.; Chem. Phys. Lett. **246**, 40 (1995).

102 Johnson, B. G.; Gill, P. M. W.; Pople, J. A.; J. Chem. Phys. **98**, 5612 (1993).

103 (a) Fast, P. L.; Sanchez, M. L.; Truhlar, D. G.; Chem. Phys. Lett. **306**, 407 (1999). (b) Curtiss, L. A.; Redfern, P. C.; Raghavachari, K.; Rassolov, V.; Pople, J. A.; J. Chem. Phys. **110**, 4703 (1999). (c) Curtiss, L. A.; Raghavachari, K.; Redfern, P. C.; Rassolov, V.; Pople, J. A.; J. Chem. Phys. **109**, 7764 (1998).

104 Lynch, B. J.; Zhao, Y.; Truhlar, D. G.; http://comp.chem.umn.edu/database/

105 Montgomery, Jr., J. A.; Frisch, M. J.; Ochterski, J. W.; Petersson, G. A.; J. Chem. Phys. **110**, 2822 (1999).

106 Hammond, G. S.; J. Am. Chem. Soc. **77**, 334 (1955).

107 Agmon, N.; J. Chem. Soc., Faraday Trans. 2 **74**, 388 (1978).

108 Miller, A. R.; J. Am. Chem. Soc. **100**, 1984 (1978).

109 (a) Lee, W. T.; Masel, R. I.; J. Phys. Chem. A **102**, 2332 (1998). (b) Bulat, F. A.; Toro-Labbé, A.; J. Phys. Chem. A **107**, 3987 (2003).

110 van Mourik, T.; Wilson, A. K.; Peterson, K. A.; Woon, D. E.; Dunning, Jr., T. H.; "The Effect of Basis Set Superposition Error (BSSE) on the Convergence of Molecular Properties Calculated with the Correlation Consistent Basis Sets." In *Advances in Quantum Chemistry*, vol 31; Löwdin, P., Ed.; Academic Press: San Diego, CA, 1998; pp. 105-135.

111 Fast, P. L.; Sánchez, M. L.; Truhlar, D. G.; Chem. Phys. Lett. **306**, 407 (1999).

REFERENCES

Abdur-Rashid, K.; Clapham, S. E.; Hadzovic, A.; Harvey, J. N.; Lough, A. J.; Morris, R. H.; J. Am. Chem. Soc. **2002**, *124*, 15104.

Abdur-Rashid, K.; Faatz, M.; Lough, A. J.; Morris, R. H.; J. Am. Chem. Soc. **2001**, *123*, 7473.

Agmon, N.; J. Chem. Soc., Faraday Trans. 2 **74**, 388 (1978).

Aliagas, I.; Gronert, S.; J. Phys. Chem. A **102**, 2609 (1998).

Allen, F. H. *Acta Crystallogr.*, *Sect. B* **2002**, *58*, 380.

Althorpe, S. C.; Clary, D. C.; Annu. Rev. Phys. Chem. **54**, 493 (2003).

Arndtsen, B. A.; Bergman, R. G.; Mobley, T. A.; Peterson, T. H. *Acc. Chem. Res.* **1995**, *28*, 154.

Au, S. M.; Huang, J. S.; Yu, W. Y.; Fung, W. H.; Che, C. M.; *J. Am. Chem. Soc.* **1999**, *121*, 9120.

Baboul, A. G.; Curtiss, L. A.; Redfern, P. C.; Raghavachari, K.; J. Chem. Phys. **110**, 7650 (1999).

Bach, T.; Korker, C. *Eur. J. Org. Chem.* **1998**, *5*, 1033.

Bader, R.F.W.; *Atoms in Molecules – A Quantum Theory*, Oxford University Press, Oxford, **1990**.

Bales, B.; Brown, P.; Dehestani, A.; Mayer, J. M. *J. Am. Chem. Soc.* **2005**, *127*, 2832.

Barrie, J. D.; Dunn, B.; Holilingsworth, G.; Zink, J. I. *J. Phys. Chem*. **1989**, 93, 3958.

Bart, S. C.; Lobkovsky, E.; Bill, E.; Chirik, P. J. *J. Am. Chem. Soc.* **2006**, *128*, 5302.

Basch, H.; Hoz, S.; J. Phys. Chem. A **101**, 4416 (1997).

Bauschlicher, C. W.; Chem. Phys. Lett. **246**, 40 (1995).

Becke, A. D. *J. Chem. Phys.* **1993**, *98*, 5648.

Belli, J.; Jensen, C. M. *Organometallics* **1996**, *15*, 1532.

Bennett, J. L.; Wolczanski, P. T. *J. Am. Chem. Soc.* **1997**, *119*, 10696.

Bennett, J. L.; Wolczanski, P. T. *J. Am. Chem. Soc.* **1994**, *116*, 2179.

Bergman, R. G.; Cundari, T. R.; Gillespie, A. M.; Gunnoe, T. B.; Harman, W. D.; Klinkman, T. R.; Temple, M. D.; White, D. P. *Organometallics* **2003**, *22*, 2331.

Binkley, J. S.; Pople, J. A.; Hehre, W. J. *J. Am. Chem. Soc.* **1980**, *102*, 939.

Blowers, P.; Zheng, X.; Homan, K.; Chem. Eng. Comm. **190**, 1233 (2003).

Betley, T. A.; Peters, J. C. *J. Am. Chem. Soc.* **2003**, *125*, 10782.

Boese, A. D.; Oren, M.; Atasoylu, O.; Martin, J. M. L.; Kállay, M.; Gauss, J.; J. Chem. Phys. **120**, 9 (2004).

Boys, S.; Bernardi, F. *Mol. Phys.*, **1970**, *90*, 553.

Braga, A. A. C.; Maseras, F.; Urbano, J.; Caballero, A.; Mar Diaz-Requejo, M.; Perez, P. J. *Organometallics* **2006**, *25*, 5292.

Brink, G. J.; Arends, I. W. C. E.; Sheldon, R. A. *Chem. Rev.* **2004**, *104*, 4105.

Brown, S. D.; Betley, T. A.; Peters, J. C. *J. Am. Chem. Soc.* **2003**, *125*, 322.

Brown, S. D.; Peters, J. C. *J. Am. Chem. Soc.* **2004**, *126*, 4538.

Brown, S. N.; Mayer, J. M. *J. Am. Chem. Soc.* **1996**, *118*, 12119; Brown, S. N.; Mayer, J. M. *Organometallics* **1995**, *14*, 2951; Brown, S. N.; Mayer, J. M. *J. Am. Chem. Soc.* **1994**, *116*, 2219.

Bryant, J. R.; Taves, J. E.; Mayer, J. M. *Inorg. Chem.* **2002**, *41*, 2769.

Bryukov, M. G.; Slagle, I. R.; Knyazev, V. D.; J. Phys. Chem. A **105**, 6900 (2001).

Bulat, F. A.; Toro-Labbé, A.; J. Phys. Chem. A **107**, 3987 (2003).

Burdett, J. *Molecular Shapes*; John Wiley & Sons: New York, NY, 1980; p 173.

Burini, A.; Bravi, R.; Fackler, J. P., Jr.; Galassi, R; Grant, T. A.; Omary, M. A; Pietroni, B. R.; Staples, R. J. *Inorg. Chem.* **2000**, *39*, 3158.

Burini, A.; Fackler, J. P., Jr.; Galassi, R., Grant, T. A.; Omary, M. A.; Rawashdeh-Omary, M. A.; Pietroni, B. R.; Staples, R. J. *J. Am. Chem. Soc.* **2000**, *122,* 11264.

Burini, A.; Mohamed, A. A.; Fackler, J. P., Jr. *Comments Inorg. Chem.* **2003**, *24*, 253.

Carvajal, M. A.; Alvarez, S.; Novoa, J. J. *Chem. Eur. J.* **2004**, *10*, 2117.

Chen, H.; Schlecht, S.; Semple, T. C.; Hartwig, J. F. *Science* **2000**, *287*, 1995.

Clapham, S. E.; Hadzovic, A.; Morris, R. H.; Coord. Chem. Rev. **2004**, *248*, 2201.

Clodfelter, S. A.; Doede, T. M.; Brennan, B. A.; Nagle, J. K.; Bender, D. P.; Turner, W. A.; LaPunzia, P. M. *J. Am. Chem. Soc.* **1994**, *116*, 11379.

Conley, B. L.; Ganesh, S. K.; Gonzales, J. M.; Tenn, W. J., III; Young, K. J. H.; Oxgaard, J.; Goddard, W. A., III; Periana, R. A. *J. Am. Chem. Soc.* **2006**, *128*, 9018.

Conner, D.; Jayaprakash, K. N.; Cundari, T. R.; Gunnoe, T. B.; *Organometallics* **2004**, *23*, 2724.

Conner, D.; Jayaprakash, K. N.; Gunnoe, T. B.; Boyle, P. D. *Inorg. Chem.* **2002**, *41*, 3042.

Conner, D.; Jayaprakash, K. N.; Wells, M. B.; Manzer, S.; Gunnoe, T. B.; Boyle, P. D. *Inorg. Chem.* **2003**, *42*, 4759.

Corchado, J. C.; Espinosa-García, J.; Hu, W.-P.; Rossi, I.; Truhlar, D. G.; J. Phys. Chem. **99**, 687 (1995).

Corchado, J. C.; Espinosa-García, J.; Roberto-Neto, O.; Chuang, Y.-Y.; Truhlar, D. G.; J. Phys. Chem. A **102**, 4899 (1998).

Crabtree, R. H. *J. Chem. Soc., Dalton Trans.* **2001**, 2437.

Crabtree, R. H. *Chem. Rev.* **1995**, *95*, 987.

Crabtree, R. H. *Chem. Rev.* **1985**, *85*, 245.

Cummins, C. C.; Baxter, S. M.; Wolczanski, P. T. *J. Am. Chem. Soc.* **1988**, *110*, 8731.

Cummins, C. C.; Schaller, C. P.; Van Duyne, G. D.; Wolczanski, P. T.; Chan, A. W. E.; Hoffmann, R. *J. Am. Chem. Soc.* **1991**, *113*, 2985.

Cundari, T.R. *J. Am. Chem. Soc.* **1994**, *116*, 340.

Cundari, T. R. *J. Am. Chem. Soc.* **1992**, *114*, 10557.

Cundari, T. R.; Gordon, M. S. *J. Am. Chem. Soc.* **1993**, 115, 4210.

Cundari, T. R.; Klinckman, T. R.; Wolczanski, P. T. *J. Am. Chem. Soc.* **2002**, *124*, 1481.

Cundari, T. R.; Stevens, W. J.; Sommerer, S. O. *J. Chem. Phys.*, **1993**, *98*, 5555.

Curtiss, L. A.; Raghavachari, K.; Redfern, P. C.; Rassolov, V.; Pople, J. A.; J. Chem. Phys. **109**, 7764 (1998).

Curtiss, L. A.; Redfern, P. C.; Raghavachari, K.; Rassolov, V.; Pople, J. A.; J. Chem. Phys. **110**, 4703 (1999).

Davies, D. L.; Donald, S. M. A.; Macgregor, S. A. *J. Am. Chem. Soc.* **2005**, *127*, 13754; Davies, D. L.; Donald, S. M. A.; Al-Duaij, O.; Macgregor, S. A.; Pölleth, M. *J. Am. Chem. Soc.* **2006**, *128*, 4210.

Dedieu, A.; Hoffmann, R. *J. Am. Chem. Soc.* **1978**, *100*, 2074.

de Fremont, P.; Stevens, E. D.; Fructos, M. R.; Mar Diaz-Requejo, M.; Perez, P. J.; Nolan, S. P. *Chem. Comm.* **2006**, *19*, 2045.

DeYonker, N. J.; Cundari, T. R.; Wilson, A. K.; J. Chem. Phys. **124**, 114104 (2006).

DeYonker, N. J.; Grimes, T. V.; Yockel, S.; Dinescu, A.; Mintz, B.; Cundari, T. R.; Wilson, A. K.; J. Chem. Phys. **125**, 104111 (2006).

DeYonker, N. J.; Ho, D. S.; Wilson, A.K.; and Cundari, T. R.; *J. Phys. Chem. A,* **2007**, *26*, 910.

DeYonker, N. J.; Peterson, K. A.; Steyl, G.; Wilson, A. K.; and Cundari, T. R.; J. Phys. Chem. A *in press* (2007).

Dias, H. V. R.; Diyabalanage, H. V. K.; Eldabaja, M. G.; Elbjeirami, O.; Rawashdeh-Omary, M. A.; Omary, M. A. *J. Am. Chem. Soc.* **2005***, 127,* 7489.

Dias, H. V. R.; Diyabalanage, H. V. K.; Rawashdeh-Omary, M. A.; Franzman, M. A.; Omary, M. A. *J. Am. Chem. Soc.* **2003**, *125*, 12072.

Doyle, M. P. *J. Org. Chem.* **2006**, *71*, 9253. (d) Doyle, M. P. *Topics in Organometallic Chemistry* **2004**, 203.

Dunning, Jr., T. H.; J. Chem. Phys. **90**, 1007 (1989).

Dunning, Jr., T. H.; Peterson, K. A.; Wilson, A. K.; J. Chem. Phys. **114**, 9244 (2001).

Dyker, G. *Angew. Chem. Int. Ed.* **1999**, *38*, 1698.

Eckert, N. A.; Vaddadi, S.; Stoian, S.; Flaschenriem, C. J.; Cundari, T. R.; Munck, E.; Holland, P. L. *Angew. Chem., Int. Ed.* **2006**, *45*, 6868.

Ehlert, M. K.; Rettig, S. J.; Storr, A.; Thompson, R. C.; Trotter, J. *Can. J. Chem.* **1990**, *68*, 1444.

Fast, P. L.; Sánchez, M. L.; Truhlar, D. G.; Chem. Phys. Lett. **306**, 407 (1999).

Feng. Y.; Gunnoe, T. B.; Grimes, T. V.; Cundari, T. R. *Organometallics* **2006**, *25*, 5456.

Feng, Y.; Lail, M.; Barakat, K. A.; Cundari, T. R.; Gunnoe, T. B.; Petersen, J. L. *J. Am. Chem. Soc.* **2005**, 127, 14174.

Feng, Y.; Lail, M.; Foley, N. A.; Gunnoe, T. B.; Barakat, K. A.; Cundari, T. R.; Petersen, J. L. *J. Am. Chem. Soc.* **2006**, *128*, 7982.

Fernández-Ramos, A.; Miller, J. A.; Klippenstein, S. J.; Truhlar, D. G.; Chem. Rev. **106**, 4518 (2006).

Foley, N. A.; Lail, M.; Lee, J. P.; Gunnoe, T. B.; Cundari, T. R.; Petersen, J. L. *J. Am. Chem. Soc.* **2007**, 129, 6765.

Fox, D. J.; Bergman, R. G. *Organometallics* **2004**, *23*, 1656.

Fridgen, T. D.; McMahon, T. B.; J. Phys. Chem. A **107**, 668 (2003).

Frisch, M. J. *et al.* Gaussian 03, Revision C.02, Gaussian, Inc., Wallingford CT, **2004**.

Fryzuk, M. D.; Montgomery, C. D.; Rettig, S. J.; Organometallics **1991**, *10*, 467.

Fujisawa, K.; Ishikawa, Y.; Miyashita, Y.; Okamoto, K.-I. *Chem. Lett.* **2004**, *33*, 66.

Fulton, J. R.; Bouwkamp, M. W.; Bergman, R. G *J. Am. Chem. Soc.* **2000**, *122*, 8799.

Fulton. J. R.; Sklenak, S.; Bouwkamp, M. W.; Bergman, R. G. *J. Am. Chem. Soc.* **2002**, *124*, 4722.

Goj, L. A.; Gunnoe, T. B. *Curr. Org. Chem.* **2005**, *9*, 671.

Goldberg, K.I., Goldman, A.S., Eds. *Activation and Functionalization of C-H Bonds*; ACS Symposium Series 885; American Chemical Society: Washington, D.C., **2004**.

Goldman, A. S.; Roy, A. H.; Huang, Z.; Ahuja, R.; Schinski, W.; Brookhart, M. *Science* **2006**, *312*, 257.

Goldsmith, C. R.; Jonas, R. T.; Stack, T. D. P. *J. Am. Chem. Soc.* **2002**, *124*, 83.

Goumri, A.; Laakso, D.; Rocha, J.-D. R.; Smith, C. E.; Marshall, P.; J. Chem. Phys. **102**, 161 (1995).

Goumri, A.; Rocha, J.-D. R.; Laakso, D.; Smith, C. E.; Marshall, P.; J. Phys. Chem. A **103**, 11328 (1999).

Goumri, A.; Rocha, J.-D. R.; Laakso, D.; Smith, C. E.; Marshall, P.; J. Chem. Phys. **101**, 9405 (1994).

Grotjahn, D. B.; Sheridan, P. M.; Jihad, I. A.; Ziurys, L. M. *J. Am. Chem. Soc.* **2001**, *123*, 5489.

Guari, Y.; Sabo-Etienne, S.; Chaudret, B. *Eur. J. Inorg. Chem.* **1999**, 1047.

Gunnoe, T. B.; *Eur. J. Inorg. Chem.* **2007**, 1185.

Guo, R.; Morris, R. H.; Song, D.; J. Am. Chem. Soc. **2005**, *127*, 516.

Hammond, G. S.; J. Am. Chem. Soc. **77**, 334 (1955).

Hand, M. R.; Rodriquez, C. F.; Williams, I. H.; Balint-Kurti, G. C.; J. Phys. Chem. A **102**, 5958 (1998).

Heiden, Z. M.; Rauchfuss, T. B.; J. Am. Chem. Soc. **2006**, *128*, 13048.

Ho, D. S.; DeYonker, N. J.; Wilson, A.K.; and Cundari, T. R.; J. Phys. Chem. A **110**, 31, (2006).

Holland, A. W.; Bergman, R. G. *J. Am. Chem. Soc.* **2002**, *124*, 14684.

Hollingsworth, G.; Barrie, J. D.; Dunn, B.; Zink, J. I. *J. Am. Chem. Soc.* **1988**, *110*, 6569.

Hoyt, H. M.; Michael, F. E.; Bergman, R. G. *J. Am. Chem. Soc.* **2004**, *126*, 1018.

Hu, X.; Meyer, K. *J. Am. Chem. Soc.* **2004**, *126*, 16322.

Jaguar, version 5.5; Schrodinger, Inc.: Portland, OR (www.schrodinger.com).

Jayaprakash, K. N.; Conner, D.; Gunnoe, T. B. *Organometallics* **2001**, *20*, 5254.

Jenkins, D. M.; Betley, T. A.; Peters, J. C. *J. Am. Chem. Soc.* **2002**, *124*, 11238.

Jensen, M. P.; Mehn, N. P.; Que, L. *Angew. Chem. Int. Ed.* **2003**, *42*, 4357.

Jiang, Y.; Alvarez, S.; Hoffmann, R. *Inorg. Chem.* **1985**, *24*, 749.

Jodkowski, J. T.; Rayez, M.-T.; Rayez, J.-C.; Bércez, T.; Dóbé, S.; J. Phys. Chem. A **103**, 3750 (1999).

Johnson, B. G.; Gill, P. M. W.; Pople, J. A.; J. Chem. Phys. **98**, 5612 (1993).

Jonas, R. T.; Stack, T. D. P. *J. Am. Chem. Soc.* **1997**, *119*, 8566.

Jones, W. D. *Acc. Chem. Res.* **2003**, *36*, 140.

Jones, W. D.; Feher, F. J. *Acc. Chem. Res.* **1989**, *22*, 91.

Jones, C. J.; Taube, D. J.; Ziatdinov, V. R.; Periana, R. A.; Nielsen, R. J.; Oxgaard, J.; Goddard, W.A., III *Angew. Chem., Int. Ed.* **2004**, *43*, 4626.

Jursic, B. S.; Theochem **499**, 223 (2000).

Kanzelberger, M.; Singh, B.; Czerw, M.; Krogh-Jespersen, K.; Goldman, A. S. *J. Am. Chem. Soc.* **2000**, *122*, 11017.

Karton, A.; Rabinovich, E.; Martin, J. M. L.; Ruscic, B.; J. Chem. Phys. **125**, 144108 (2006).

Kendall, R. A.; Dunning, Jr., T. H.; Harrison, R. J.; J. Chem. Phys. **96**, 6796 (1992).

Kogut, E.; Wiencko, H. L.; Zhang, L.; Cordeau, D.; Warren, T. H. *J. Am. Chem. Soc.* **2005,** *127*, 11248.

Korchowiec, J.; Kawahara, S.; Matsumura, K.; Uchimaru, T.; Sugie, M.; J. Phys. Chem. A **103**, 3548 (1999).

Krogh-Jespersen, K.; Czerw, M.; Summa, N.; Renkema, K. B.; Achord, P. D.; Goldman, A. S. *J. Am. Chem. Soc.* **2002**, *124*, 11404.

Kua, J.; Xu, X.; Periana, R. A.; Goddard, W. A., III *Organometallics* **2002**, *21*, 511.

Labinger, J. A.; Bercaw, J. E. *Nature* **2002**, *417*, 507.

Lail, M.; Bell, C. M.; Cundari, T. R.; Conner, D.; Gunnoe, T. B.; Petersen, J. L. *Organometallics* **2004**, *23*, 5007.

Lam, W. H.; Jia, G.; Lin, Z.; Lau, C. P., Eisenstein, O.; *Chem. Eur. J.* **2003**, *9*, 2775.

Larsen, A. S.; Wang, K.; Lockwood, M. A.; Rice, G. L.; Won, T. J.; Lovell, S.; SadЛek, M.; Tureček, F.; Mayer, J. M. *J. Am. Chem. Soc.* **2002**, *124*, 10113.

Lee, W. T.; Masel, R. I.; J. Phys. Chem. A **102**, 2332 (1998).

Lin, M.; Chen, S.; Garcia-Zayas, E. A.; Sen, A. *J. Am. Chem. Soc.* **2001**, *123*, 1000.

Linstrom, P. J., Mallard, W.G., Eds., *NIST Chemistry WebBook, NIST Standard Reference Database Number 69*, **2005**, National Institute of Standards and Technology, Gaithersburg MD, 20899 (http://webbook.nist.gov).

Liu, F.; Pak, E. B.; Singh, B.; Jensen, C. M.; Goldman, A. S. *J. Am. Chem. Soc.* **1999**, *121*, 4086.

Lynch, B. J.; Fast, P. L.; Harris, M.; Truhlar, D. G.; J. Phys. Chem. A **104**, 4811 (2000).

Lynch, B. L.; Truhlar, D. G.; J. Phys. Chem. A **105**, 2936 (2001).

Lynch, B. J.; Zhao, Y.; Truhlar, D. G.; http://comp.chem.umn.edu/database/

Martin, J. M. L.; Chem. Phys. Lett. **259**, 669 (1996).

Martin, J. M. L.; de Oliveira, G.; J. Chem. Phys. **111**, 5 (1999).

Martin, J. M. L.; Oliveira, G.; J. Chem. Phys. **111**, 1843 (1999).

Mayer, J. M. *Annu. Rev. Phys. Chem.* **2004**, *55*, 363.

Mayer, J. M. *Acc. Chem. Res.*, **1998**, *31*, 441.

Mayer, J. M.; Made, E. A.; Roth, J. P.; Bryant, J. R.; Matsuo, T.; Dehestani, A.; Bales, B. C.; Watson, E. J.; Osako, T.; Vallient-Saunders, K.; Lam, W. H.; Hrovat, D. A.; Borden, W. T., Davidson, E. R. *J. Mol. Catal. A* **2006**, *251*, 24.

Mehrotra, P. K.; Hoffmann, R. *Inorg. Chem.* **1978**, *17*, 2187.

Mendizabal, F.; Pyykkö, P.; Runeberg, N. *Chem. Phys. Lett.*, **2003**, *370*, 733.

Merz, K. M., Jr.; Hoffmann, R. *Inorg. Chem.* **1988**, *27*, 2120.

Meunier, B. Ed.; *Biomimetic Oxidations Catalyzed by Transition Metal Complexes*; Imperial College Press: River Edge, NJ, **1999**.

Miller, A. R.; J. Am. Chem. Soc. **100**, 1984 (1978).

Mindiola, D. J.; Hillhouse, G. L. *Chem. Comm.* **2002**, *17*, 1840.

Mindiola, D. J.; Hillhouse, G. L. *J. Am. Chem. Soc*. **2001**, *123*, 4623.

Montgomery, Jr., J. A.; Frisch, M. J.; Ochterski, J. W.; Petersson, G. A.; J. Chem. Phys. **110**, 2822 (1999).

Moore, C.E. *Atomic Energy Levels*; Nat. Bur. Stand.: Washington, 1958; Vol. III.

Murata, K.; Konishi, H.; Ito, M.; Ikariya, T.; Organometallics **2002**, *21*, 253.

Nagle, J. K.; Brennan, B. A. *J. Am. Chem. Soc.* **1988**, *110*, 5931.

Omary, M. A.; Mohamed, A. A.; Rawashdeh-Omary, M. A.; Fackler, J. P., Jr. *Coord. Chem. Rev.* **2005**, *249*, 1372.

Omary, M. A.; Patterson, H. H. *J. Am. Chem. Soc.* **1998**, *120*, 7696.

Omary, M. A.; Rawashdeh-Omary, M. A.; Gonser, M. W. A.; Elbjeirami, O.; Grimes, T.; Cundari, T. R.; Diyabalanage, H, V. K.; Palehepitiya Gamage, C. S.; Dias, H. V. R. *Inorg. Chem.* **2005***, 44*, 8200.

Omary, M. A.; Sinha, P.; Bagus, P. S.; Wilson, A. K. *J. Phys. Chem. A* **2005***, 109,* 690.

Omary, M. A.; Webb, T. R.; Assefa, Z.; Shankle, G. E.; Patterson. H. H. *Inorg. Chem*. **1998**, *37*, 1380

Oxgaard, J.; Goddard, W. A., III; *J. Am. Chem. Soc.* **2004**, *126*, 442.

Oxgaard, J.; Muller, R. P.; Goddard, W. A., III,; Periana, R. A. *J. Am. Chem. Soc.* **2004**, *126*, 352.

Oxgaard, J.; Periana, R. A.; Goddard, W. A., III; *J. Am. Chem. Soc.* **2004**, *126*, 11658.

Oxgaard, J.; Tenn, III, W. J.; Nielsen, R. J.; Periana, R. A.; Goddard, W. A., III; *Organometallics* **2007**, *26*, 1565.

Parthiban, S.; Martin, J. M. L.; J. Chem. Phys. **114**, 6014 (2001).

Parthiban, S.; Oliveira, G.; Martin, J. M. L.; J. Phys. Chem. A **105**, 895 (2001).

Periana, R. A.; Bhalla, G.; Tenn, W. J., III; Young, K. J. H.; Liu, X. Y.; Mironov, O.; Jones, C. J.; Ziatdinov, V. R. *J. Mol. Catal. A* **2004**, *220*, 7.

Periana, R. A.; Ortmann, D. A. 223rd ACS National Meeting, Orlando, FL, April 7-11, **2002**, INOR-157.

Periana, R. A.; Ortmann, D. A.; Dagmara, A.; Mironov, O. A. 224th ACS National Meeting, Boston, MA, August 18-22, **2002**, INOR-465.

Periana, R. A.; Taube, D. J.; Evitt, E. R.; Loffler, D. G.; Wentrcek, P. R.; Voss, G.; Masuda, T. *Science* **1993**, *253*, 340.

Periana, R. A.; Taube, D. J.; Gamble, S.; Taube, H.; Satoh, T.; Fujii, H. *Science* **1998**, *280*, 560.

Peterson, K. A.; Woon, D. E.; Dunning, Jr., T. H.; J. Chem. Phys. **100**, 7410 (1994).

Poblet, J. M.; Bénard, M. *Chem. Commun.*, **1998**, 1179.

Pople, J. A.; Head-Gordon, M.; Fox, D. J.; Raghavachari, K.; Curtiss, L. A.; J. Chem. Phys. **90**, 5622 (1989).

Pu, J.; Truhlar, D. G.; J. Phys. Chem. A **109**, 773 (2005).

Pyykkö, P. *Angew. Chem. Int. Ed.* **2004**, *43*, 4412.

Pyykkö, P.; *Chem. Rev.*, **1997**, *97*, 597.

Pyykkö, P.; Runeberg, N.; Mendizabal, F. *Chem. Eur J.*, **1997**, *3*, 1451.

Rawashdeh, M. A.; Omary, M. A.; Patterson, H. H.; Fackler, J. P., Jr. *J. Am. Chem. Soc.* **2001**, *123,* 11237.

Rawashdeh-Omary, M. A.; Omary, M. A.; Fackler, J. P., Jr.; Galassi, R.; Pietroni, B. R.; Burini, A. *J. Am. Chem. Soc.* **2001**, *123*, 9689.

Rawashdeh-Omary, M. A.; Omary, M. A.; Patterson, H. H. *J. Am. Chem. Soc.* **2000**, *122,* 10371.

Renkema, K. B.; Kissin, Y. V.; Goldman, A. S. Journal *J. Am. Chem. Soc.* **2003**, *125*, 7770.

Ritleng, V.; Sirlin, C.; Pfeffer, M. *Chem. Rev.* **2002**, *102*, 1731.

Roth, J. P.; Yoder, J. C.; Won, T. J.; Mayer, J. M. *Science* **2001**, *294*, 2524.

Sadow, A. D.; Tilley, T. D. 224th ACS National Meeting, Boston, MA, August 18-22, 2002, INOR-563.

Sadow, A. D.; Tilley, T. D. *J. Am. Chem. Soc.* **2005**, *127*, 643.

Sæbø, S.; Pulay, P. *Theor. Chim. Acta* **1986**, *69*, 357.

Sæbø, S.; Tong, W. *J. Chem. Phys.*, **1993**, *98*, 2170.

Sandoval, C. A.; Ohkuma, T.; Muniz, K.; Noyori, R.; J. Am. Chem. Soc. **2003**, *125*, 13490.

Schafer, D. F., II; Wolczanski, P. T. *J. Am. Chem. Soc.* **1998**, *120*, 4881.

Schaller, C. P.; Bonanno, J. B.; Wolczanski, P. T. *J. Am. Chem. Soc.* **1994**, *116*, 4133.

Schaller, C. P.; Cummins, C. C.; Wolczanski, P. T. *J. Am. Chem. Soc.* **1996**, *118*, 591.

Schaller, C. P.; Wolczanski, P. T. *Inorg. Chem.* ***1993***, *32*, 131.

Schilstra, M. J.; Veldink, G. A.; Vliegenthart, J. F. G. *Biochemistry* **1994**, *33*, 3974.

Schuchardt, K.L.; Didier, B.T.; Elsethagen, T.; Sun, L.; Gurumoorthi, V.; Chase, J.; Li, J.; Windus, T.L.; *J. Chem. Inf. Model* **2007**, 10.1021/ci600510j

Schwartz, M.; Marshall, P.; Berry, R. J.; Ehlers, C. J.; Petersson, G. A.; J. Phys. Chem. A **102**, 10074 (1998).

Sen, A. *Acc. Chem. Res.* **1998**, *31*, 550.

Shilov, A. E.; Shteinman, A. A. *Acc. Chem. Res.* **1999**, *32*, 763.

Shilov, A. E.; Shul'pin, G. B. *Chem. Rev.* **1997**, *97*, 2879.

Singh, K.; Long, J. R.; Stavropoulos, P. *J. Am. Chem. Soc.* **1997**, *119*, 2942.

Singh, K.; Long, J. R.; Stavropoulos, P. *Inorg. Chem.* **1998**, *37*, 1073.

Slaughter, L. M.; Wolczanski, P. T.; Klinckman, T. R.; Cundari, T. R. *J. Am. Chem. Soc.* **2000**, *122*, 7953.

So, S. P.; Chem. Phys. Lett. **313**, 307 (1999).

Stahl, S.; Labinger, J. A.; Bercaw, J. E. *Angew. Chem., Int. Ed.* **1998**, *37*, 2181.

Stevens, W. J.; Basch, H.; Krauss, M. *J. Chem. Phys.* **1984**, *81*, 6026.

Stevens, W. J.; Krauss, M.; Basch, H.; Jasien, P. G. *Can. J. Chem.* **1992**, *70*, 612.

Tajti, A.; Szalay, P. G.; Császár, A. G.; Kállay, M.; Gauss, J.; Valeev, E. F.; Flowers, B. A.; Vázquez, J.; Stanton, J. F.; J. Chem. Phys. **121**, 23 (2004).

Tenn, W. J., III; Young, K. J. H.; Bhalla, G.; Oxgaard, J.; Goddard, W. A., III; Periana, R. A. *J. Am. Chem. Soc.* **2005**, *127*, 14172.

Thompson, M. E.; Baxter, S. M.; Bulls, A. R.; Burger, B. J.; Nolan, M. C.; Santarsiero, B. D.; Schaefer, W. P.; Bercaw, J. E. *J. Am. Chem. Soc.* **1987**, *109*, 203.

Thyagarajan, S.; Shay, D. T.; Incarvito, C. D.; Rheingold, A. L.; Theopold, K. H. *J. Am. Chem. Soc,* **2003,** *125,* 4440.

Truong, T. N.; Evans, T. J.; J. Phys. Chem. **98**, 9558. (1994).

van Mourik, T.; Wilson, A. K.; Peterson, K. A.; Woon, D. E.; Dunning, Jr., T. H.; "The Effect of Basis Set Superposition Error (BSSE) on the Convergence of Molecular Properties Calculated with the Correlation Consistent Basis Sets." In *Advances in Quantum Chemistry*, vol 31; Löwdin, P., Ed.; Academic Press: San Diego, CA, 1998; pp. 105-135.

Vedernikov, A. N.; Caulton, K. G. *Chem. Comm.* **2004**, *2*, 162.

Verma, A. K.; Nazif, T. N.; Achim, C.; Lee, S. C. *J. Am. Chem. Soc.* **2000**, *122*, 11013.

Vorontsov, I. I.; Kovalevsky, A. Y.; Chen, Y.-S.; Graber, T.; Gembicky, M.; Novozhilova, I. V.; Omary, M. A.; Coppens, P. *Phys. Rev. Lett.* **2005**, *94*, 193003

Walsh, P. J.; Hollander, F. J.; Bergman, R. G. *J. Am. Chem. Soc.* **1988**, *110*, 8729.

Wang, B.; Hou, H.; Gu, Y.; J. Phys. Chem. A **105**, 156 (2001).

Waterman, R.; Hillhouse, G. L. *J. Am. Chem. Soc*. **2003**, *125*, 13350.

WebElements Scholar, http://www.webelements.com/, Accessed January **2007**.

Webster, C. E.; Fan, Y.; Hall, M. B.; Kunz, D.; Hartwig, J. F. *J. Am. Chem. Soc.* **2003**, *125*, 858.

Weinhold, F.; Landis, C. R. *Chem. Ed.: Research and Practice in Europe* **2001**, *2*, 91.

White-Morris, R. L.; Olmstead, M. M.; Jiang, F.; Balch, A. L. *Inorg. Chem.* **2002**, *41*, 2313.

White-Morris, R. L.; Olmstead, M. M.; Jiang, F.; Tinti, D. S.; Balch, A. L. *J. Am. Chem. Soc.* **2002**, *124*, 2327.

Wilson, A. K.; Woon, D. E.; Peterson, K. A.; Dunning, Jr., T. H.; J. Chem. Phys. **110**, 7667 (1999).

Wilson, A. K.; Woon, D. E.; Peterson, K. A.; Dunning, Jr., T. H.; Abstr. Pap. – Am. Chem. Soc. **213**, 60 (1997).

Winter, M. *WebElements (Professional Edition).* http://www.webelements.com/

Woon, D. E.; Dunning, Jr., T. H.; J. Chem. Phys. **117**, 10548 (2002).

Woon, D. E.; Dunning, Jr., T. H.; J. Chem. Phys. **103**, 4572 (1995).

Woon, D. E.; Dunning, Jr., T. H.; J. Chem. Phys. **100**, 2975 (1994).

Xu, X.; Fu, G.; Goddard, W. A., III; Periana, R. A. *Studies Surf. Sci. Catal.* **2004**, *147*, 499.

Xu, Z.-F.; Li, S.-M.; Yu, Y.-X.; Li, Z.-S.; Sun, C. C.; J. Phys. Chem. A **103**, 4910 (1999).

Yang, G.; Raptis, R. G. *Inorg. Chem.* **2003**, *42*, 261.

Yu, X.; Li, S.-M.; Liu, J.-Y.; Xu, Z.-F.; Li, Z.-S.; Sun, C.-C.; J. Phys. Chem. A **103**, 6402 (1999).

Yu, Y.-X.; Li, S.-M.; Xu, Z.-F.; Li, Z. S.; Sun, C.-C.; Chem. Phys. Lett. **302**, 281 (1999).

Zhang, J.; Gunnoe, T. B.; Petersen, J. L.; *Inorg. Chem.* **2005**, *44*, 2895.

Zhao, Y.; González-García, N.; Truhlar, D. G.; J. Phys. Chem. A **109**, 2012 (2005).

Zhu, K.; Achord, P. D.; Zhang, X.; Krogh-Jespersen, K.; Goldman, A. S. *J. Am. Chem. Soc.* **2004**, *126*, 13044.